FINAL REPORT
presented to the
US ARMY RESEARCH OFFICE
on contract DAAH04-95-1-0527
Hot Electron Effect and Quantum
Magnetotransport in Quantum Wires

UNIVERSITY OF
NEBRASKA-LINCOLN

College of Engineering and Technology
University of Nebraska–Lincoln
Lincoln, Nebraska 68588-0501

SF 298 MASTER COPY KEEP THIS COPY FOR REPRODUCTION PURPOSES

REPORT DOCUMENTATION PAGE

Form Approved
OMB NO. 0704-0188

1. AGENCY USE ONLY *(Leave blank)*	2. REPORT DATE	3. REPORT TYPE AND DATES COVERED
	June 19, 1997	Final report

4. TITLE AND SUBTITLE
Hot Electron and Quantum Magnetotransport in Quantum Wires

5. FUNDING NUMBERS
DAAH04-95-1-0527

6. AUTHOR(S)
Supriyo Bandyopadhyay

7. PERFORMING ORGANIZATION NAMES(S) AND ADDRESS(ES).
University of Notre Dame

8. PERFORMING ORGANIZATION REPORT NUMBER

9. SPONSORING / MONITORING AGENCY NAME(S) AND ADDRESS(ES)
U.S. Army Research Office
P.O. Box 12211
Research Triangle Park, NC 27709-2211

10. SPONSORING / MONITORING AGENCY REPORT NUMBER
ARO 32161.2-EL

11. SUPPLEMENTARY NOTES
The views, opinions and/or findings contained in this report are those of the author(s) and should not be construed as an official Department of the Army position, policy or decision, unless so designated by other documentation.

12a. DISTRIBUTION / AVAILABILITY STATEMENT
Approved for public release; distribution unlimited.

12 b. DISTRIBUTION CODE

13. ABSTRACT *(Maximum 200 words)*

This report details the result of theoretical investigation carried out to study hot electron effects and magneto-optical properties of quantum wires. Many surprising features emerged, such as the quenching of acoustic phonon interaction by a magnetic field, an anomalous electron cooling effect, a temperature inversion effect, the possibility of a negative transport lifetime, giant enhancements in the second- and third-order optical nonlinearities in a quantum wire, and the possibility of efficient, low loss waveguiding of polaritons in arrays of quantum wires.

14. SUBJECT TERMS	15. NUMBER IF PAGES
Quantum wires, magnetotransport, hot electrons, excitons, optical non-linearity, polaritons	16. PRICE CODE

17. SECURITY CLASSIFICATION OR REPORT	18. SECURITY CLASSIFICATION OF THIS PAGE	19. SECURITY CLASSIFICATION OF ABSTRACT	20. LIMITATION OF ABSTRACT
UNCLASSIFIED	UNCLASSIFIED	UNCLASSIFIED	UL

FINAL REPORT
presented to the
US ARMY RESEARCH OFFICE
on contract DAAH04-95-1-0527
Hot Electron Effect and Quantum
Magnetotransport in Quantum Wires

Hot Electron and Quantum Magnetotransport[1]

FINAL REPORT

S. Bandyopadhyay

June 1997

US Army Research Office

CONTRACT NO. DAAH04-95-1-0527

University of Nebraska
Licoln, Nebraska 68588

[1]This contract was awarded to University of Notre Dame, the author's previous employer. The author is presently with the University of Nebraska.

1 Foreward

This report covers the period August 15, 1995 to December 31, 1996. This was the duration of grant DAAH04-95-1-0527. During this time, extensive theoretical studies of hot electron and quantum magnetotransport in quantum wires was undertaken under the author's supervision. One graduate student was supported for part his program at the University of Notre Dame. He received a Ph.D. degree in Electrical Engineering in December 1996 and is currently a post-doctoral research associate at the University of Nebraska. He will be joining the Department of Electrical Engineering at the University of California-Los Angeles as a research associate starting August 1, 1997.

This research resulted in five journal/book publications and six conference publications which are attached in the appendix.

A Table of Contents is not included since the main body of the report is less than 10 pages.

2 Technical Report

2.1 Statement of problem

Two distint problems were studied: (a) hot electron magneto-transport, and (b) quantum magneto-optical properties of quantum wires. In the first case, we started with the Schrödinger equation in a quantum wire subjected to a magnetic field. This equation was solved numerically using a finite difference scheme developed by us [1] to yield the electron wave functions, energy-dispersion relations and the density of states. From these, electron-phonon and electron-impurity scattering rates were calculated using Fermi's Golden Rule [2-8]. These were then used in a Monte Carlo simulator to find electron velocity versus field characteristics, electron energy and other transport parameters [6,7].

To study magneto-optical properties, we solved the Schrödinger equation for an exciton in a quantum wire subjected to a magnetic field. This was based on a variational approach [9-28]. The solutions yield exciton binding energies and other parameters, which are then used to calculate bi-exciton parameters [10,12,14]. Third-order dielectric susceptibility $\chi^{(3)}$ was calculated using the rotating wave approximation. This third-order non-linearity arises from exciton-exciton interaction and population saturation of the excitonic state [11,16-18]. Furthermore, second-order susceptibility $\chi^{(2)}$ was also calculated. It arises from inter-subband transitions and giant dipoles associated with them [13,19,22,23,27]. Finally, exciton-polariton transport in an array of quantum wires has also been investigated [20,28].

2.2 Summary of most important results

The following findings were the most remarkable:

1. It was found that a magnetic field quenches intra-subband electron-bulk acoustic phonon scattering rates in a quantum wire by several orders of magnitude. This has important implications for the celebrated integral Quantum Hall effect and may partially explain its robustness. The quenching occurs because the dominant scattering mechanism is backscattering which involves transitions between *oppositely* travelling states. In the presence of a magnetic field, these states are localized along opposite edges of the wire ("edge states") with very little overlap between their wave functions. As a result, the matrix element for transition between these states is drastically reduced.

2. A magnetic field increases electron-surface optical phonon scattering since the field skews the wave functions of electrons towards the surfaces (or edges) of the quantum wire thus increasing the overlap between the surface phonon modes and the electron wave function.

3. A magnetic field has two different effects on electron-confined polar optical phonon scattering. On the one hand, it reduces the overlap between an electron wave function and a phonon mode with the same index because of the skewing of the former, but on the other hand, it opens new channels of scattering by breaking the orthogonality between the electron wave function and a phonon mode with different index. Usually, the second effect wins, resulting in a increase in the electron-confined optical phonon scattering rates.

4. The *ensemble average* transport lifetime in a quantum wire can be *negative* if the Fermi velocity (determined by carrier concentration) is less than the sound velocity. Such a negative lifetime can cause very low field velocity overshoot.

5. There can be an anomalous cooling effect whereby the electron temperature can fall *below* the lattice temperature when an electric field is applied over a quantum wire. The electrons

gain energy from the electric field, but lose energy at a faster rate by emitting phonons. As a result, the electron gas cools in an electric field.

6. The electron temperature at a lattice temperature of 300 K can be *less* than the electron temperature at a lattice temperature of 77 K when a magnetic field is present since phonon emission (and hence energy relaxation) is more efficient at 300 K.

7. Both exciton and biexciton binding energies in a quantum wire are enhanced by a magnetic field. This effect is opposite to that caused by an electric field. Whereas an electric field reduces the binding energy by exerting equal and opposite forces on an electron and hole, a magnetic increases the binding energy by squeezing an electron and hole wave function closer together. There is a whole bevy of magneto-optic effects that are analogs of well-known electro-optic effects.

8. Both second- and third-order susceptibiltiesof a quantum wire are enhanced by a magnetic field. The magnetic field allows one to tune the differential non-linear refractive index and absorption in a quantum wire thereby allowing flexible device design.

9. A magnetic field can be used to spectrally separate regions of high refractive index and high absorption. As a result, it is possible to sustain polariton transport in an array of quantum wires where both efficient waveguiding and low-loss propagation is possible. This has serious implications for optical communications.

2.3 Important publications resulting from the grant

1. N. Telang and S. Bandyopadhyay, "Magnetic Field Dependence of Energy and Momentum Relaxation Rates of Hot Carriers in a Quantum Wire Subjected to a Magnetic Field", *Phys. Low Dimensional Struct.* 9/10, 63-74 (1996).

2. A. Svizhenko, A. Balandin and S. Bandyopadhyay "Giant Dipole Effect and Second Harmonic Generation in Quantum Wires Biased with a Magnetic Field", *J. Appl. Phys.* (in press).

3. A. Balandin and S. Bandyopadhyay, "Dielectric Confinement of Magneto- Excitons and Biexcitons in Quantum Wires", submitted to *Zh. Eksp. Teor. Fiz.: JETP.*

4. A. Balandin, A. Svizhenko and S. Bandyopadhyay, "Non-linear optical mixing in quantum wires", to appear in *Quantum Confinement IV*: Proc. of the 191st Meeting of the Electrochemical Society; Fourth International Symposium on Quantum Confinement: Nanoscale Materials, Devices and Systems, Montreal, Canada, May 4-9, 1997.

5. A. Balandin and S. Bandyopadhyay, "Polariton transport in semiconductor quantum wires", to appear in *Quantum Confinement IV*: Proc. of the 191st Meeting of the Electrochemical Society; Fourth International Symposium on Quantum Confinement: Nanoscale Materials, Devices and Systems, Montreal, Canada, May 4-9, 1997.

6. A. Balandin, A. Svizhenko and S. Bandyopadhyay, "Refractive Index of a Quantum Wire Around a Polariton Resonance", to be presented at the Tenth International Conference on Superlattices, Microstructures and Microdevices, Lincoln, Nebraska, USA.

7. A. Svizhenko, A. Balandin and S. Bandyopadhyay, "Linear and Non-linear Magneto-optical Properties of a Quantum Wire Associated with Inter-Magnetoelectric Subband Resonances", to be presented at the Tenth International Conference on Superlattices, Microstructures and Microdevices, Lincoln, Nebraska, USA.

8. A. Balandin, A. Svizhenko and S. Bandyopadhyay, "Effective Breaking of Inversion Symmetry in a Quantum Wire with a Magnetic Field", to be presented at the International Conference on Nanostructures, NANO'97, Repino, Russia, June (1997).

9. S. Bandyopadhyay, A. Balandin and A. Svizhenko, "Dielectric Enahancement of the Oscillator Strengths and Binding Engeries of Magneto- Excitons and Biexcitons in a Quantum Wire" Spring Meeting of the American Physical Society, Kansas City, MO, 1997.

10. A. Svizhenko, A. Balandin and S. Bandyopadhyay, "Giant Dipole Effect and Second Harmonic Generation in Magnetic Field Biased Quantum Wires", Spring Meeting of the American Physical Society, Kansas City, MO, 1997.

11. S. Balandin and S. Bandyopadhyay, "Exciton-Polariton Transport in Quantum Wires", March Meeting of the American Physical Society, Kansas City, MO, 1997.

2.4 Personnel

1. Prof. Supriyo Bandyopadhyay, principal investigator

2. Dr. Nina Telang, Research Engineer, Motorola, Inc, Austin, TX

3. Dr. Alexander Balandin, post-doctoral associate, University of Nebraska

Dr. Balandin was a graduate student working on this grant who received his Ph.D. in December 1996.

3 Reference

1. S. Chaudhuri and S. Bandyopadhyay, "Numerical Calculation of Hybrid Magnetoelectric States in an Electron Waveguide", *J. Appl. Phys.*, 71, 3027 - 3029 (1992); S. Bandyopadhyay, S. Chaudhuri, B. Das and M. Cahay, "Features of quantum magnetotransport and electromigration in mesoscopic systems" *Superlattices and Microstructures*, 12, 123 - 132 (1992); S. Chaudhuri, S. Bandyopadhyay, and M. Cahay, "Spatial Distribution of the Current, Fermi Carriers, Potential and Electric Field in a Disordered Quantum Wire Subjected to a Magnetic Field" *Phys. Rev. B* 47, 12649 (1993).

2. N. Telang and S. Bandyopadhyay, "Quenching of Acoustic Phonon Scattering of Electrons in Semiconductor Quantum Wires Induced by a Magnetic Field" *Appl. Phys. Lett.* 62, 3161 (1993).

3. N. Telang and S. Bandyopadhyay, "The Effect of a Magnetic Field on Electron Phonon Scattering Rates", *Phys. Rev. B*, 48, 18002 (1993).

4. N. Telang and S. Bandyopadhyay, "Modulation of Electron Phonon Scattering in Quantum Wires by a Magnetic Field", *Semicon. Sci. Technol.* 9, 955-957 (1994).

5. N. Telang and S. Bandyopadhyay, "Negative Transport Lifetimes in Quantum Wires", *Phys. Rev. Lett.*, 73, 1683-1685 (1994).

6. N. Telang and S. Bandyopadhyay, "Effect of a Magnetic Field on Hot Electron Transport in a Quantum Wire", *Appl. Phys. Lett.* 66, 1623-1625 (1995).

7. N. Telang and S. Bandyopadhyay, "Monte Carlo Simulation of Hot Electron Magnetotransport in Quantum Wires at Low, Intermediate and High Electric Fields", *Phys. Rev. B* 51, 9728 (1995).

8. N. Telang and S. Bandyopadhyay, "Magnetic Field Dependence of Energy and Momentum Relaxation Rates of Hot Carriers in a Quantum Wire Subjected to a Magnetic Field", *Phys. Low Dimensional Struct.* 9/10, 63-74 (1996).

9. A. Balandin and S. Bandyopadhyay, "Excitons in a Quantum Wire Subjected to a Magnetic Field", *Phys. Rev. B* 52, 8312 (1995).

10. A. Balandin and S. Bandyopadhyay, "Magneto-Biexcitonic States in a Quantum Wire", *Phys. Rev. B* 54, 5712 (1996).

11. A. Balandin and S. Bandyopadhyay, "Theoretical Studies of the Effects of a Magnetic Field on the Excitonic Non-Linear Optical Properties of Quantum Wires", *Phys. Rev. B* 54, 5721 (1996).

12. A. Balandin and S. Bandyopadhyay, "Biexcitons in a Quantum Wire Subjected to a Magnetic Field", in *Quantum Confinement III: Quantum Wires and Dots*, Eds. M. Cahay, S. Bandyopadhyay, J-P Leburton and M. Razeghi, (The Electrochemical Society, Inc., Pennington, New Jersey, 1996), p. 117.

13. A. Svizhenko, A. Balandin and S. Bandyopadhyay "Giant Dipole Effect and Second Harmonic Generation in Quantum Wires Biased with a Magnetic Field", *J. Appl. Phys.* (in press).

14. A. Balandin and S. Bandyopadhyay, "Dielectric Confinement of Magneto- Excitons and Biexcitons in Quantum Wires", submitted to *Zh. Eksp. Teor. Fiz.: JETP.*

15. A. Balandin and S. Bandyopadhyay, "Binding Energy and Length of Quasi One-dimensional Excitons in a Magnetic Field", *Superlattices and Microstructures* 19, 97 (1996).

16. A. Balandin and S. Bandyopadhyay, "Non-linear Differential Refractive Index and Absorption in Quantum Wires in the Presence of a Magnetic Field", *Superlattices and Microstructures* (in press).

17. A. Balandin, A. Svizhenko and S. Bandyopadhyay, "Third-order Magneto-excitonic Non-linearities in Quantum Wires", presented at Nanostructures 96, St. Petersburg, Russia, June 24-28, 1996 (also in Abstracts of Invited Lectures and Contributed Papers, Nanostructures 96, Russian Academy of Sciences, p. 294).

18. A. Balandin and S. Bandyopadhyay, "Non-linear Differential Refractive Index and Absorption in Quantum Wires in the Presence of a Magnetic Field", presented at the Ninth International Conference on Superlattices and Microstructures, Liege, Belgium, July 14-19 (1996).

19. A. Balandin, A. Svizhenko and S. Bandyopadhyay, "Non-linear optical mixing in quantum wires", presented at the 191st Meeting of the Electrochemical Society; Fourth International Symposium on Quantum Confinement: Nanoscale Materials, Devices and Systems, Montreal, Canada, May 4-9, 1997.

20. A. Balandin and S. Bandyopadhyay, "Polariton transport in semiconductor quantum wires", presented at the 191st Meeting of the Electrochemical Society; Fourth International Symposium on Quantum Confinement: Nanoscale Materials, Devices and Systems, Montreal, Canada, May 4-9, 1997.

21. A. Balandin, A. Svizhenko and S. Bandyopadhyay, "Refractive Index of a Quantum Wire Around a Polariton Resonance", to be presented at the Tenth International Conference on Superlattices, Microstructures and Microdevices, Lincoln, Nebraska, USA.

22. A. Svizhenko, A. Balandin and S. Bandyopadhyay, "Linear and Non-linear Magneto-optical Properties of a Quantum Wire Associated with Inter-Magnetoelectric Subband Resonances", to be presented at the Tenth International Conference on Superlattices, Microstructures and Microdevices, Lincoln, Nebraska, USA.

23. A. Balandin, A. Svizhenko and S. Bandyopadhyay, "Effective Breaking of Inversion Symmetry in a Quantum Wire with a Magnetic Field", to be presented at the International Conference on Nanostructures, NANO'97, Repino, Russia, June (1997).

24. S. Bandyopadhyay, A. E. Miller and A. Balandin, **Non-linear Optical Properties of Self-Assembled Structures: Theory and Experiment**, to be presented at the International Conference on Laser Surface Processing, Limoges, France, Septmeber 8-12, 1997.

25. A. Balandin, A. Svizhenko and S. Bandyopadhyay, "Non-linear magneto-optical properties of quantum wires", presented at the Midwest Solid State Physics Symposium, University of Nebraska, Lincoln, October 17, 1996.

26. S. Bandyopadhyay, A. Balandin and A. Svizhenko, "Dielectric Enahancement of the Oscillator Strengths and Binding Engeries of Magneto- Excitons and Biexcitons in a Quantum Wire" Spring Meeting of the American Physical Society, Kansas City, MO, 1997.

27. A. Svizhenko, A. Balandin and S. Bandyopadhyay, "Giant Dipole Effect and Second Harmonic Generation in Magnetic Field Biased Quantum Wires", Spring Meeting of the American Physical Society, Kansas City, MO, 1997.

28. S. Balandin and S. Bandyopadhyay, "Exciton-Polariton Transport in Quantum Wires", March Meeting of the American Physical Society, Kansas City, MO, 1997.

APPENDIX

Publications.

Abstract Submitted
for the MAR97 Meeting of
The American Physical Society

Sorting Category: 17.b

Giant Dipole Effect and Second Harmonic Generation in Magnetic-Field-Bised Semiconductor Quantum Wires
ALEXEI SVIZHENKO, *Department of Electrical Engineering, University of Notre Dame, Notre Dame, IN.*, ALEXANDER BALANDIN, SUPRIYO BANDYOPADHYAY, *Department of Electrical Engineering, University of Nebraska, Lincoln, NE.* — We have theoretically studied the giant dipole effect in magnetic-field-biased semiconductor quantum wires. The dipoles are associated with transitions between magneto-electric subbands within the conduction band; some of these transitions are forbidden in the absence of the magnetic field. The possibility of second harmonic generation in a quantum wire biased with a magnetic field has also been examined. We will show that the simultaneous presence of a symmetric confinement (electrostatic) potential and an external magnetic field may lead to uneven charge distribution along the width of the wire which breaks the inversion symmetry in a generic quantum well or wire. This results in a non-zero third-order susceptibility and associated optical nonlinearity. This work was supported by the US Army Research Office under contract DAAH04-95-1-0586 and DAAH04-95-1-0527.

Alexander Balandin
abalandi@engrs.unl.edu
Department of Electrical Engineering
University of Nebraska, Lincoln, NE.

[X] Prefer Oral Session
[ ] Prefer Poster Session

Date submitted: December 3, 1996

Electronic form version 1.2

Abstract Submitted
for the MAR97 Meeting of
The American Physical Society

Sorting Category: 17.b

Dielectric Enhancement of the Oscillator Strengths and Binding Energies of Magneto-Excitons and Magneto-Biexcitons in Quantum Wires SUPRIYO BANDYOPADHYAY, ALEXANDER BALANDIN, *Department of Electrical Engineering, University of Nebraska, Lincoln, NE.*, ALEXEI SVIZHENKO, *Department of Electrical Engineering, University of Notre Dame, Notre Dame, IN.*
— We will report a partly variational calculation of magneto- exciton and biexciton (excitonic molecule) binding energies in a rectangular semiconductor quantum wire taking into account dielectric confinement effects. The discontinuity of the dielectric constant at the boundaries between the wire and surrounding medium causes redistribution of electric field which leads to higher binding energies of excitons and biexcitons. The dielectric confinement effects are introduced via the image-charge method. Strong dielectric enhancement of the exciton binding energies (up to 2.5 times) and oscillator strengths is found for quantum wires of the dimensions comparable to the exciton Bohr radius. The enhancement decreases substantially in a magnetic field because of a charge cancellation effect. This work was supported by the US Army Research Office under contract DAAH04-95-1-0586 and DAAH04-95-1-0527.

Alexander Balandin
abalandi@engrs.unl.edu
Department of Electrical Engineering
University of Nebraska, Lincoln, NE.

[X] Prefer Oral Session
[ ] Prefer Poster Session

Date submitted: December 3, 1996

Electronic form version 1.2

Abstract Submitted
for the MAR97 Meeting of
The American Physical Society

Sorting Category: 17.b

Exciton-Polariton Transport in an Array of Semiconductor Quantum Wires ALEXANDER BALANDIN, SUPRIYO BANDYOPADHYAY, *Department of Electrical Engineering, University of Nebraska, Lincoln, NE.* — Polariton effects play an important role in low temperature absorption of bulk and nanostructured semiconductors in the spectral range close to the exciton resonance frequencies. The formation of polaritons (exciton-photon coupled states) modifies the transport of light through the medium. In particular, the medium of propagation becomes substantially more transparent provided that the exciton-polariton coherence length, critical temperature and exciton decay parameter meet certain criteria. We will show that in a properly designed array of quasi one-dimensional structures (quantum wires) of dimensions comparable to the exciton Bohr radius, the application of an external magnetic field can strongly increase the critical exciton-polariton coherence length and the critical temperature. Our numerical results are based on a partially variational calculation of the exciton longitudinal-transverse splitting as a function of wire dimensions and magnetic flux density. The temperature dependence is evaluated under the assumption that interactions with acoustic and polar optical phonons are the dominant scattering mechanisms for excitons. This work was supported by the US Army Research Office under contract DAAH04-95-1-0586 and DAAH04-95-1-0527.

Alexander Balandin
abalandi@engrs.unl.edu
Department of Electrical Engineering
University of Nebraska, Lincoln, NE

[X] Prefer Oral Session
[ ] Prefer Poster Session

Date submitted: December 3, 1996

Electronic form version 1.2

Submitted to Zh. Eksp. Teor (JETP)

Dielectric Confinement of Magneto- Excitons and Biexcitons in Quantum Wires

A. Balandin*and S. Bandyopadhyay
Department of Electrical Engineering
University of Nebraska
Lincoln, Nebraska 68588 U.S.A.

The[1] effect of dielectric confinement on magneto- excitons and biexcitons in a quantum wire, surrounded by a medium with lower dielectric cosntant, is investigated theoretically. For free-standing wires, very strong dielectric enhancement of binding energies and oscillator strengths, along with a concomitant decrease in radii, is found for wires whose widths are comparable to the effective Bohr radius of the exciton. In GaAs wires, the combination of dielectric confinement, quantum confinement and magnetostatic confinement can make both the exciton and biexciton binding energies exceed the room-temperature thermal energy for realistic wire widths. We also show how a magnetic field can be used to experimentally separate the effect of dielectric confinement and quantum confinement.

*On leave from the Moscow Institute of Physics and Technology, Dolgoprudny, Russia
[1]PACS Indices: 78.20.Ls, 73.20.Dx, 78.66.-w

I. INTRODUCTION

Quasi one-dimensional structures (quantum wires) exhibit enhanced exciton and biexciton binding energies and oscillator strengths which endow them with strong non-linear optical properties[1–5]. The enhancements accrue primarily from quantum confinement which is spatial confinement of the electron and hole wavefunctions in a quasi one-dimensional region. This confinement can be increased further by a magnetic field which "squeezes" the electron and hole wave functions into edge-states or cyclotron orbits. At the same time, if the medium surrounding the wire has a smaller dielectric constant, then the effective dielectric constant of the entire system is reduced which then reduces the screening of the attractive interaction between an electron and a hole. As a result, an electron and a hole become even more tightly bound and this increases the binding energy and oscillator strengths further[6–8]. In this paper, we examine this latter effect - the so-called "dielectric confinement" - in the presence of a magnetic field.

While dielectric confinement effects in quantum wells and dots have been studied[9,10], scant attention has been given to quantum wires. So far, the very few theoretical treatements that have been reported for wires have concentrated narrowly on specific geometries and carrier density regimes. In ref. [11], the effect of dielectric confinement on exciton binding energy was found variationally for cylindrical wires whose radii R were much smaller that the exciton Bohr radius a_B. The mathematical model in this work is valid only when $R << a_B$ and is therefore of limited use. Ref. [12] treated a wedge shaped wire. We consider a wire of rectangular cross-section. To our knowledge, ours is also the first study where the effect of an external magnetic field has been taken into account. Furthermore, we have also examined the

effect of dielectric confinement on *biexcitons*. This is an extremely important topic since exciton-exciton interaction leading to the formation of biexcitons (and possibly higher order excitonic complexes) is the major source of optical non-linearity in quantum wires[13,14]. Increased biexciton binding energies translate into increased third-order dielectric susceptibility (and therefore increased optical non-linearity) in quantum wires. Finally, any increase in biexciton binding energy makes these complexes more stable and therefore improves the chances of experimental observation.

This paper is organized as follows. In the next section, we present the theory. This is followed by results and finally the conclusion.

II. THEORY

A. Dielectrically confined magneto-excitons

We consider a quantum wire of rectangular cross-section as shown in Fig. 1 (a) with infinite potential barriers located at $y = \pm L_y/2$ and $z = \pm L_z/2$. A magnetic field of flux density B is applied along the z-direction. For nondegenerate and isotropic bands, the Hamiltonian of a free Wannier-Mott exciton in this system is given within the envelope-function approximation by

$$\begin{aligned} \hat{H^X} &= \frac{\hat{P_X}^2}{2M} + \frac{\hat{p_x}^2}{2\mu} + \frac{\hat{p_{y_e}}^2 + \hat{p_{z_e}}^2}{2m_e} + \frac{\hat{p_{y_h}}^2 + \hat{p_{z_h}}^2}{2m_h} \\ &+ \frac{eB(y_e - y_h)}{M}\hat{P_X} + eB(y_e/m_e + y_h/m_h)\hat{p_x} + \frac{e^2B^2}{2}(y_e^2/m_e + y_h^2/m_h) \\ &+ U_C(x_e, x_h, y_e, y_h, z_e, z_h) + U_S(y_e, y_h, z_e, z_h) + U_D(y_e, y_h, z_e, z_h), \end{aligned} \tag{1}$$

where we have chosen the Landau gauge for the magnetic vector potential

$$\vec{A} = (-By, 0, 0).$$

The quantities $m_e, m_h, (x_{e,h}, y_{e,h}, z_{e,h})$ are the effective masses (coordinates) of electrons and holes respectively, $1/\mu(= 1/m_e + 1/m_h,)$ is the reduced mass, $M(= m_e + m_h)$ is the total mass, $U_C(x_e, x_h, y_e, y_h, z_e, z_h)$ is the electron-hole Coulomb interaction energy, $U_S(y_e, y_h, z_e, z_h)$ is the spatial confinement potential energies for electrons and holes along the transverse y and z directions, and $U_D(y_e, y_h, z_e, z_h)$ is the dielectric confinement for electrons and holes along y and z directions arising from the redistribution of the electric field due to the discontinuity of the dielectric constant at the wire interfaces. We neglect Zeeman splitting since the Landé g-factor is small in most technologically important semiconductors.

For convenience, we replaced $x_{e,h}$-coordinates in Eq. (1) by the center-of-mass (X) and relative coordinate (x):

$$X = (m_e x_e + m_h x_h)/M,$$

$$x = x_e - x_h.$$

For free-standing quantum wires (surrounded by air or vacuum), we can assume hard-wall boundary conditions:

$$\begin{aligned} U_S(y_e, y_h, z_e, z_h) &= 0, \quad z_{e,h} < L_z \ \wedge \ y_{e,h} < L_y \\ &= \infty, \quad \textit{otherwise.} \end{aligned} \tag{2}$$

Finite barrier heights introduce only small corrections for wires with width and thickness $>$ 50 Å; therefore, our results are quite general for wires of realistic widths.

The Coulomb interaction between any two charged particles in a quantum wire is given by its full three-dimensional form

$$U_C(x_e, x_h, y_e, y_h, z_e, z_h) = \pm \frac{e^2}{4\pi\epsilon_w[(x_e - x_h)^2 + (y_e - y_h)^2 + (z_e - z_h)^2]^{1/2}}, \tag{3}$$

where ϵ_w is the dielectric constant of the wire.

To calculate the dielectric confinement energy, U_D, we adopt the image-charge method which is known to provide good qualitative agreement with experiments[8,15,16]. The image-charge method, which is well-established in electrostatics, accounts for the electric field induced by charged particles in parallel or spherical geometries by means of imaginary charges placed in surrounding media.[17] The values of the image-charges are determined from the continuity conditions for the electrostatic potentials and the normal components of the displacement vector at the interfaces. Following the derivation of Refs. [9, 10], we can write the dielectric confinement potential of an electron-hole pair within the quantum wire as

$$U_D \equiv U_{self}^{(e)} + U_{self}^{(h)} + U_{attr}^{(e-h)}, \tag{4}$$

where

$$U_{self}^{(e)} = \frac{e^2}{2\epsilon_w} \sum_{l=-\infty}^{\infty} \sum_{m=-\infty}^{\infty} \frac{\xi^{|l|+|m|}}{[(y_e - y_{e,l,m})^2 + (z_e - z_{e,l,m})^2]^{1/2}}, \tag{5}$$

$$U_{self}^{(h)} = \frac{e^2}{2\epsilon_w} \sum_{l=-\infty}^{\infty} \sum_{m=-\infty}^{\infty} \frac{\xi^{|l|+|m|}}{[(y_h - y_{h,l,m})^2 + (z_h - z_{h,l,m})^2]^{1/2}}, \tag{6}$$

$$U_{attr}^{(e-h)} = -\frac{e^2}{\epsilon_w} \sum_{l=-\infty}^{\infty} \sum_{m=-\infty}^{\infty} \frac{\xi^{|l|+|m|}}{[(x_e - x_h)^2 + (y_e - y_{h,l,m})^2 + (z_e - z_{h,l,m})^2]^{1/2}}. \tag{7}$$

and

$$(x_\alpha, y_{\alpha,l,m}, z_{\alpha,l,m}) = (x_\alpha, L_y l + (-1)^l y_\alpha, L_z m + (-1)^m z_\alpha),$$

with $\alpha = e$ or h; and $l, m = -\infty, ..., \infty$. The $l = m = 0$ term is excluded from the summation in Eqs. (5)-(7). The dielectric constant of the surrounding medium is assumed to be less than the dielectric constant of the wire material ($\epsilon_b < \epsilon_w$), which is usually the case in real systems. Finally, the quantity

$\xi = (\epsilon_w - \epsilon_b)/(\epsilon_w + \epsilon_b)$ is a measure of the *dielectric misfit* between the quantum wire material (dielectric constant ϵ_w) and the boundary material (dielectric constant ϵ_b).

One can see from Eq. (4) that the dielectric confinement term, U_D, is written as a sum of two positive self-energy terms resulting from repulsive interactions of electron -"electron image" (hole - "hole image"); and a negative term which is due to attractive interaction between electron - "hole image" (hole - "electron image"). The summations over the infinite series in Eqs. (5) - (7) come about because any charge image, in turn, creates another image in the opposite flat boundary of the wire (see Fig. 1 (b)).

For materials with a small dielectric misfit (e.g. CdS dispersed in alumina for which $\xi \approx 0.5$), one can retain only the first order terms ($|l| + |m| = 1$) in Eqs. (5) - (7); for material systems with higher dielectric misfit (such as GaAs surrounded by air for which $\xi \approx 0.9$), higher order terms are required. For the sake of illustration, we will write the first order terms in U_D explicitly. Setting $l = 0$ and $m = \pm 1$ we obtain the terms which correspond to interactions of the electron and hole with their images in the flat boundaries along z direction (L_z is the thickness of the wire). Similarly, setting $m = 0$ and $l = \pm 1$ we obtain the terms which correspond to interactions of the electron and hole with their images in the flat boundaries along y direction (L_y is the width of the wire). Combining these terms together, we get

$$U_{self}^{(e)} = +\frac{1}{2}\frac{e^2}{\epsilon_w}\left(\frac{\epsilon_w - \epsilon_b}{\epsilon_w + \epsilon_b}\right)\left\{\frac{1}{|2z_e - L_z|} + \frac{1}{|2z_e + L_z|} + \frac{1}{|2y_e - L_y|} + \frac{1}{|2y_e + L_y|}\right., \tag{8}$$

$$U_{self}^{(h)} = +\frac{1}{2}\frac{e^2}{\epsilon_w}\left(\frac{\epsilon_w - \epsilon_b}{\epsilon_w + \epsilon_b}\right)\left\{\frac{1}{|2z_h + L_z|} + \frac{1}{|2z_h - L_z|}\right. \tag{9}$$

$$+ \frac{1}{|2y_h + L_y|} + \frac{1}{|2y_h - L_y|}\},$$

and

$$U_{attr}^{(e-h)} = -\frac{e^2}{\epsilon_w}\left(\frac{\epsilon_w - \epsilon_b}{\epsilon_w + \epsilon_b}\right)\{\frac{1}{\sqrt{x^2 + y^2 + (L_z + z_e + z_h)^2}} \tag{10}$$
$$+ \frac{1}{\sqrt{x^2 + y^2 + (L_z - z_e - z_h)^2}}$$
$$+ \frac{1}{\sqrt{x^2 + (L_y + y_e + y_h)^2 + z^2}}$$
$$+ \frac{1}{\sqrt{x^2 + (L_y - y_e - y_h)^2 + z^2}}\}.$$

The exciton ground state in the system described by the Hamiltonian of Eq. (1) is found variationally by minimizing the expectation value $< \Psi|\hat{H^X}|\Psi >$ where the exciton wave function Ψ is properly normalized. We will be interested only in excitonic states that can be accessed optically. Under optical excitation, the center-of-mass motion can be neglected since the photon momentum is too small to create states of significant center-of-mass kinetic energy. Therefore, the wave function of an optically generated exciton (s symmetry only) with center-of-mass momentum $\hat{P_X} = 0$ is given by

$$\Psi \equiv \Psi(x, y_e, y_h, z_e, z_h) = g_t(x, \eta)\psi_e(y_e, z_e)\psi_h(y_h, z_h) \tag{11}$$
$$= g_t(x, \eta)\phi_e(y_e)\phi_h(y_h)\chi_e(z_e)\chi_h(z_h),$$

where g is the x-component of the exciton wave function, and ϕ and χ are respectively the y- and z-components of independently confined electron and hole making up an exciton.

The separation of the wave function into a product of g, ϕ and χ in Equation (11) is permissible only in the limit of weak Coulomb interaction between the charged particles, i.e. for materials with relatively large dielectric

constants (narrow gap semiconductors). The z-component $\chi_{e,h}(z_{e,h})$ is not affected by a magnetic field oriented along the z-direction. Therefore, it is a particle-in-a-box state:

$$\chi_{e,h}(z_{e,h}) = \sqrt{\frac{2}{L_z}} cos(\pi \frac{z_{e,h}}{L_z}). \tag{12}$$

The y-component of the electron and hole wave functions, $\phi_{e,h}(y_{e,h})$, are affected by the magnetic field and are calculated numerically. This is done by solving the one-particle Schrödinger equation using a finite difference scheme.[18]

Finally, the x-component of the wave function (i.e. the component along the free direction or wire axis) is given by a Gaussian-type "orbital" function:

$$g_\eta(x, \eta) = \frac{1}{\eta^{1/2}} (\frac{2}{\pi})^{1/4} e^{-(x/\eta)^2} \tag{13}$$

The ground state exciton binding energies E_B^X can now be found using the relation[9]

$$E_B^X = E_{conf}^{e1} + E_{conf}^{hh1} + E_{self}^{(e)} + E_{self}^{(h)} - E^{tot}. \tag{14}$$

Here $E_{conf}^{e1}, E_{conf}^{hh1}$ are the lowest electron and the highest heavy hole magneto-electric subband energies in the quantum wire measured from the bottom of the bulk conduction band and the top of the bulk valence band respectively. The total energy E^{tot} is determined by minimizing the expectation value of the total Hamiltonian by varying the parameter η, i.e.,

$$E^{tot} = min_\eta < \Psi | \hat{H^X} | \Psi >, \tag{15}$$

and the electron self-energy $E_{self}^{(e)}$ is given as

$$E_{self}^{(e)} = < \psi_e(y_e, z_e) | U_{self}^{(e)} | \psi_e(y_e, z_e) > . \tag{16}$$

The hole self-energy is obtained from the last expression by substituting the hole index "h" in place of the electron index "e."

The evaluation of self-energy integrals in Equation (16) is not straightforward because of the unphysical divergences associated with the "poles" of the self-energies in Equations (8) and (9). These divergences are a consequence of assuming that the dielectric constant changes abruptly at the wire interface (this is also equivalent to assuming that the induced surface charge has no spatial extension). In order to avoid these divergences, we adopt the approach of ref. [19] and assume that the surface charge is located symmetrically with respect to the boundary and has a spatial extension δ less than the lattice constant. The self-energy terms are then calculated as "principal values" with the replacement

$$\frac{1}{|2z_e \pm L_z|} \quad ---> \quad \frac{|2z_e \pm L_z|}{(2z_e \pm L_z)^2 + \delta^2} \tag{17}$$

Unlike the self-energy integrals, the Coulomb integrals $< \Psi|U_C|\Psi >$ and $< \Psi|U_{attr}|\Psi >$ are "proper" integrals as long as U_C and U_{attr} of Eqs. (3) and (10) are treated in their full three-dimensional form. Despite the characteristic $1/r$ singularity, these integrals do not diverge because in two or three dimensions, the surface element $2\pi r dr$ or the volume element $4\pi r^2 dr$ goes to zero as rapidly as, or more rapidly than, r. Consequently, the integrals $< \Psi|U_C|\Psi >$ and $< \Psi|U_{attr}|\Psi >$ are always finite if U_C and U_{attr} are treated in their three-dimensional form. We cannot do the same for the self-energy terms because they depend only on one coordinate - z or y - and hence the integration is effectively one-dimensional. Therefore, it becomes necessary to introduce the artificial parameter δ. Nonetheless, we always verify that the final result of any calculation does not depend sensitively on δ. Typically, several orders of magnitude variation in δ introduces only a few percent

variation in the final result.

B. Dielectrically confined magneto-biexcitons

In order to study the effect of dielectric confinement on magneto-biexcitons, we use the same quantum wire geometry as in Fig. 1(a). Our mathematical model will be based on several assumptions. First, we consider the regime of intermediate carrier densities, n, for which the Wigner-Seitz radius $\rho_s \equiv (3/4\pi n)^{1/3} >> a_B$, where a_B is again the Bohr radius of the exciton. Extremely high carrier densities (excitation levels) may lead to dissociation of all excitonic complexes and formation of the electron-hole plasma which is not within the scope of this work. Second, we neglect any polariton effects which, in fact, may be important for very narrow wires.[20,21]

For nondegenerate and isotropic bands, the Hamiltonian of a biexciton in a quantum wire subjected to a magnetic field is given in the envelope-function approximation by[22]

$$\begin{aligned} H^{\hat{X}X} &= -\frac{\hbar^2}{2\mu}\left(\frac{\partial^2}{\partial x_{1a}^2}+\frac{\partial^2}{\partial x_{2b}^2}\right)-\frac{\hbar^2}{m_h}\left(\frac{\partial^2}{\partial x_{ab}^2}-\frac{\partial^2}{\partial x_{1a}\partial x_{ab}}+\frac{\partial^2}{\partial x_{2b}\partial x_{ab}}\right) \\ &\quad -\frac{\hbar^2}{2m_e}\left(\frac{\partial^2}{\partial {y_1}^2}+\frac{\partial^2}{\partial {y_2}^2}+\frac{\partial^2}{\partial {z_1}^2}+\frac{\partial^2}{\partial {z_2}^2}\right) \\ &\quad -\frac{\hbar^2}{2m_h}\left(\frac{\partial^2}{\partial {y_a}^2}+\frac{\partial^2}{\partial {y_b}^2}+\frac{\partial^2}{\partial {z_a}^2}+\frac{\partial^2}{\partial {z_b}^2}\right) \\ &\quad +\frac{e^2B^2}{2}\left(\frac{y_1^2+y_2^2}{m_e}+\frac{y_a^2+y_b^2}{m_h}\right)+\frac{eBi\hbar}{m_e}\left(y_1\frac{\partial^2}{\partial x_{1a}}+y_2\frac{\partial^2}{\partial x_{2b}}\right) \\ &\quad +\frac{eBi\hbar}{m_h}\left(y_a\frac{\partial^2}{\partial x_{1a}}+(y_b-y_a)\frac{\partial^2}{\partial x_{ab}}+y_b\frac{\partial^2}{\partial x_{2b}}\right) \\ &\quad + V_C(x_e,x_h,y_e,y_h,z_e,z_h)+V_S(y_e,y_h,z_e,z_h)+V_D(y_e,y_h,z_e,z_h), \end{aligned} \tag{18}$$

where V_S is the spatial confinement potential along the y and z directions, V_C is the Coulomb interaction between various charged entities, and V_D is the dielectric confinement for all four particles comprising a biexciton. The electron coordinates bear numerical subscripts 1 and 2 while the hole coordinates bear alphabetical subscripts a and b. For convenience, we again

replace the coordinates in Eq. (18) by the center-of-mass (X) and relative coordinates ($x_{\alpha,\gamma)}$ using the following transformations[22,23]

$$\begin{aligned} X &= [m_e(x_1+x_2)+m_h(x_a+x_b)]/2(m_e+m_h), \qquad (19)\\ x_{1a} &= x_1-x_a \\ x_{2b} &= x_2-x_b \\ x_{ab} &= x_a-x_b, \end{aligned}$$

where $\alpha,\gamma = 1,2,a,b$, and $\alpha \neq \gamma$.

As in Eq. (2), the spatial confinement potential V_S is given by

$$\begin{aligned} V_S(y_{1,a},y_{2,b},z_{1,a},z_{2,b}) &= 0, \quad z_{1,a,2,b} < L_z \ \wedge \ y_{1,a,2,b} < L_y \qquad (20)\\ &= \infty, \quad otherwise. \end{aligned}$$

The Coulomb interaction term is given by

$$V_{Coulomb} = \frac{e^2}{4\pi\epsilon}\{\frac{(-1)}{\sqrt{x_{1a}^2+r_{1a}^2}}+\frac{(-1)}{\sqrt{x_{1b}^2+r_{1b}^2}}+\frac{(-1)}{\sqrt{x_{2b}^2+r_{2b}^2}}+$$

$$\frac{(-1)}{\sqrt{x_{2a}^2+r_{2a}^2}}+\frac{1}{\sqrt{x_{ab}^2+r_{ab}^2}}+\frac{1}{\sqrt{x_{12}^2+r_{12}^2}}\}, \qquad (21)$$

where

$$r_{\alpha\gamma}^2 = (y_\alpha-y_\gamma)^2+(z_\alpha-z_\gamma)^2,$$

$$x_{\alpha,\gamma} = x_\alpha - x_\gamma,$$

with $\alpha,\gamma = 1,2,a,b$, and $\alpha \neq \gamma$.

The dielectric confinement term V_D is analogous to Eqs. (4)-(7). The only principally different terms which appear in the biexciton problem and are not present in the exciton problem are the repulsive electron - "another electron-image" (hole - "another hole-image") interactions. These terms have the same structure as the attractive terms but bear the opposite sign. For

the sake of illustration, we have written the first-order terms explicitly in the Appendix.

The variational procedure for calculating the biexciton binding energies is the same as that reported in ref. [22, 23]. The trial wave function is chosen to be a singlet state with the electron-hole pair contributions given by the Gaussian-type "orbital" functions:

$$\Phi = \frac{1}{S}\{\psi_{1a}\psi_{2b} + \psi_{2a}\psi_{1b}\}G_{ab}(x_{ab}), \tag{22}$$

where

$$\psi_{\alpha\gamma} = g_{\alpha\gamma}\phi_{\alpha}(y_{\alpha})\chi_{\alpha}(z_{\alpha})\phi_{\gamma}(y_{\gamma})\chi_{\gamma}(z_{\gamma}), \tag{23}$$

with

$$G_{ab}(x_{ab}) = e^{-x_{ab}^2/\tau^2}, \tag{24}$$

and

$$g_{1a} = e^{-x_{1a}^2/\eta^2}, \tag{25}$$

$$g_{2b} = e^{-x_{2b}^2/\eta^2}, \tag{26}$$

$$g_{2a} = e^{-(x_{2b}-x_{ab})^2/\eta^2}, \tag{27}$$

$$g_{1b} = e^{-(x_{1a}+x_{ab})^2/\eta^2}, \tag{28}$$

The wave functions $g_{\alpha\gamma}$ are Gaussian orbitals whose "spread" η and τ are variational parameters. It is obvious that these parameters physically correspond to the electron-hole and hole-hole separations along the length of the quantum wire. The quantity S is a normalization constant and $\phi_{e,h}(y_{e,h})$

$[\chi_{e,h}(z_{e,h})]$ are y-components [z-components] of the wave functions of independently confined electrons and holes as in the previous section.

In our own previous calculation of the magneto-biexciton binding energies in ref. [22], we employed two variational parameters: η and τ. The use of only two variational parameters tacitly assumes that the electron-hole separation in a biexciton is the same as that in a free exciton. In the present work, we do away with this assumption and improve on our previous calculations by including a third variational parameter η^*, which allows the electron-hole pair within the biexciton to relax. This is done following Ref. [24]. The biexciton binding energy E_B^{XX} is found from the relation

$$E_B^{XX} = min_{\tau,\eta^*} < \Psi|H^{XX}|\Psi > -2min_{\eta} < \psi|H^{X}|\psi >, \qquad (29)$$

where $min_{\tau,\eta^*} < \Psi|H^{XX}|\Psi >$ is found by minimizing the expectation value of the Hamiltonian H^{XX} with respect to the hole-hole variational parameter τ and the electron-hole relaxation parameter η^*, while $min_{\eta} < \psi|H^{X}|\psi >$ is found as described in the previous section.

Before concluding this section, we should make a few remarks about the numerical details. As we have already mentioned in the previous section, the Coulomb terms treated in their full three-dimensional form do not cause divergence, and can be handled without introducing any ad hoc truncation procedure. However, this strategy is also CPU-costly since the number of independent coordinates (spatial dimensions) increases threefold. The calculation of the expectation value of the biexciton Hamiltonian involves evaluation of multi-dimensional integrals ($n = 9$) in real space. The evaluation is achieved by iterated applications of product Gauss formulas. The integral is first estimated by a two-point tensor product formula in each coordinate direction. Then for $i = 1, ..., n$ the routine calculates a new estimate by dou-

bling the number of points in the $i-$th direction, but halving the number immediately afterwards if the new estimate is not appreciably different.

III. RESULTS AND DISCUSSION

A. Magnetoexciton and magnetobiexciton binding energies

All the results that we present in this section are relevant to free-standing GaAs quantum wires surrounded by vacuum or air. Electron and hole effective masses are assumed to be $0.067\mathrm{m}_0$ and $0.5\mathrm{m}_0$ respectively. The relative permittivity of GaAs, ϵ_w, is taken as 12.9. The dielectric misfit between GaAs and vacuum is estimated to be $\xi = 0.856$.

The binding energies of dielectrically confined magneto-excitons are calculated from Eqs. (14) - (16). In order to give some idea about the relative scale of the terms in Eq. (14), we present in Fig. 2 the confinement energies (the magneto-electric subband bottom energies E^{el}_{conf} and E^{hh1}_{conf}) as functions of the wire width for two different values of a magnetic flux density. The fundamental band gap energy E_G in Fig. 2 is assumed to be zero for clarity. Although not shown in the figure, the values of the self-energy terms are about 20-30% higher than the corresponding confinement energies.

In Fig. 3, we present the ground state binding energy of a dielectrically confined exciton as a function of wire width L_y. For comparison, the binding energy without dielectric confinement effects is shown by the dashed line. The dash-dotted curve in Fig. 3 represents the case when only first order terms in Eq. (5)-(7) were taken into account. As one can see the discrepancy between this curve and the solid curve which is obtained using higher order terms (up to 4th) is quite pronounced. This difference is always appreciable

for material systems with large values of dielectric misfit $\xi > 0.5$. When the dielectric misfit is not large (e.g. the GaAs/AlGaAs system rather than the GaAs/vacuum system), just the first order correction may be enough. The binding energy always decreases with increasing wire width for all cases as expected because of decreasing spatial (electrostatic) confinement. For a 200 Å thick wire, the exciton ground state binding energy is enhanced by approximately 2.7 times because of dielectric confinement. Note that the binding energy is larger than the room-temperature thermal energy (kT = 26 meV) for wire widths less than 300 Å.

The exciton radius (or more correctly the longitudinal length) along the x direction is given analytically as $\rho \equiv \sqrt{< x^2 >} = \eta/2^{1/4}$ for the chosen trial wave function in Equation (11). This radius is shown in Fig. 4 as a function of the wire width with and without dielectric confinement taken into account. It is interesting to note that the ratio $(\beta \equiv \rho - \rho_D)/\rho$ shows very weak dependence on the wire width L_y. Here ρ_D is the the exciton radius in a system with dielectric confinement and ρ is the same without dielectric confinement.

In Fig. 5 we present the dependence of the exciton radius on magnetic flux density for two cases: (i) with dielectric confinement, and (ii) without dielectric confinement. The important thing to note is that the difference between the two curves decreases with increasing magnetic flux density. The exciton radii ratio β depends quite strongly on magnetic field. For the wire with dimensions $L_y \times L_z = 500\mathring{A} \times 200\mathring{A}$, the ratio can be approximated as $\beta = 0.128 - 0.0062B$, where B is in tesla. This monotonically decreasing dependence of β on B can be easily explained. A magnetic field squeezes the exciton wave function along all directions,[3,23] pushing the electron and

the hole closer together. As a result, the exciton increasingly approximates a truly electrically neutral uncharged single particle rather than a bound electron-hole pair. Since a chargeless particle has no image charge, the dielectric confinement effect falls off rapidly.

The strong dependence of β on magnetic field has a very important implication. It appears that because of this feature, a magnetic field can be used to separate the effects of spatial confinement and dielectric confinement on the exciton radius. This could not be done by varying the wire width or spatial confinement (e.g. in split-gate quantum wires) since evidently β does not depend sufficiently strongly on L_y (recall Fig. 4).

Fig. 6 shows the corresponding dependence of the exciton binding energy on the magnetic flux density for the same wire dimensions as in Fig. 5. As one can see, the difference between binding energies with and without dielectric confinement, ΔE_B^X, does not depend on the magnetic field as strongly as the difference between the radii. The magnitude of the dielectric enhancement of the binding energy is in a good qualitative agreement with experimental results published for quantum wells[8,15]. Unfortunately, no data are available yet for quantum wires so that a quantitative comparison is not possible.

The increase in the binding energy and the decrease in the radius as a result of dielectric confinement can be simply ascribed to a lowering of the effective dielectric constant (and hence the screening) in the entire system due to the image charges. A magnetic field reduces the image-charge effect because it squeezes the electron and hole togther thereby tending to condense them into an uncharged single particle. Cosnequently, a magnetic field quenches the dielectric confinement.

In Fig. 7 we present the dependence of the exciton radius on dielectric

misfit with and without the magnetic field present. As one should expect, the radius decreases with increasing misfit for both cases provided that the dielectric constant of the surrounding material is lower than that of the wire. This is simply a validation of the fact that a higher dielectric misfit results in a higher dielectric confinement. Furthermore, the exciton radius is more sensitive to dielectric confinement if there is no magnetic field. The physics of it is intuitively obvious: the wave function of the exciton in a quantum wire subjected to the field (10 tesla) is already compressed due to strong magnetostatic confinement and does not "feel" the additional dielectric confinement as much.

The corresponding dependence of the exciton binding energy on the dielectric misfit is shown in Fig. 8. It is interesting to note that the dependence is almost exactly *linear*: for the magnetic flux density of 10 tesla it can be approximated by the interpolation formula $E_B^X \approx 9.240 + 16.376\,\xi + 0.089\,\xi^2$ where the pre-factor of the quadratic term is more than two-orders of magnitude smaller than that of the linear term.

In Fig. 9 (a) we present the magneto-biexciton binding energy as a function of the magnetic field for two cases: with dielectric confinement and without it. As we can see, the overall behavior of the binding energy is similar to that in the case of magneto-excitons, although the dielectric confinement effect is not so pronounced. The weaker effect is probably caused by the fact that there are like-charged entities (two holes and two electrons) in a biexciton that repel. As a result, the dielectric confinement effect is not so strong. Fig. 9 (b) shows the biexciton binding energy as a function of the wire width. It is interesting to note that in the presence of dielectric confinemen ("+"marked curve) the binding energy exceeds the room-temperature

thermal energy of 26 meV for wire width less than 100 $\AA$. Application of an external magnetic field allows to exceed room-temperature thermal energy for even wider wires.

III. DIELECTRIC ENHANCEMENT OF OSCILLATOR STRENGTH

In this section, we examine the effect of dielectric confinement on oscillator strength. In order to calculate the oscillator strength of the exciton transition, we need to evaluate the momentum matrix element which is given by[25]

$$|M_{cv}^{X}|^2 = |\frac{1}{2\pi}\int d\vec{k_{||}} g_t(x,\eta) M_{cv}(\vec{k_{||}})|^2, \tag{30}$$

where M_{cv} is the valence-band to conduction-band dipole matrix element and $\vec{k_{||}} = k_x\hat{x}$ is the wave vector along the unconfined direction of the wire. When the $\vec{k_{||}}$ dependence of M_{cv} is neglected, Eq. (30) reduces to the simple expression

$$|M_{cv}^{X}|^2 = |M_{cv}|^2 |g_t(x=0,\eta)|^2. \tag{31}$$

The exciton oscillator strength per unit length can be written as follows

$$f_{1s} = \frac{2}{m_o \hbar\omega_{go}} |M_{cv}^{X}|^2. \tag{32}$$

Here $\hbar\omega_{go}$ is the exciton ground state energy and m_o is the free electron mass. The oscillator strength of the excitonic transition is proportional to the square of the valence-band to conduction-band momentum matrix element M_{cv}, and to the probability of finding the electron and hole in the same unit cell,[26] i.e., the square of the exciton relative-motion orbital wave function $g_t(x=0,\eta)$.

In Fig. 10 we present the oscillator strength of the exciton transition per unit length of the wire as a function of the wire width for two cases: (i) with

dielectric confinement; (ii) without dielectric confinement . As one can see, the dielectric constant discontinuity (dielectric confinement effect) causes a 20 % increase in the oscillator strength for the entire range of the wire dimensions. The overall behavior of the oscillator strength curve is in an excellent agreement with the data presented in Ref. [25] for the parabolic model approximation. The absolute value of the oscillator strength was calculated using the following material parameters: the fundamental band gap $E_G = 1.519$ eV, the Kane matrix element $E_p = 23$ eV (related to momentum matrix element), and the density of carriers per unit area $n_s = 7.89 \times 10^{14}\ /cm^2$. For the 200 Å wire, the oscillator strength is about 0.85/nm without dielectric confinement which is close to the value of 0.38/nm found in ref. [25] for the same wire dimensions. The slight difference is due to different values of effective masses assumed in ref. [25].

Fig. 11 shows the oscillator strength as a function of a magnetic flux density. The magnetic field induced quenching of the dielectric confinement effect is more pronounced in this figure than in the plot for the exciton binding energy. Since

$$f_{1s} \propto \int \alpha(\hbar\omega) d\omega, \tag{33}$$

it appears that the integrated absorption, a quantity easily measured experimentally, is quite sensitive to magnetic field.

The matrix element M_{cv}^{XX} for the exciton-biexciton transition is given by the overlap integral between the exciton and biexciton wave functions[27] which is in our notation

$$M_{cv}^{XX} = M_{cv} \int_{-\infty}^{+\infty} d\vec{x} \int_{\Sigma} d\vec{y} d\vec{z} \Psi \Phi, \tag{34}$$

where Ψ is the exciton wave function given by Eq. (11), Φ is the biexciton wave function given by Eq. (22), $d\vec{x} \equiv dx_{ab} dx_{2b}$, $d\vec{y} \equiv dy_a dy_b dy_1 dy_2$, $d\vec{z} \equiv$

$dz_a dz_b dz_1 dz_2$, and Σ is a square region defined by wire lateral dimensions. In order to capture only the internal motion of the biexciton, the following conditions are imposed over the coordinates while performing the integration: $x_{1a} = x_1 - x_a = 0,\ y_1 - y_a = 0,\ z1 - z_a = 0$. This condition keeps first hole (subscript "a") and first electron (subscript "1") at the same place while allowing the other electron and hole to move (here the adjective "first" should be interpreted loosely since of course both electrons and holes are indistinguishable particles).

We have evaluated the integral in Eq. (34) numerically. Our results showed that the exciton-biexciton matrix element (or the corresponding oscillator strength) increases only slightly with introduction of dielectric confinement. In order to obtain some intuition into the origin of this weak dependence, we reproduce here the analytical result for this quantity obtained for analogous but simpler trial wave functions. In Ref. [27] the exciton-biexciton wave function overlap was evaluated analytically for simple "Gaussian-type" orbital trial functions, and the exciton - biexciton transition matrix element was found to be (in our notation)

$$|M_{cv}^{XX}|^2 = |M_{cv}|^2 [2\frac{\tau}{a_B}\sqrt{\pi}]^D |g_t(0,\eta)|^2 a_B^D, \tag{35}$$

where τ is the inter-hole distance in the biexciton and D denotes the dimensionality of the system. For quasi one-dimensional structures ($D = 1$) and with no magnetic field present, the oscillator strength is proportional to τ and inversely proportional to the exciton radius η (since g_t is proportional to $1/\sqrt{\eta}$). Because both these quantities are about *equally* affected by the dielectric confinement, they cancel each other's effect so that the overall oscillator strength is relatively insensitive to dielectric confinement.

Finally, in Fig. 12 we present the exciton-biexciton transition oscillator

strength as a function of the magnetic flux density for two wire widths. The sublinear behavior of the oscillator strengths at high values of the magnetic flux density is due to strong compression of the biexciton wave function for $B > 8$ tesla.

IV. CONCLUSION

In conclusion, we have theoretically studied the effects of dielectric confinement on the binding energies, radii and oscillator strengths of magnetoexcitons and biexcitons. Dielectric confinement increases the binding energy and oscillator strength while decreasing the radius. A magnetic field tends to reduce the effect of dielectric confinement by squeezing the charged entities (electrons and holes) together into an effective chargeless single particle. Although a magnetic field reduces the dielectric enhancement of the binding energy, it also introduces additional contribution to the binding energy because it squeezes the electrons and holes together. As a result, the net binding energy increases monotonically with magnetic field. The resultant effect of quantum confinement, dielectric confinement and magnetostatic confinement may make both the exciton and biexciton binding energies exceed the room temperature thermal energy in quantum wires of reasonable dimension which has important ramifications for the experimental observation of these entities in room temperature experiments.

ACKNOWLEDGEMENTS

This work was supported by the US Army Research Office under grants DAAH04-95-1-0586 and DAAH04-95-1-0527. One of the authors, A.B., is indebted to Dr. S. Tikhodeev and Dr. E. Zhukov for insightful discussions.

V. APPENDIX

The electron - image-hole (hole - image-electron) attractive terms for the first electron ("1") and the first hole ("a") composing the biexciton are analogous to Eq. (10) and can be written as follows

$$\begin{aligned} U_{attr}^{(1-a)} &= -\frac{e^2}{\epsilon_w}\left(\frac{\epsilon_w-\epsilon_b}{\epsilon_w+\epsilon_b}\right)\Big\{\frac{1}{\sqrt{x_{1a}^2+y_{1a}^2+(L_z+z_1+z_a)^2}} \\ &+ \frac{1}{\sqrt{x_{1a}^2+y_{1a}^2+(L_z-z_1-z_a)^2}} \\ &+ \frac{1}{\sqrt{x_{1a}^2+(L_y+y_1+y_a)^2+z_{1a}^2}} \\ &+ \frac{1}{\sqrt{x_{1a}^2+(L_y-y_1-y_a)^2+z_{1a}^2}}\Big\}. \end{aligned} \tag{36}$$

Here and throughout the Appendix we have used the same notation for the coordinates as in the text. The remaining attraction terms $U_{attr}^{(2-b)}$, $U_{attr}^{(2-a)}$, and $U_{attr}^{(1-b)}$ can be obtained by formal substitution of appropriate indices in Eq. (36).

The self-energy terms are analogous to Eqs. (8), (9) and for the first hole are given by

$$\begin{aligned} U_{self}^{(a)} &= +\frac{1}{2}\frac{e^2}{\epsilon_w}\left(\frac{\epsilon_w-\epsilon_b}{\epsilon_w+\epsilon_b}\right)\Big\{\frac{1}{|2z_a-L_z|}+\frac{1}{|2z_a+L_z|} \\ &+ \frac{1}{|2y_a-L_y|}+\frac{1}{|2y_a+L_y|}. \end{aligned} \tag{37}$$

The rest of the self-energy terms, $U_{self}^{(1)}$, $U_{self}^{(2)}$, and $U_{self}^{(b)}$ can be obtained by formal substitution of appropriate indices in Eq. (37).

The only new terms which appear in the biexciton problem, but do not appear in the exciton problem, are the repulsive terms between electron - "another electron image" (hole - "another hole image"). These terms have the same structure as the attractive terms but with the opposite sign. The

repulsive term for the electrons can be written as

$$
\begin{aligned}
U_{repuls}^{(1-2)} &= +\frac{e^2}{\epsilon_w}\left(\frac{\epsilon_w-\epsilon_b}{\epsilon_w+\epsilon_b}\right)\Big\{\frac{1}{\sqrt{x_{1a}^2+y_{1a}^2+(L_z+z_1+z_a)^2}} \\
&+ \frac{1}{\sqrt{x_{12}^2+y_{12}^2+(L_z-z_1-z_2)^2}} \\
&+ \frac{1}{\sqrt{x_{12}^2+(L_y+y_1+y_2)^2+z_{12}^2}} \\
&+ \frac{1}{\sqrt{x_{12}^2+(L_y-y_1-y_2)^2+z_{12}^2}}\Big\}.
\end{aligned}
\tag{38}
$$

Again, the rest of the repulsive terms $U_{repuls}^{(a-b)}$ can be obtained by formal substitution of appropriate indices in Eq. (38).

The group of attractive terms contains 16×2 separate interactions, the group of self-energy terms has 16 interactions and the group of the repulsive terms has 8×2 separate interaction. Combining these terms together, we have 64 terms accounting for the Coulomb interaction between all charged entities composing the biexciton and their images in the four plane boundaries of the wire.

REFERENCES

[1]. T. Someya, H. Akiyama, H. Sakakai, *Phys. Rev. Lett.*, **74**, 3664 (1995); R. Rinaldi, R. Cingolani, M. Lepore, M. Ferrara, I. M. Catalano, F. Rossi, L. Rota, E. Molinari, P. Lugli, U. Marti, D. Martin, F. Morier-Gemoud, P. Ruterana, and F. K. Reinhart, *Phys. Rev. Lett.*, **73**, 2899 (1994).

[2]. F. L. Madarasz, F. Szmulowicz, F. K. Hopkins, and D. L. Dorsey, *Phys. Rev. B*, **49**, 13528 (1994); F. L. Madarasz, F. Szmulowicz, F. K. Hopkins, and D. L. Dorsey, *ibid.*, **52**, 8964 (1995); F. L. Madarasz, F. Szmulowicz, F. K. Hopkins, and D. L. Dorsey, *J. Appl. Phys.*, **75**, 639 (1994).

[3]. A. Balandin and S. Bandyopadhyay, *Phys. Rev. B*, **52**, 8312 (1995); A. Balandin and S. Bandyopadhyay, *Superlatt. and Microst.*, Vol. 19, No. 2, 97 (1996).

[4]. H. Gotoh, H. Ando, H. Kanbe, *Appl. Phys. Lett.*, **68**, 2132 (1996).

[5]. A. D'Andrea, L. Pilozzi, *Journal de Physique IV*, Vol. 3 , 385 (1993).

[6]. L.V. Keldysh., *JETP Lett.*, **29**, 658 (1965).

[7]. N.S. Rytova, *Dokl. Akad. Nauk.*, **163**, 118 (1965, in Russian).

[8]. L.V. Kulik, V.D. Kulakovskii, M. Bayer, A. Forchel, N.A. Gippius, S.G. Tikhodeev, *Phys. Rev. B.*, **54**, R2335 (1996).

[9]. M. Kumagai, T. Takagahara, *Phys. Rev. B.*, **40**, 12359 (1989).

[10]. T. Takagahara, *Phys. Rev. B.*, **47**, 4569 (1993).

[11]. E.A. Muljarov, S.G. Tikhodeev, reprints of the *Rossiiskaya Akademia Nauk: Institut Obschei Fiziki*, Moscow, 1995 (in Russian); also see E.A. Muljarov, N.A. Gippius, A.V. Kvit, G.Ya. Zueva, G.N. Mikhailova, A.M.

Prokhorov, S.G. Tikhodeev, "Nanostructures: Phys. and Tech.," Int. Symp. Abs., St. Petersburg, Russia, 1994, p. 127.

[12]. E.A. Andryushin, A.P. Silin, *Sov. Phys. Solid State*, **30**, 1871 (1988); E.A. Andryushin, A.P. Silin, *Sov. Phys. Solid State*, **35**, 971 (1993).

[13]. T. Ishihara, *Phys. Status. Solidi.*, **159**, 371 (1990).

[14]. A. Balandin and S. Bandyopadhyay, *Phys. Rev. B*, **54**, 5721 (1996); A. Balandin and S. Bandyopadhyay, *Superlatt. and Microst.*, Vol. 20, (in press, 1996); A. Balandin, S. Bandyopadhyay, A. Svizhenko, "Nanostructures: Phys. and Tech.," Int. Symp. Abs., St. Petersburg, Russia, 1996, pp. 294-297.

[15]. A.L. Yablonskii, A.B. Dzyubenko, S.G. Tikhodeev, L.V. Kulik, V.D. Kulakovskii, *JETP Lett.*, **64**, No. 1, 51 (1996).

[16]. E.A. Muljarov, S.G. Tikhodeev, N.A. Gippius, *Phys. Rev. B.*, **51**, 14370 (1995).

[17]. See for example D.V. Sivukhin, *General Physics: Electrisity*, (Nauka, Moscow, 1983), pp. 90-101 (in Russian); also for the case of spherical geometry see A. Balandin, M.S. thesis, Moscow Institute of Physics and Technology, Dolgoprudny, 1991.

[18]. S. Chaudhuri and S. Bandyopadhyay, *J. Appl. Phys.*, **71**, 3027 (1992).

[19]. Tran Thoai, D.B., Zimmermann, R., Grundmann, M., Bimberg, D., *Phys. Rev. B.*, **42**, 5906 (1990).

[20]. A. L. Ivanov and H. Haug *Phys. Status. Solidi. (b)*, **188**, 61 (1995).

[21]. Actually, in a pump-probe experimental setup, the polariton effects are important only for long enough excitation pulses whose temporal width is

greater than the inverse polariton gap frequency Ω. In our case, we can assume that the optical excitation pulse is relatively short, $\tau < 1/\Omega$; E.S. Koteles, in *Excitons*, edited by E.I. Rashba and M.D. Struge, Modern Problems in Condenced Matter Sciences (North-Holland, Amsterdam, 1982), p.83.

[22]. A. Balandin and S. Bandyopadhyay, *Phys. Rev. B*, **54**, 5712 (1996);

[23]. A. Balandin and S. Bandyopadhyay, in *Quantum Confinement: Physics and Applications* (Electrochemical Society, Inc., Pennington, New Jersey, 1996), edited by M. Cahay *et al.,* pp. 117-128; A. Balandin, PhD. dissertation, University of Notre Dame, 1996.

[24]. R. O. Klepfer, F. L. Madarasz and F. Szmulowicz, *Phys. Rev. B.*, **51**, 4633 (1995).

[25]. I. Suemune, L.A. Coldren, *IEEE J. Quantum Electron.*, Vol. 24, No. 8, 1778 (1988).

[26]. S. Schnitt-Rink, D.S. Chemla, D.A.B. Miller, *Phys. Rev. B.*, **32**, 6601 (1985).

[27]. L. Banyai, I. Galbraith, H. Haug, *Phys. Rev. B.*, **38**, 3931 (1988).

FIGURE CAPTIONS

[1]. (a) The geometry of the wire. (b) Schematic structure of the wire along y direction and illustration of the image-charge method. The original charge is indicated by a double circle and the induced image charges are given by single circles.

[2]. The magneto-electric subband bottom energies E_{conf}^{el} and E_{conf}^{hh1} as functions of the wire width for two different values of a magnetic flux density. The wire thickness is 200 Å. The two upper curves correspond to the electrons and the two lower to the holes. The curves delineated by "o" are plotted for zero magnetic flux density and those delineated by "+" are plotted for a 10 tesla magnetic field. The fundamental band gap energy E_G is assumed to be zero for clarity.

[3]. Exciton binding energy in a GaAs quantum wire as a function of the wire width L_y for three different cases: (i) without dielectric confinement (dashed line); (ii) with only first order correction due to the dielectric confinement (dash-dotted line); and (iii) with complete dielectric confinement (solid line). In the last case, up to fourth order correction was sufficient for convergence. The thickness of the wire along the z-direction is 200$\mathring{A}$.

[4]. Exciton longitudinal radii versus wire width with and without dielectric confinement. When there is no magnetic field present, the exciton radius increases monotonically with increasing wire width. The thickness along the z-direction is 200$\mathring{A}$.

[5]. Exciton longitudinal radii as a function of a magnetic flux density with ("+") and without ("o") dielectric confinement. The thickness along the z-direction is 200$\mathring{A}$.

[6]. Exciton binding energy versus magnetic field. All parameters are the same as in Fig. 5. The inset shows exciton binding energy as a function of the dielectric misfit.

[7]. Exciton radius as a function of the dielectric misfit for two values of the magnetic field: (i) B=0 tesla ("o") and (ii) B=10 tesla ("+"). The thickness along the z-direction is $200\mathring{A}$ and the width is $500\mathring{A}$.

[8]. Exciton binding energy as a function of the dielectric misfit for two values of the magnetic field: (i) B=0 tesla ("o"); (ii) B=10 tesla ("+"). The thickness along the z-direction is $200\mathring{A}$ while the width is $500\mathring{A}$.

[9]. (a) Biexciton binding energy in a GaAs quantum wire as a function of magnetic flux density. (b) Biexciton binding energy in a GaAs quantum wire as a function of wire width. No magnetic field is present. The thickness along the z-direction is $200\mathring{A}$ and the width is $500\mathring{A}$ for both cases.

[10. Exciton oscillator strength as a function of wire width with ("+") and without ("o") dielectric confinement. The thickness along the z-direction is $200\mathring{A}$.

[11]. Exciton oscillator strength as a function of a magnetic flux density with ("+") and without ("o") dielectric confinement. The thickness along the z-direction is $200\mathring{A}$ and the width is $500\mathring{A}$.

[12]. The exciton-biexciton transition oscillator strength as a function of a magnetic flux density. For the curve delineated by "o" the thickness along the z-direction is $200\mathring{A}$ and the width is $500\mathring{A}$. For the curve delineated by "+" the thickness along the z-direction is $200\mathring{A}$ and the width is $700\mathring{A}$.

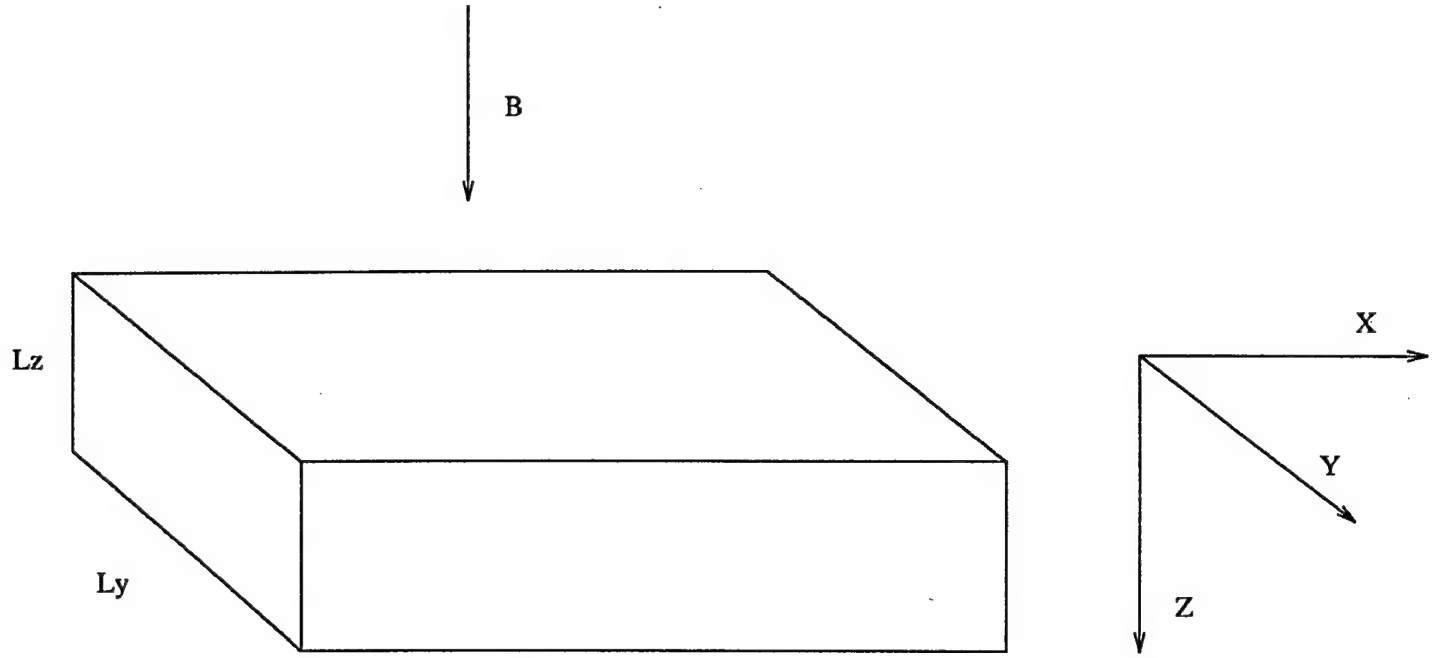

Fig. 1(a)

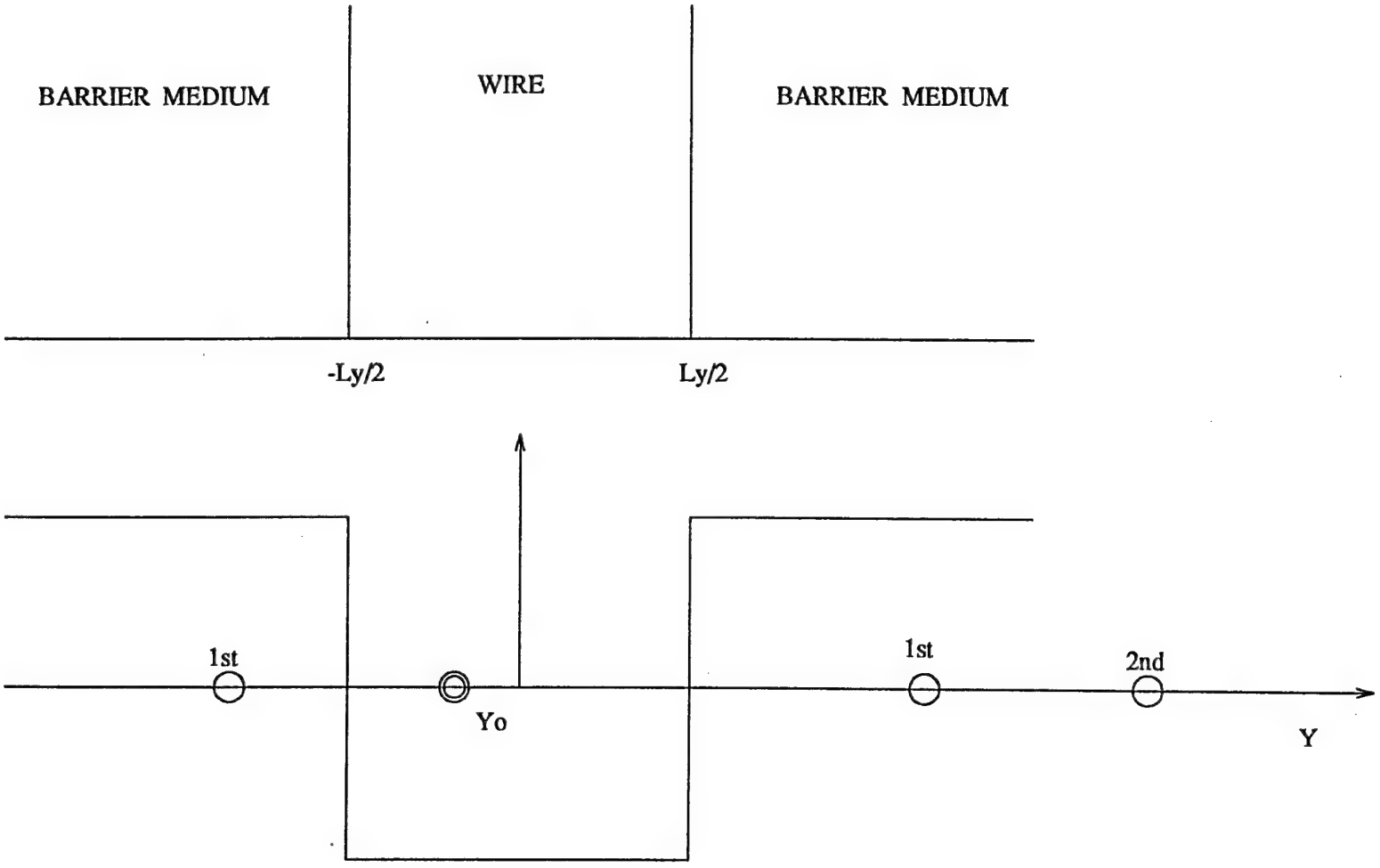

Fig. 1(b)

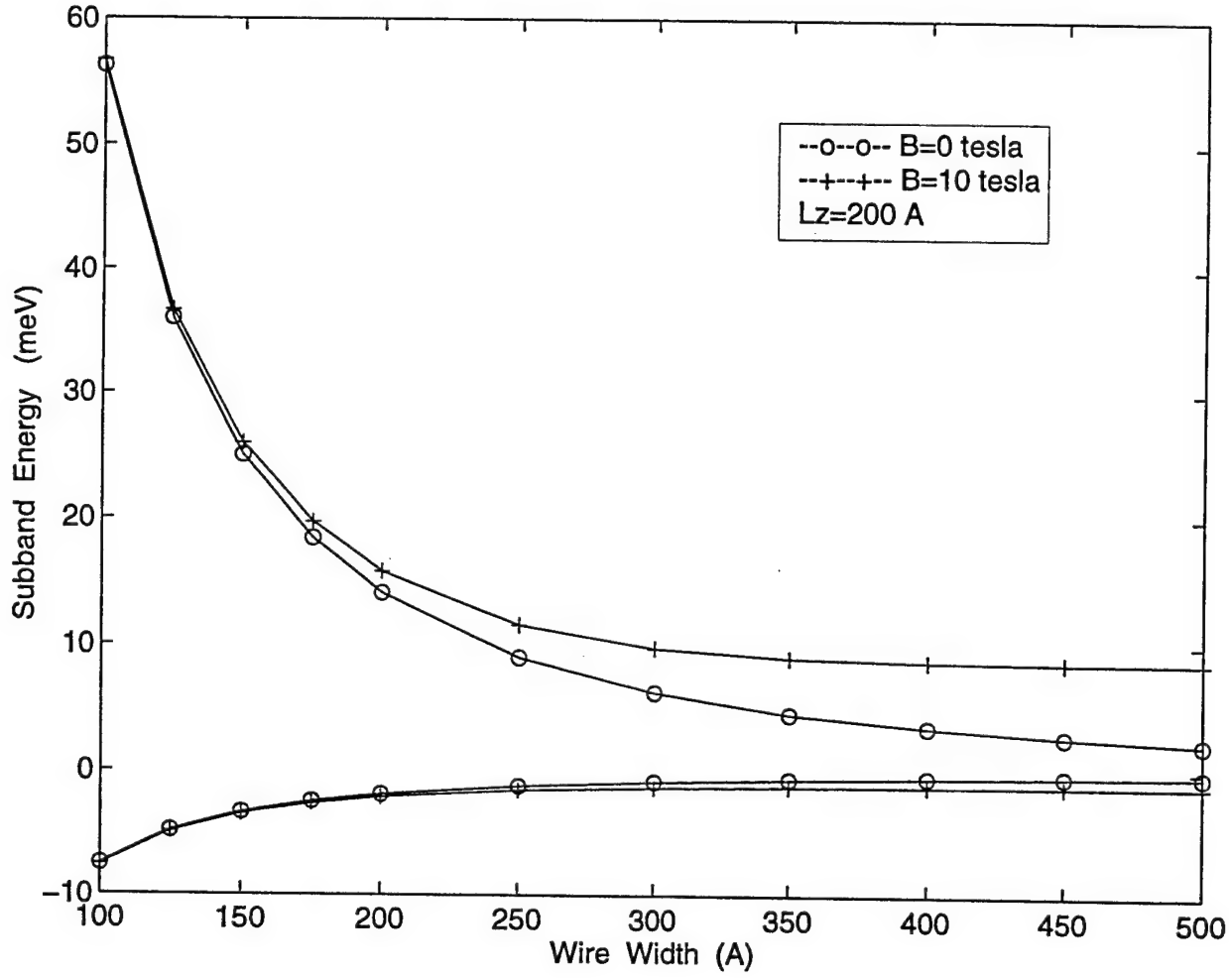
--o--o-- B=0 tesla
--+--+-- B=10 tesla
Lz=200 A
Subband Energy (meV)
Wire Width (A)
60
50
40
30
20
10
0
−10
100
150
200
250
300
350
400
450
500

Fig. 2

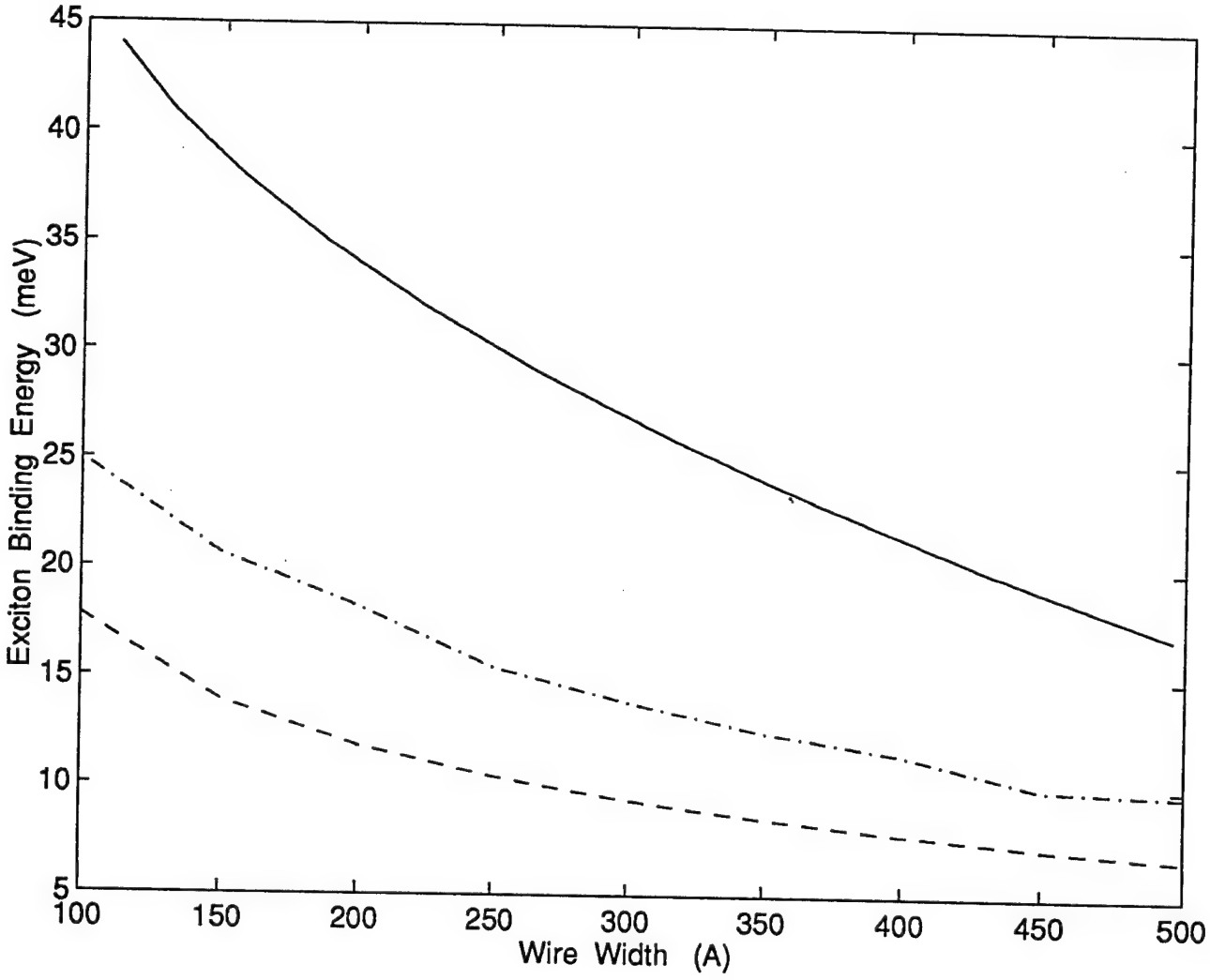
45
40
35
30
25
20
15
10
5
Exciton Binding Energy (meV)
100
150
200
250
300
350
400
450
500
Wire Width (A)

Fig. 3

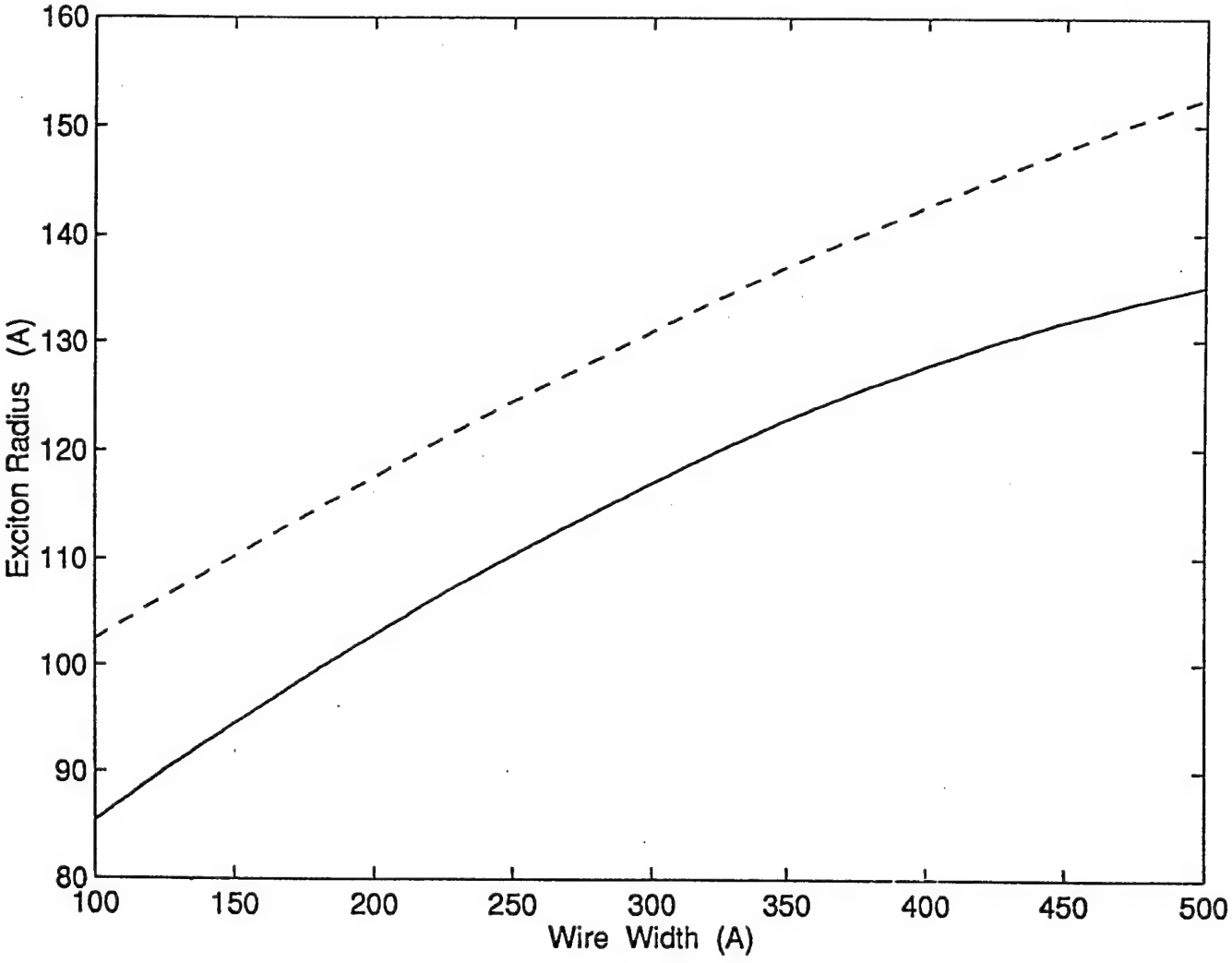
160
150
140
130
120
110
100
90
80
Exciton Radius (A)
100
150
200
250
300
350
400
450
500
Wire Width (A)

Fig. 4

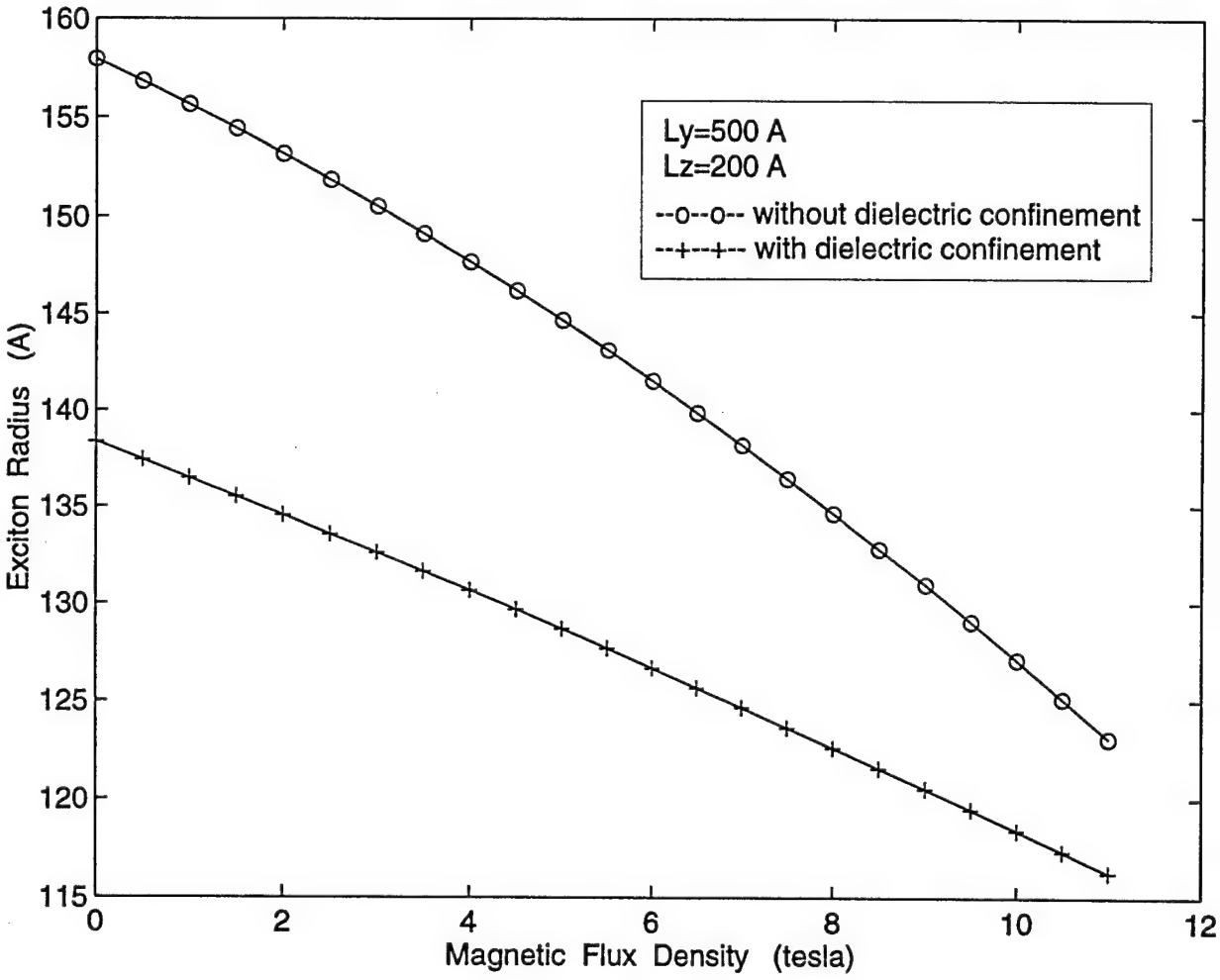
Ly=500 A
Lz=200 A
--o--o-- without dielectric confinement
--+--+-- with dielectric confinement
Exciton Radius (A)
Magnetic Flux Density (tesla)
160
155
150
145
140
135
130
125
120
115
0
2
4
6
8
10
12

Fig. 5

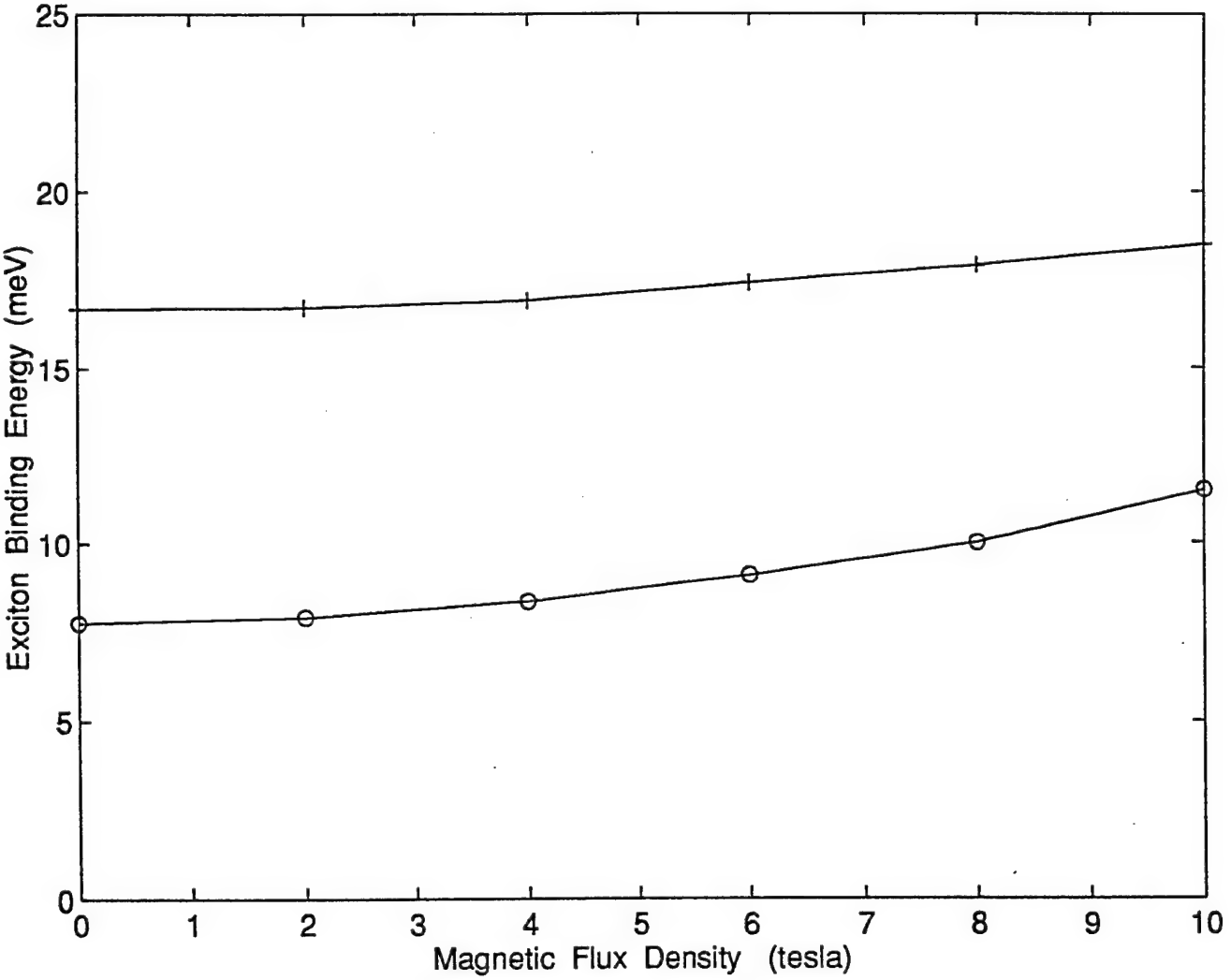
25
20
15
10
5
0
Exciton Binding Energy (meV)
0
1
2
3
4
5
6
7
8
9
10
Magnetic Flux Density (tesla)

Fig. 6

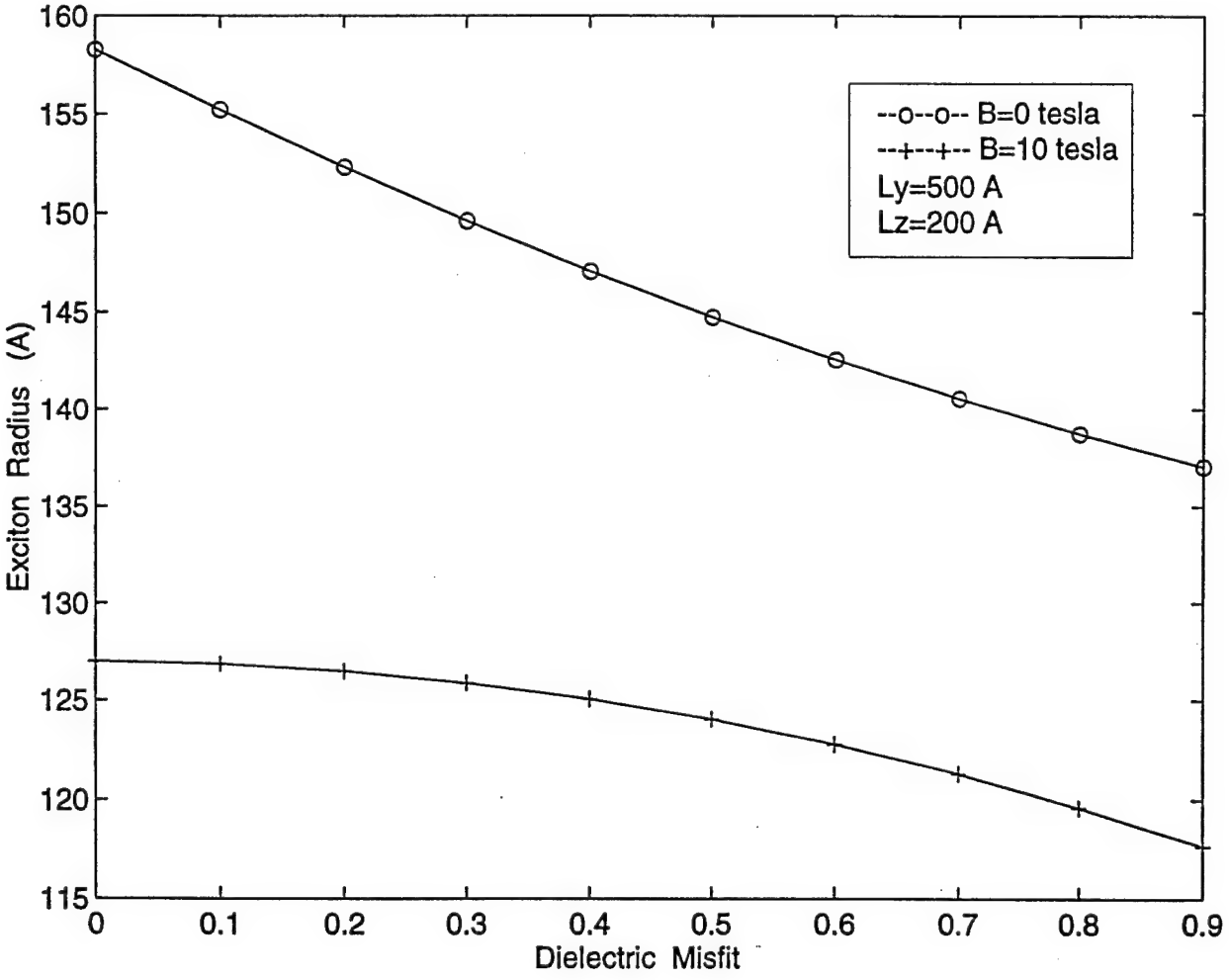
160
155
150
145
140
135
130
125
120
115
Exciton Radius (A)
0
0.1
0.2
0.3
0.4
0.5
0.6
0.7
0.8
0.9
Dielectric Misfit
--o--o-- B=0 tesla
--+--+-- B=10 tesla
Ly=500 A
Lz=200 A

Fig. 7

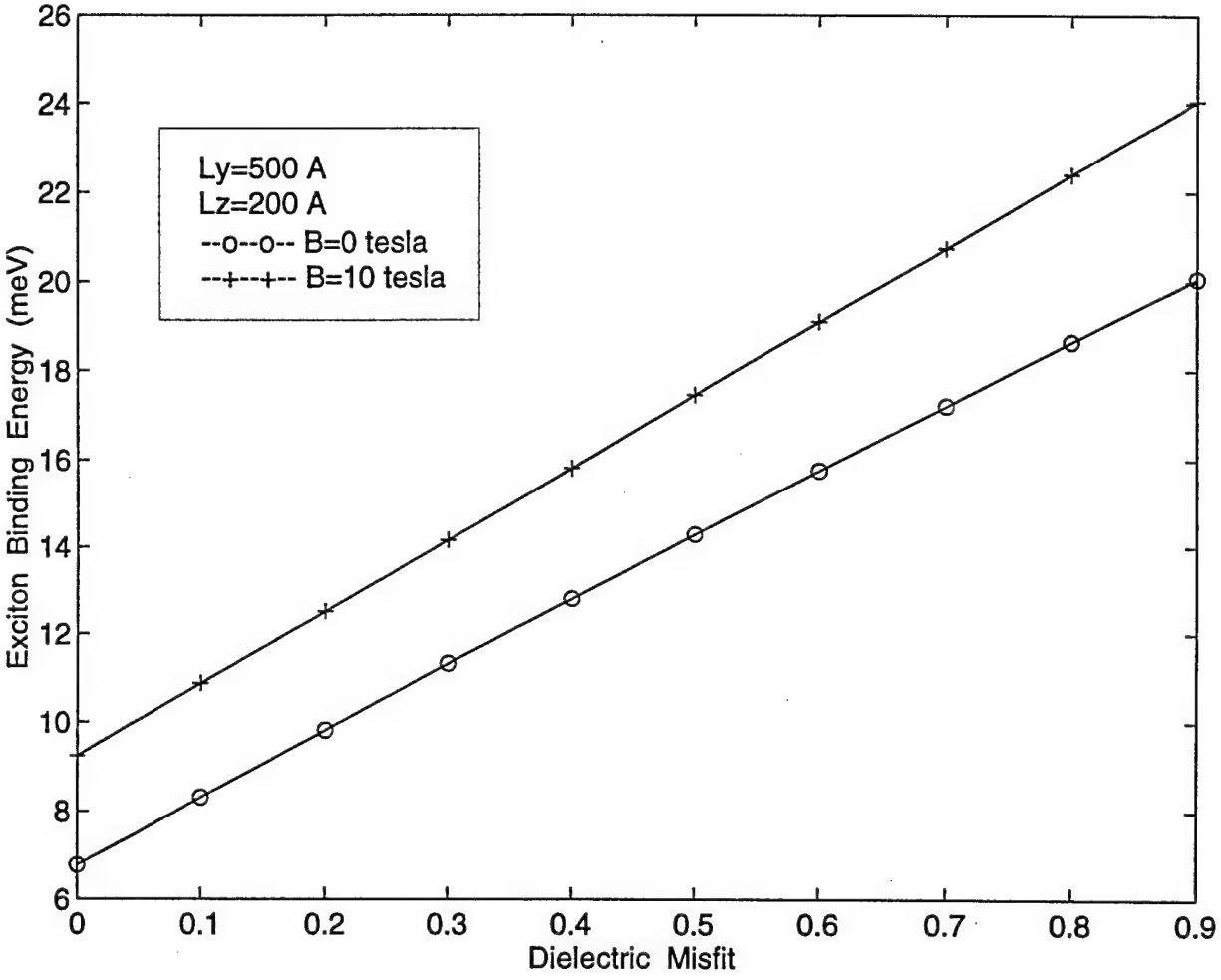
Ly=500 A
Lz=200 A
--o--o-- B=0 tesla
--+--+-- B=10 tesla
Exciton Binding Energy (meV)
Dielectric Misfit
26
24
22
20
18
16
14
12
10
8
6
0
0.1
0.2
0.3
0.4
0.5
0.6
0.7
0.8
0.9

Fig. 8

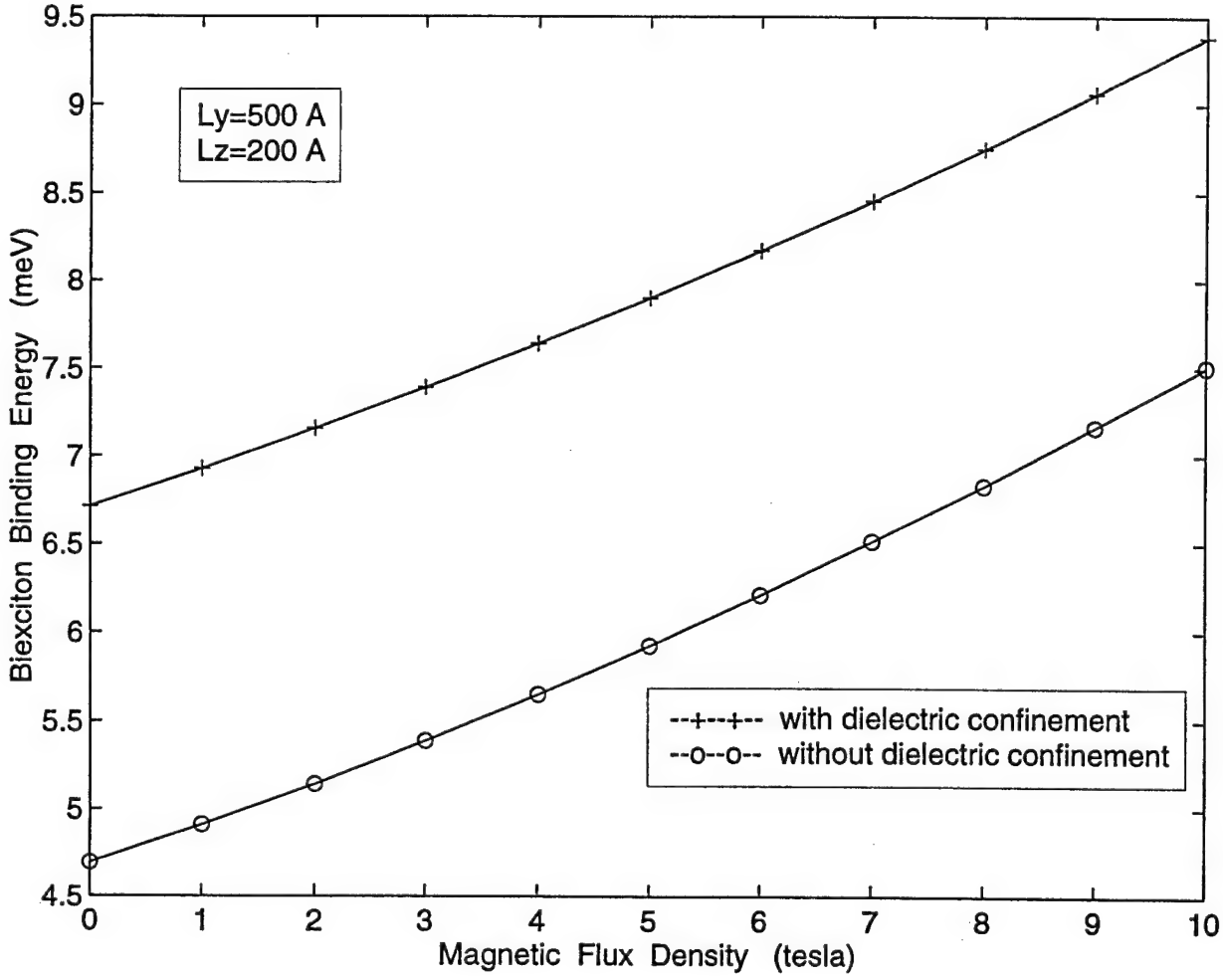
Ly=500 A
Lz=200 A
--+--+-- with dielectric confinement
--o--o-- without dielectric confinement
Biexciton Binding Energy (meV)
Magnetic Flux Density (tesla)
9.5
9
8.5
8
7.5
7
6.5
6
5.5
5
4.5
0
1
2
3
4
5
6
7
8
9
10

Fig. 9(a)

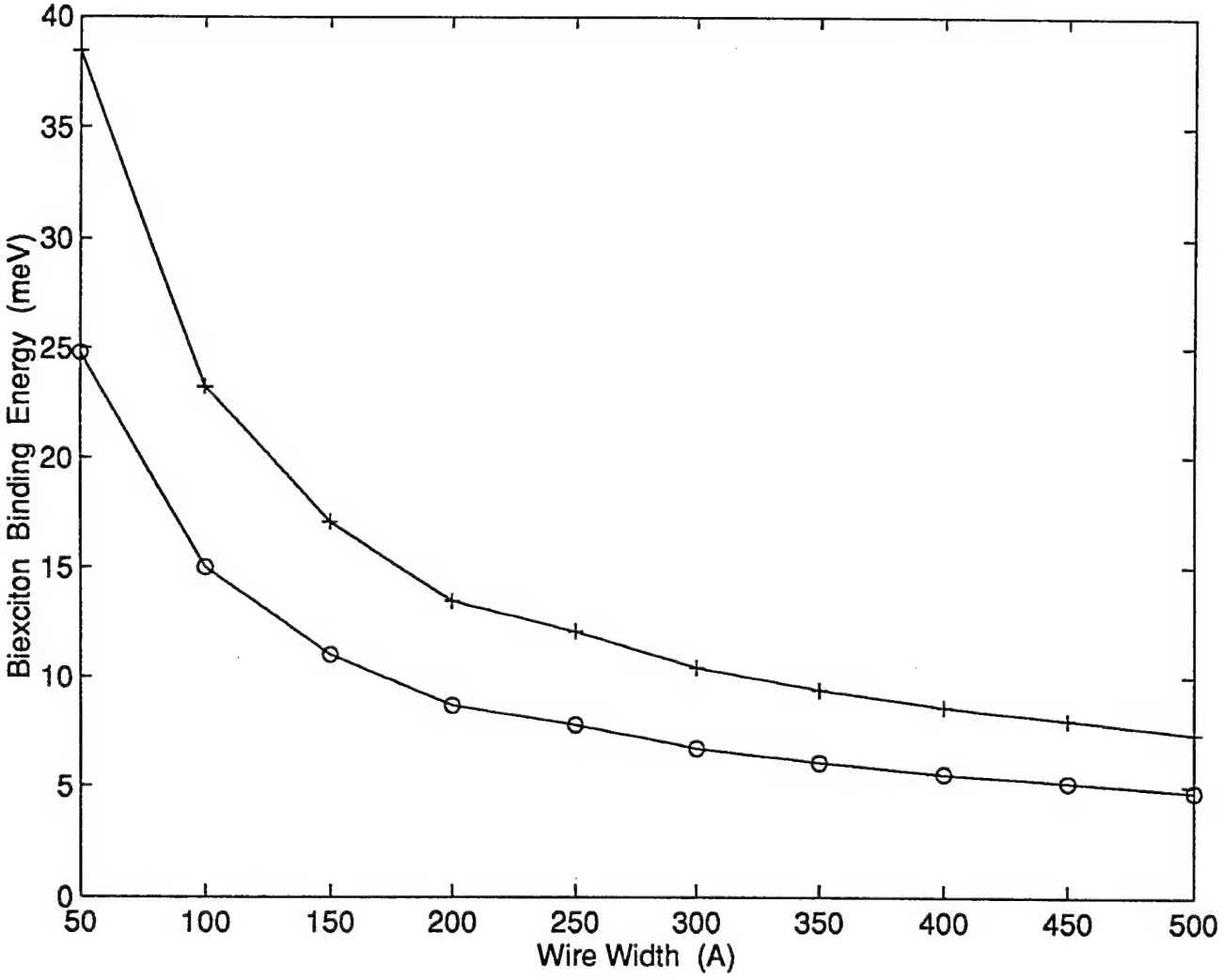
Biexciton Binding Energy (meV)
Wire Width (A)
0
5
10
15
20
25
30
35
40
50
100
150
200
250
300
350
400
450
500

Fig. 9(b)

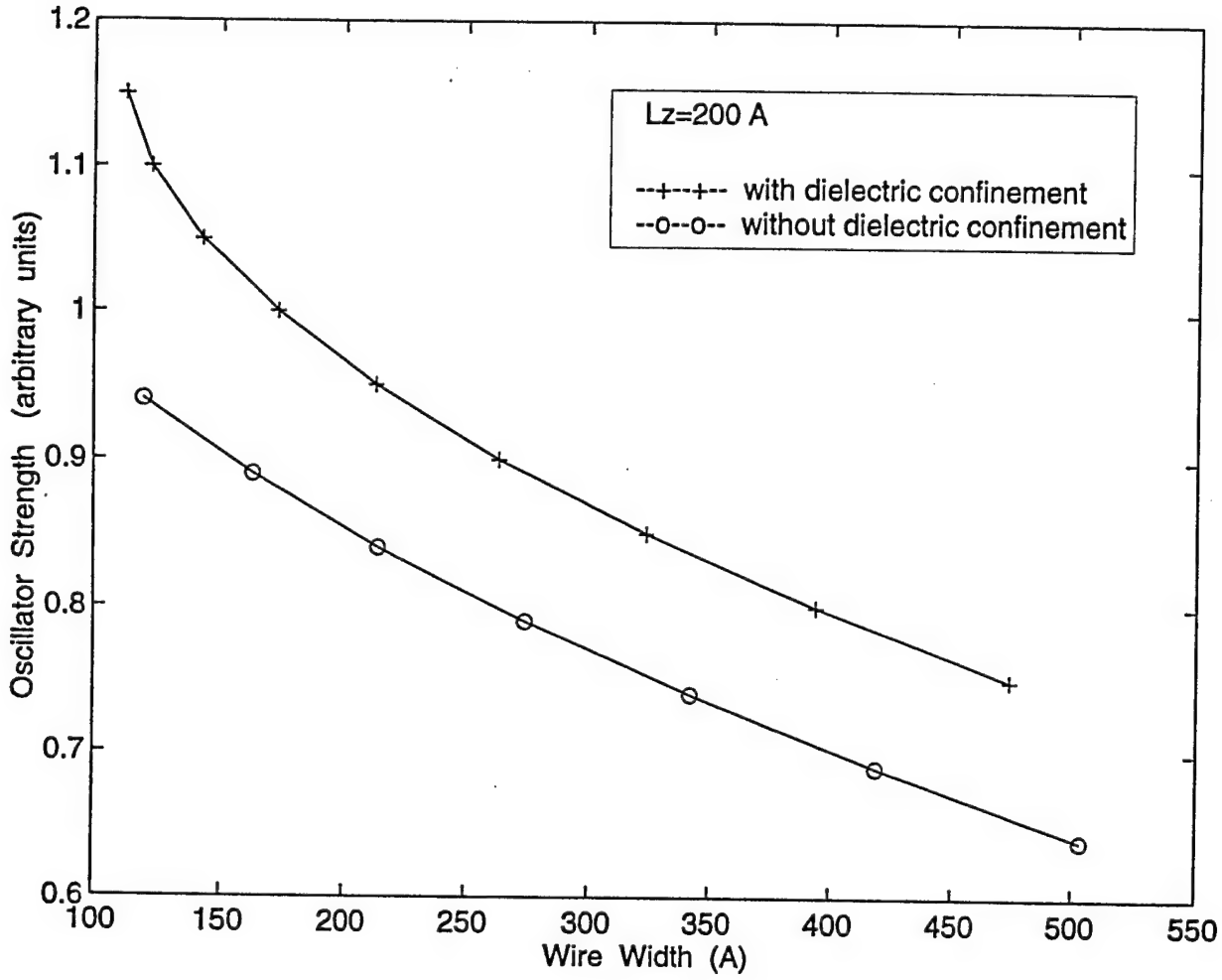
Lz=200 A
--+--+-- with dielectric confinement
--o--o-- without dielectric confinement
Oscillator Strength (arbitrary units)
Wire Width (A)
1.2
1.1
1
0.9
0.8
0.7
0.6
100
150
200
250
300
350
400
450
500
550

Fig. 10

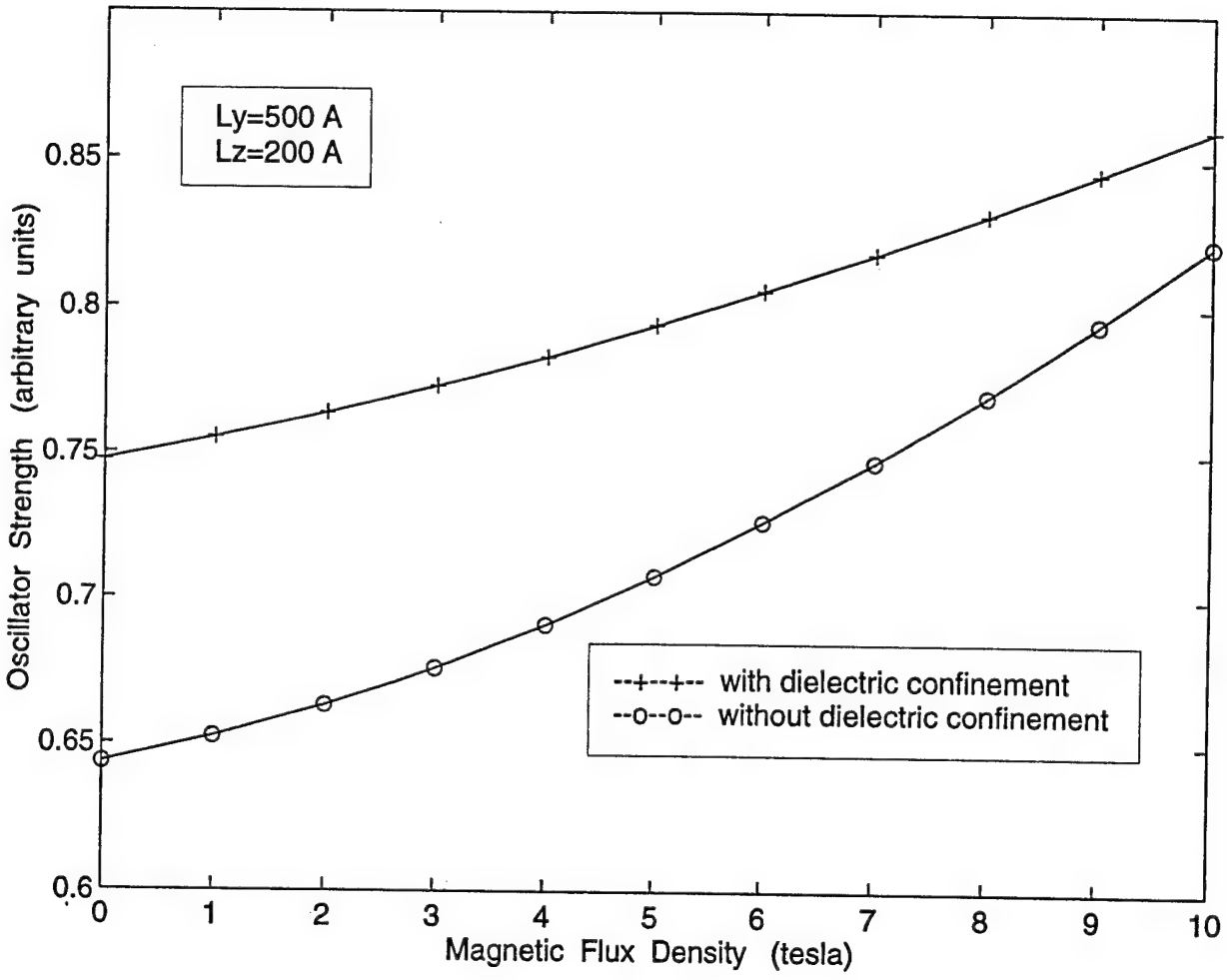
Ly=500 A
Lz=200 A
0.85
0.8
0.75
0.7
0.65
0.6
Oscillator Strength (arbitrary units)
0
1
2
3
4
5
6
7
8
9
10
Magnetic Flux Density (tesla)
--+--+-- with dielectric confinement
--o--o-- without dielectric confinement

Fig. 11

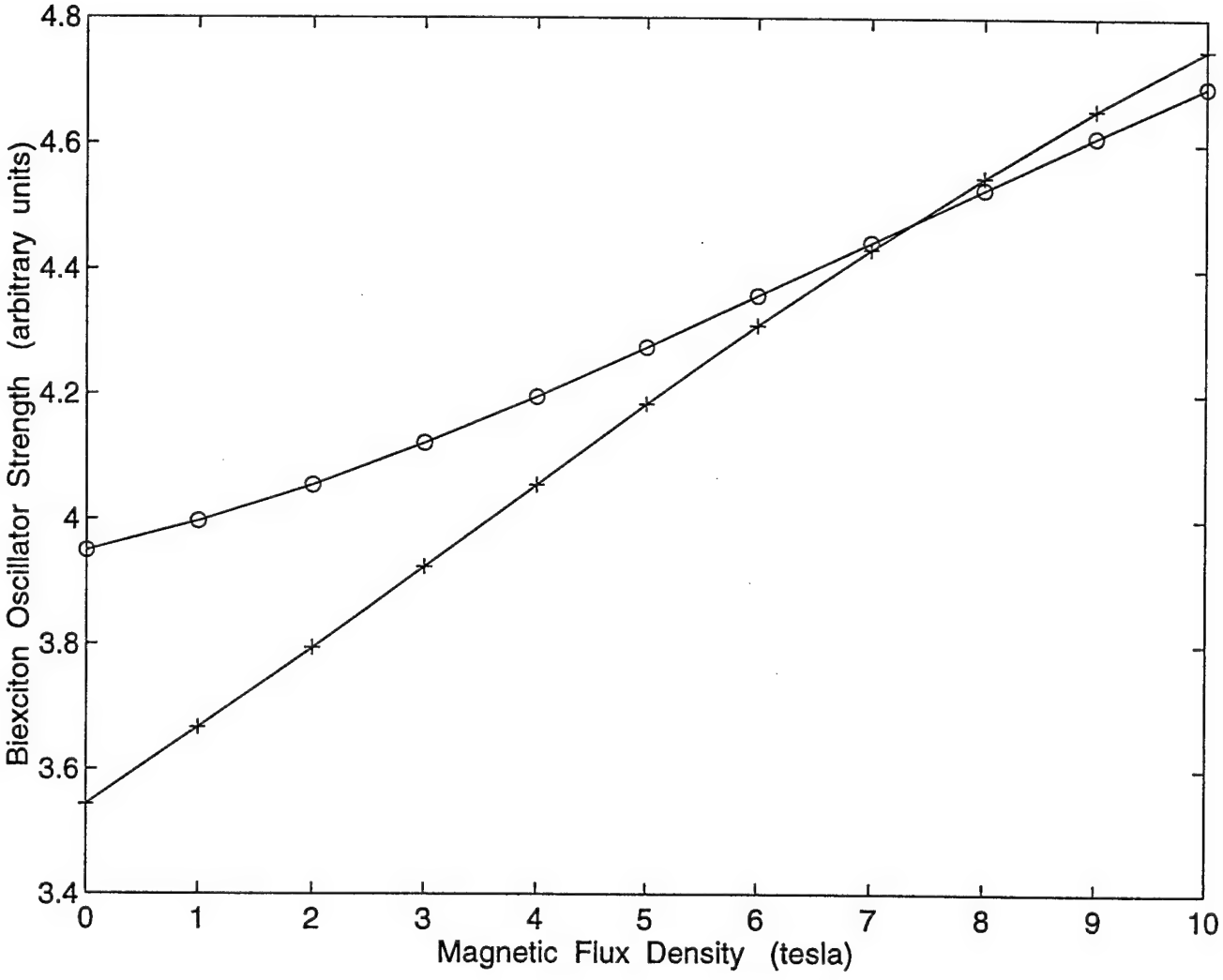
4.8
4.6
4.4
4.2
4
3.8
3.6
3.4
Biexciton Oscillator Strength (arbitrary units)
0
1
2
3
4
5
6
7
8
9
10
Magnetic Flux Density (tesla)

Fig. 12

Phys. Low-Dim. Struct., **9/10***(1996)pp.63–74*

Magnetic Field Dependence of Momentum and Energy Relaxation Rates of Hot Electrons in a Quantum Wire

N.Telang†, S.Bandyopadhyay‡

†*Motorola, Inc. Austin, Texas 78721, USA*
‡*Department of Electrical Engineering*
University of Nebraska, Lincoln, Nebraska 68588-0511, USA

(Received 26 September 1996, accepted for publication 2 October 1996)

We have calculated the momentum and energy relaxation rates of hot electrons in a quantum wire subjected to a magnetic field. These rates have been determined for both forward (where the electron velocity does not change sign) and backward (where the electron velocity changes sign) scattering. A magnetic field suppresses both momentum and energy relaxation rates associated with non-polar acoustic and surface optical phonon scattering. For polar acoustic and polar optical phonon scattering, it suppresses the momentum relaxation rate, but increases the energy relaxation rate. The suppression of momentum relaxation rate leads to an increase in the drift velocity and mobility of electrons, which is beneficial for electronic device applications.

1. Introduction

It is now well-established that a magnetic field suppresses *back*-scattering of electrons in quantum wires. The field spatially separates *oppositely* traveling electron states ("edge-states") thereby reducing the overlap between their wave functions and the matrix element for backscattering [1–4]. While this has many important consequences, perhaps the most noteworthy is the celebrated integral quantum Hall effect whose origin may lie in this phenomenon [5].

In this paper, we have calculated the momentum and energy relaxation rates of electrons in a quantum wire subjected to a magnetic field. Since the momentum relaxation rate is primarily determined by backscattering (large change in momentum) as opposed to forward scattering (small change in momentum),

we expect a drastic suppression of momentum relaxation and a concomitant increase in electron mobility when a magnetic field is present. Furthermore, it is known that the field will enhance confined longitudinal polar and surface optical phonon emission rates [4] so that an increase in the energy relaxation rates can be expected as well. The latter will reduce the electron temperature and hence the Johnson noise. This provides the motivation for our work.

2. Theory

The momentum and energy relaxation rates, τ_m and τ_E, associated with any type of scattering (for an electron with energy E in a subband with transverse indices μ and ν) are calculated from the corresponding scattering rate $S(E_{\mu,\nu}, E'_{\mu',\nu'})$ as follows

$$\frac{1}{\tau_m(E_{\mu,\nu})} = \sum_{E'_{\mu',\nu'}} S(E_{\mu,\nu}, E'_{\mu',\nu'})(1 - f(E'_{\mu',\nu'}))\frac{(k - k')}{k} \tag{1}$$

$$\frac{1}{\tau_E(E_{\mu,\nu})} = \sum_{E'_{\mu',\nu'}} S(E_{\mu,\nu}, E'_{\mu',\nu'})(1 - f(E'_{\mu',\nu'}))\frac{(E_{\mu,\nu} - E'_{\mu',\nu'})}{E_{\mu,\nu}} \tag{2}$$

where k is the electron wavevector in the unconfined direction and f is the occupation probability or the electron distribution function which is negligible compared to unity for a non-degenerate electron gas. The primed and unprimed quantities correspond to the initial and final states of the electron. The calculations of the scattering rates, $S(E_{\mu,\nu}, E'_{\mu',\nu'})$, with and without a magnetic field, are based on standard Fermi's Golden Rule and have been described by us in previous papers [1–4]. They will not be repeated here. We emphasize that these calculations are rigorous since we directly solve the Schrödinger equation in a quantum wire in the presence of a magnetic field and obtain the exact electron wavefunctions, the exact energy dispersion relations and the exact density of states in each magnetoelectric subband. Calculation of these quantities have been described by us in Ref.[6]. These exact quantities are then used in the calculations of the scattering rates.

3. Results

The prototypical system that we chose for calculating the momentum and energy relaxation rates is a free-standing rectangular $GaAs$ quantum wire with infinite potential barriers at the transverse boundaries. It has a width of 300 $\AA$ and thickness 100 $\AA$ (see Fig. 1). The magnetic field is oriented along the thickness. In all our calculations we have assumed that the phonons are unaffected

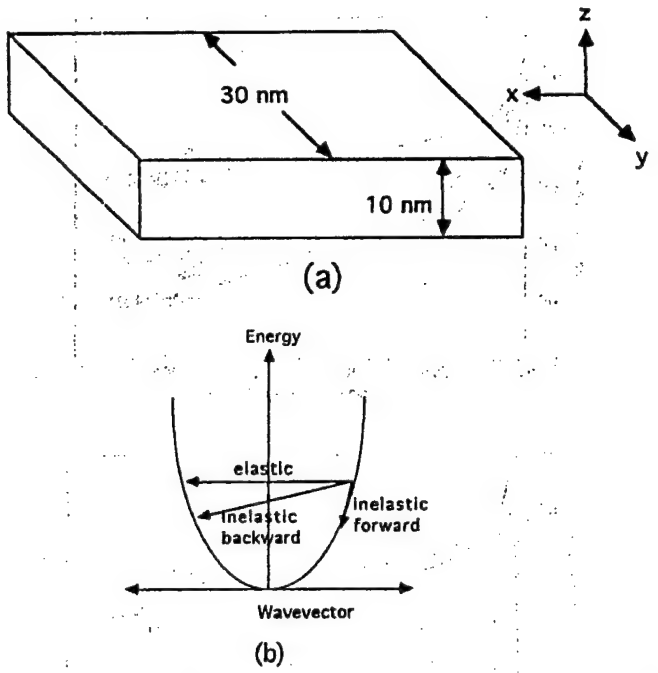

Figure 1. (a) A free-standing quantum wire with hardwall boundaries. The magnetic field is directed along the thickness. (b) Wavevector change associated with forward and backward scattering events in a subband for elastic and inelastic scattering.

by the magnetic field (owing to their heavy "masses") and are in therm namic equilibrium so that the phonon occupation probability is given by Bose-Einstein factor at the lattice temperature.

In Fig. 2a we plot the momentum relaxation rate $1/\tau_m(E_{1,1})$ as a fun of the electron kinetic energy $E_{1,1}$ in the lowest subband for non-polar aco phonon emission. We should stress that the qualitative features do not depending on the subband so that the results for the lowest subband ar solutely generic. Relaxation rates in all subbands behave in exactly the way. The solid and broken curves are results with and without a magnetic of 10 Tesla at a lattice temperature of 300 K. Only intrasubband scatteri considered for illustration. We have calculated the relaxation rates under different premises: (a) the acoustic phonon energy is zero so that the scatt is elastic, and (b) the acoustic phonon energy is $\hbar v_s q$ (where q is the ph wavevector and v_s is the longitudinal sound velocity) so that the scatteri inelastic. In the former case, there can be only backward scattering (see Fig

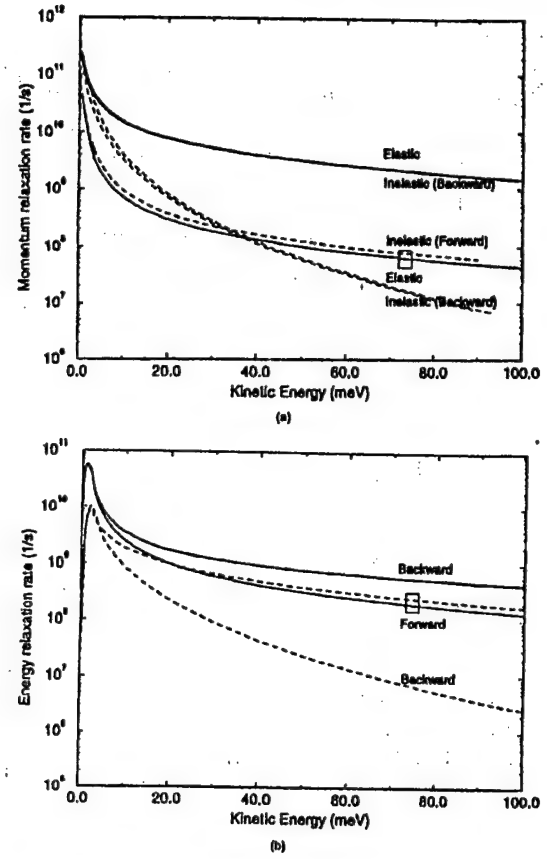

Figure 2. The relaxation rates for non-polar acoustic phonon emission for a quantum wire with and without a magnetic flux density of 10 Tesla at a temperature of 300 K. In this figure and in all subsequent figures, the solid lines are results without a magnetic field and the broken lines are results with a 10 Tesla flux density. Both the inelastic (forward and backward) and elastic rates are plotted for comparison. (a) momentum relaxation rate and (b) energy relaxation rate.

whereas in the latter case, there can be both forward and backward scattering. In the past, acoustic phonon scattering in quantum wires was mostly treated as elastic. This was shown to cause serious errors in one dimensional systems at low electron energies [7]. We therefore use a rigorous inelastic treatment, but this makes the calculation numerically challenging, especially when a magnetic

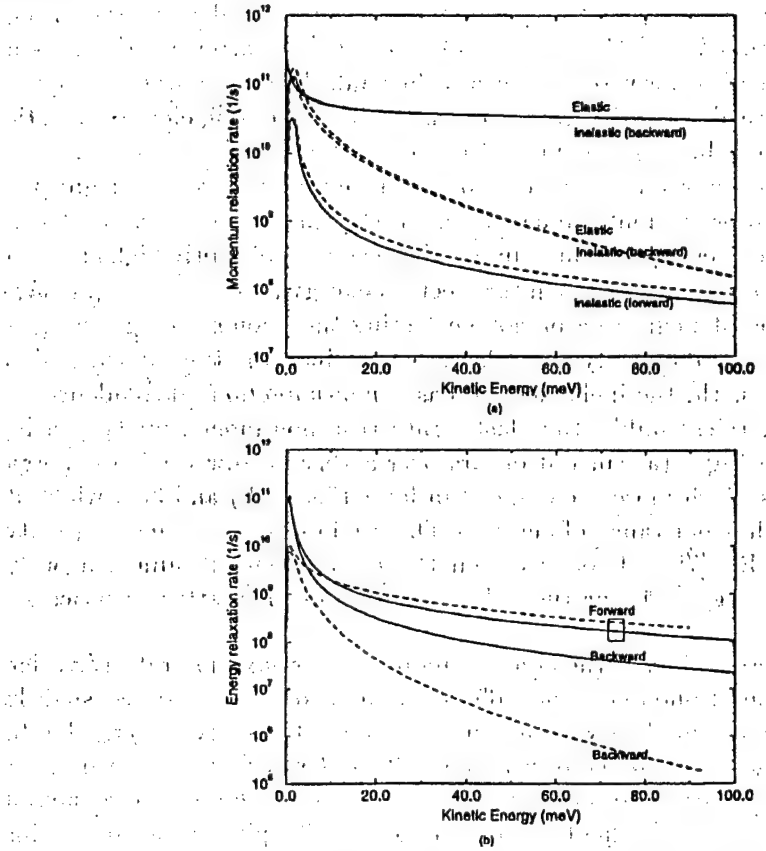

Figure 3. The relaxation rates for polar acoustic phonon emission a quantum wire with and without a magnetic flux density of 10 Tesla a temperature of 300 K. Both the inelastic (forward and backward) a elastic rates are plotted for comparison. (a) momentum relaxation r and (b) energy relaxation rate.

field is present. One must use rejection techniques to search for the ap phonon in any transition which will simultaneously conserve both en longitudinal momentum in the scattering event.

Returning to Fig. 2a, we see some interesting features. First, when netic field is present, the momentum relaxation rate for forward scat about two orders of magnitude smaller than that for backward scatteri pare the two solid curves). The reason for this can be traced to Equ

which shows unambiguously that a lot more momentum is lost when the initial and final wavevectors k and k' have opposite *signs* (backscattering) than when they have the same sign (forward scattering). Second, the difference between the backward and forward scattering rates increases with increasing electron kinetic energy. This happens because the magnitude of the momentum change $\hbar(k-k')$ increases with increasing kinetic energy (or, equivalently, increasing magnitude of $|k|$). Third, with or without a magnetic field, the elastic and inelastic (backward + forward) scattering rates are almost identical at sufficiently high electron energies. This is to be expected when the electron energy far exceeds the phonon energy at which point neglecting or not neglecting the phonon energy in comparison with the electron energy (i.e. elastic versus inelastic treatment) makes little difference. Fourth, the inelastic rate has a *non-monotonic* dependence on energy (at low energies) unlike the elastic rate (the non-monotonicity can be barely observed in Fig. 2(a) since it occurs over a very narrow range of energy below 2 meV; it is much more pronounced in later Figs. 2(b) and 3(a) where it occurs over a much wider range of energy.) The origin of this non-monotonicity was explained in Ref.[7] and follows from the requirement of simultaneously conserving both energy and longitudinal momentum in the scattering process.

When a magnetic field is turned on, the momentum relaxation rate $1/\tau_m$ due to forward emission of phonons is not affected a great deal (it increases slightly because of an increase in the electron density of states). However, $1/\tau_m$ due to backward scattering drops precipitously, regardless of whether we assume elastic or inelastic processes. The reason for this drop is the generic suppression of backscattering in a magnetic field alluded to earlier. The physical origin of this suppression was described by us in previous papers [1–4]. Briefly speaking, the Lorentz force associated with the magnetic field skews the wavefunctions of oppositely traveling states towards opposite edges of the wire, thereby reducing the overlap between their wavefunctions and the matrix element for backscattering. At high enough magnetic field, all current carrying (traveling) states collapse into "edge-states" [8] or "skipping orbit states" that hug opposite edges of the wire if they have oppositely directed velocities. In a relatively wide wire, the overlap between the wavefunctions of oppositely directed edge states becomes infinitesimally small, so that the matrix element for backscattering essentially vanishes. This can lead to a total suppression of backscattering in the quantum Hall effect regime [9] which not only causes the quantum Hall effect [5] but also accounts for its surprising robustness. Finally, it should be noted that the suppression of backscattering in a magnetic field becomes progressively more pronounced at higher electron energies since the Lorentz force responsible for the suppression has a linear dependence on the electron velocity and therefore

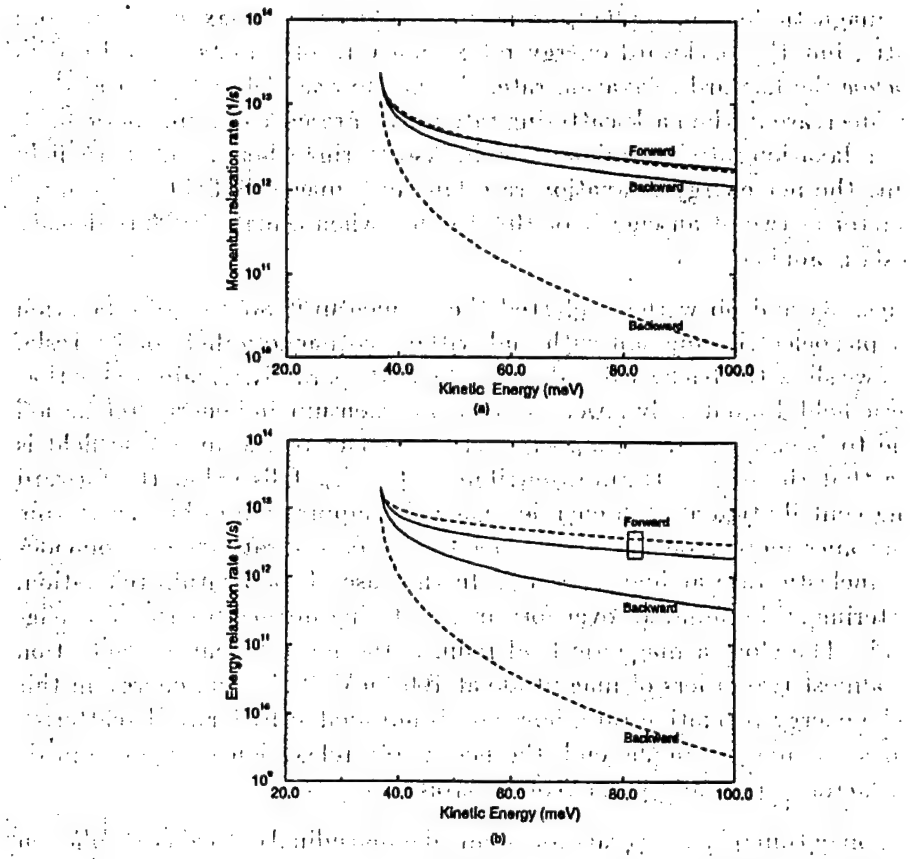

Figure 4. The relaxation rates for longitudinal optical phonon emissio for a quantum wire with and without a magnetic flux density of 10 Tesl at a temperature of 300 K. Both the inelastic (forward and backward and elastic rates are plotted for comparison. (a) momentum relaxatio rate and (b) energy relaxation rate.

on the square-root of the electron energy [10]. At an electron energy of 100 a magnetic flux density of 10 Tesla reduces the net momentum relaxatio by more than two orders of magnitude.

In Fig. 2b we have plotted the energy relaxation rate as a function electron energy both with and without a magnetic flux density of 10 Tesl temperature of 300 K. Here again we see that the rate associated with bac tering exceeds that associated with forward scattering when no magneti is present. However, the difference is not very large (about a factor of

When a magnetic field is applied, we notice that forward relaxation rate goes up slightly, but the backward energy relaxation rate plummets several orders falling *below* the forward relaxation rate. Again the reason for this is the same dramatic decrease in the backscattering rate in the presence of a magnetic field. Since the relaxation rate is dominated by backscattering when no magnetic field is present, the net energy relaxation rate falls in a magnetic field — by more than a factor of two at an energy of 100 meV — when a magnetic flux density of 10 Tesla is applied.

In Figs. 3a and 3b we have plotted the momentum and energy relaxation rates for piezoelectric emission with and without a magnetic field of 10 Tesla. Here also we show the backward and forward rates separately. Again we see that a magnetic field dramatically lowers both the momentum and energy relaxation rates due to backward scattering. In fact, the effect of the magnetic field is so strong that the backscattering contribution to $1/\tau_m$ falls below the forward scattering contribution at high energies when the suppression of backscattering events becomes more pronounced. As before, the elastic rate almost coincides with the inelastic rate at high energies. In the case of momentum relaxation, backscattering still dominates over forward scattering in the absence of a magnetic field. Therefore a magnetic field reduces the net momentum relaxation rate (by almost two orders of magnitude at 100 meV of electron energy in this case). The energy relaxation rate, however, is dominated by forward scattering which goes up slightly. In the end, the net energy relaxation rate goes up, by almost a factor of two, at 100 meV of electron energy.

The momentum relaxation rate for confined longitudinal optical (LO) phonon emission is shown in Fig. 4a. In contrast to the previous cases, forward scattering dominates since it is much easier to satisfy both energy and longitudinal momentum conservation requirements with small wavevector phonons that cause forward scattering. The much higher probability of forward scattering more than compensates for the smaller momentum change taking place in forward scattering compared to backward scattering. Surprisingly, the forward *momentum relaxation* rate is slightly suppressed by a magnetic field (at high electron energies) even though the forward scattering rate $S(E_{\mu,\nu}, E'_{\mu',\nu'})$ is known to actually increase because of the opening of many new scattering channels in a magnetic field [4]. Obviously, this counter-intuitive result is caused by the modification of the energy-dispersion relation in a magnetic field [6] which reduces the net momentum transfer associated with forward scattering at sufficiently high electron energy. Because forward scattering dominates momentum relaxation, and it is suppressed slightly at high electron energies by a magnetic field, the net momentum relaxation rate falls at high electron energies. At lower energies,

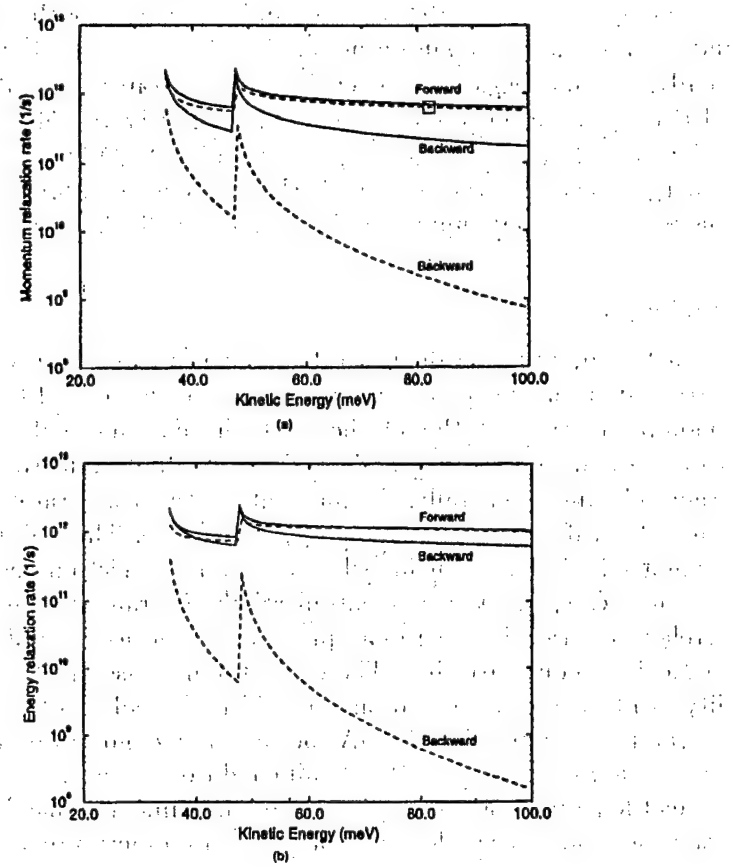

Figure 5. The relaxation rates for surface optical phonon emission for a quantum wire with and without a magnetic flux density of 10 Tesla at a temperature of 300 K. Both the inelastic (forward and backward) and elastic rates are plotted for comparison. (a) momentum relaxation rate and (b) energy relaxation rate.

forward scattering is enhanced rather than suppressed by a magnetic fiel that the net momentum relaxation rate increases. In this case, the cross takes place at an electron energy of about 58 meV.

In the case of energy relaxation via confined LO phonon emission (Fig. forward scattering is both dominant and increased by a magnetic field. energy relaxation rate is proportional to the scattering rate (since the ph energy is a constant) and the latter increases in a magnetic field [4]. In sl

the net energy relaxation rate increases and this may cool the electrons [10–12] causing a suppression of Johnson noise.

Finally, the momentum and energy relaxation rates associated with surface optical (SO) phonon emission are shown in Figs. 5a and 5b. The momentum relaxation rate shows the same features as confined LO phonons. However, the total energy relaxation rate decreases slightly since forward scattering, which dominates, is somewhat suppressed by a magnetic field.

4. Conclusion

In conclusion, we have calculated the momentum and energy relaxation rates of electrons in a quantum wire subjected to a magnetic field for different types of phonon interactions. Although the results have been calculated for the lowest subband, they are perfectly generic and the qualitative features will apply to any other subband. Generally, the momentum relaxation rate decreases, which will cause the drift velocity (or mobility) to increase. This will be more evident at sufficiently high electric fields when the average electron energy is high [12] and the suppression in the momentum relaxation rate is large. The decrease in the relaxation rate is much more pronounced for acoustic phonon scattering than optical phonon scattering. Therefore, the increase in the drift velocity (or mobility) will be much more pronounced for non-polar materials such as Ge rather than polar materials like GaAs because in Ge, non-polar acoustic phonon interactions dominate under virtually all conditions whereas in GaAs, they may dominate at low temperatures only. At the same time, the increase in the energy relaxation rate can cause a lowering of electron temperature.

Acknowledgements

This work was supported by the US Army Research Office under grant DAAH04-95-1-0527.

References

[1] N.Telang and S.Bandyopadhyay, Appl. Phys. Lett., 62 (1993) 3161; M.Masale and N.C.Constantinou, Phys. Rev., B48 (1993) 11128.

[2] N.Telang and S.Bandyopadhyay, in *Proc. of the International Workshop on Computational Electronics, Beckman Institute, University of Illinois, May 1992*, edited by R. W. Dutton. K. Hess and U. Ravaioli (Beckman Institute, Urbana, 1992); A.Y.Shik and L.J.Challis, Phys. Rev., B47 (1993) 2028.

[3] N.Telang and S.Bandyopadhyay, Semiconduc. Sci. Technol., 9 (1994) 955.

[4] N.Telang and S.Bandyopadhyay, Phys. Rev., B48 (1993) 18002.

[5] M.Büttiker, Phys. Rev., B38 (1988) 9375.

[6] S.Chaudhuri and S.Bandyopadhyay, J. Appl. Phys., 71 (1992) 3027.

[7] R.Mickevicius and V.Mitin, Phys. Rev., B48 (1993) 17194.

[8] See, for example, C.W.J.Beenakker and H.van Houten in *Solid State Physi Semiconductor Heterostructures and Nanostructures*, edited by H. Ehrenrei and D. Turnbull, (Academic, New York, 1991), Vol. 44, pp. 1–228.

[9] B.I.Halperin, Phys. Rev., B25 (1982) 2185; P.Streda, J.Kucera a A.H.McDonald, Phys. Rev. Lett., 59 (1987) 1973.

[10] N.Telang and S.Bandyopadhyay, Appl. Phys. Lett., 66 (1995) 1623.

[11] J.P.Leburton, Phys. Rev., B45 (1992) 11022.

[12] N.Telang and S.Bandyopadhyay, Phys. Rev., B51 (1995) 9728.

To appear in J. Appl. Phys.

Giant Dipole Effect and Second Harmonic Generation in Quantum Wires Biased with a Magnetic Field

A. Svizhenko
Department of Electrical Engineering
University of Notre Dame
Notre Dame, Indiana 46556

A. Balandin* and S. Bandyopadhyay
Department of Electrical Engineering
University of Nebraska
Lincoln, Nebraska 68588

We have theoretically studied giant dipoles associated with transitions between magneto-electric subbands in a quantum wire subjected to a transverse magnetic field. The strengths of these dipoles and their resonant frequencies can be varied with the magnetic field which then allows one to tune the emission wavelength of these transitions. The large magnitude of the dipole moments also leads to a strong second-harmonic component of the dielectric susceptibility which can be utilized for non-linear optical applications such as second-harmonic generation, limiting, mixing, optical switching, etc.

*On leave from the University of Notre Dame

[1]PACS Indices: 78.20.Ls, 78.55.Cr, 78.66.Fd, 73.20.Dx

I. Introduction

Direct intraband transitions between the quantized states (subbands) of the conduction band in a quantum well is a well-researched topic.[1] It has been shown both experimentally and theoretically that such transitions have very large dipole moments and narrow bandwidths. Strong infrared absorption associated with transitions between the lowest two electronic subbands in a GaAs quantum well was observed long ago by a number of experimental groups[2]. Recently, population inversion between the second and third subbands of a quantum well has been established unambiguously leading to the demonstration of the celebrated quantum cascade laser[3]. The energy separation between the subbands in a quantum well or wire can be varied by an external magnetic field which then allows one to realize a continuously tunable laser or light-emitting-device. Moreover, the field can induce forbidden transitions that make additional frequency ranges accessible, thus permitting flexible device design.

Another potential use of magnetic field biasing of quantum wells or wires is in non-linear optics. Non-linear optical properties stem from higher order dielectric susceptibilties. Specifically, the second-order susceptibility $\chi^{(2)}$ is responsible for such phenomena as mixing and second-harmonic generation. It is well-known that even-order susceptibilities vanish in structures with inversion symmetry. Consequently, finite second-order susceptibilities can be obtained in such structures only if the inversion symmetry of the conduction-band potential is broken either by an external electric field or by the intentional growth of an asymmetric well. Obviously, the former is the preferred method since an electric field can be continuously varied which allows one to tune the degree of symmetry-breaking and the magnitude of $\chi^{(2)}$.

However, this method has a practical shortcoming. An electric field tilts the potential barriers of the well thereby allowing carriers to escape by tunneling or thermionic emission. This is especially serious in GaAs/AlGaAs systems where the barrier height is relatively small. Indeed, it has been pointed out that the electronic states in a quantum confined system biased by a transverse electric field are never true bound states since the particles can always lower their energy by escaping from the well[4]. Therefore, these states have a finite lifetime. An electric field reduces the lifetime drastically and broadens the transitions.

To overcome this shortcoming, one can adopt magnetostatic biasing. A magnetic field can break inversion symmetry without tilting potential barriers and promoting carrier escape. A transverse magnetic field applied to a quantum wire exerts a Lorentz force on an electron moving along the wire. As a result, its wave function (in any subband) will be skewed towards one edge of the wire. This skewing does not tilt potential barriers to first order (the barriers may tilt slightly because of a second-order effect associated with space-charges and the self-consistent (Hall) electric field). However, it effectively breaks inversion symmetry since it causes a net charge to accumulate at either edge of the wire (the charges at the two edges have opposite signs as in the classical Hall effect). This leads to a non-vanishing even-order susceptibility in a symmetric structure. The skewing has another subtle effect. The degree to which the wave function is skewed is *different in different subbands* since an electron has different kinetic energies and hence experiences different Lorentz forces in different subbands. As a result, transitions between subbands whose wave functions have the same parity - which are forbidden without a magnetic field - are now allowed since the parities are altered by

different amounts in different subbands by the different degrees of skewing. We should point out that this effect has striking similarity with the quantum confined Lorentz effect (QCLE) previously examined by Balandin and Bandyopadhyay [5] in the context of interband transitions between conduction and valence band states rather than intraband transitions in the conduction band. In that case, the different amount of skewing of the electron and hole states quenches photoemission.

This paper is organized as follows. In the next section, we describe the theoretical formulation, followed by results. Finally, in section IV, we present the conclusions.

II. Theory

We consider a quantum wire as shown in Fig. 1 with a magnetic field applied along the z direction. The thickness along the z direction is so small (and consequently the subband separation in energy is so large) that for the range of photon energies considered, an electron cannot be excited (by real transition) into a subband which has more than two nodes along the z-direction. Such a transition will not be accessible in energy. This restriction, coupled with the fact that a magnetic field does not affect the z-component of the electron wave function, allows us to drop the z-component from further consideration. The width of the wire along the y-direction is however large enough that subbands with more than two nodes along the y-direction are accessible in energy.

In the framework of the envelope function approximation (EFA), an electron wave function can be written as the product of a Bloch wave function, periodic with the atomic lattice spacing, and an envelope wave function, describing the nonperiodic behavior. Consequently, the wave function of an

electron for a given wave vector k along the x-direction, in the nth magnetoelectric subband, at a magnetic field B can be written as

$$\Phi_n(x,y,k,B,t) = \Psi_n(x,y,k,B)u_n(x,y,k)e^{-jE_n(k,B)t/\hbar}, \quad (1)$$

where $\Psi_n(x,y,k,B)$ is an envelope function, $u_n(x,y,k)$ is a Bloch function of a conduction band and $E_n(k,B)$ is the dispersion relation of the nth magnetoelectric subband at a flux density B. The Bloch wave functions are assumed to be s states which is the usual case for semiconductors where $\hat{J} = 1/2$ for the conduction band.

The envelope function can be further decomposed into a plane wave along the unconfined x direction and confined component along y direction

$$\Psi_n(x,y,k,B) = \chi_n(y,k,B)e^{jkx} \quad (2)$$

Using the electric dipole approximation, we can write the matrix element of photoinduced inter-subband transitions within the conduction band as[6]

$$d_{f,i}(k,B) = e\int \chi_f(y,k,B)\hat{\eta}\cdot\vec{r}\chi_i(y,k,B)d\vec{r}\int u_f^*(x,y,k)u_i(x,y,k)d\Omega \quad (3)$$

where $d\Omega$ is a volume element, $\hat{\eta}$ is the unit vector along the direction of the incident photon polarization, $\vec{r} = x\vec{a}_x + y\vec{a}_y$ is the two-dimensional radius vector, and subscripts i, f stand for initial and final states respectively. The exponential term of Equation (2) is not present in Eq. (3) since for photoinduced transitions ($k_f = k_i$), the product of the exponential function and its complex conjugate is exactly unity. The volume overlap of the Bloch functions is also unity for s-states with the same wave vector. Now, if we assume that the incident light is polarized along the y-direction so that $\hat{\eta} = \hat{a_y}$, the above equation simplifies to

$$d_{f,i}(k,B) = e < \chi_f|y|\chi_i >= e\int_{-W/2}^{W/2} y\chi_f(y,k,B)\chi_i(y,k,B)dy, \qquad (4)$$

where W is the width of the quantum wire along the y-direction.

One should note here, that if there is no magnetic (or electric) field applied, the envelope functions χ_i are just particle-in-box states and the dipole moment in Eq. (4) is non zero only for the transitions between subband states of opposite parity. For a symmetric square potential well, these dipole elements (between any two states n and m) are independent of the wave vector k and can be found analytically[1] by evaluating the integral in Equation (4).

$$\begin{aligned} d_{f,i} = e < \chi_f|y|\chi_i > &= eW\frac{8}{\pi^2}\frac{mn}{(m^2-n^2)^2}, \quad if\ n\ and\ m\ have\ opposite\ parity \\ &= 0, \quad otherwise \end{aligned} \qquad (5)$$

However, when a magnetic field is applied, the skewing of the wave functions changes the integral in Equation (4) and alters the selection rules. Generally, the skewing causes three effects. First, it makes the dipole moment depend on the wave vector k (since the degree of skewing depends on k). Second, it reduces the dipole moment for transitions between states of opposite parity (since the integral in Equation (4) decreases), and third, it allows forbidden transitions between states of the same parity (since the integral in Equation (4) no longer vanishes for states of the same parity).

It is clear from Equation (4) that to calculate the dipole moments in the presence of a magnetic field, all we need to compute are the wave functions $\chi_{f,i}(y,k,B)$ at a given magnetic field B, for given magnetoelectric subbands f and i, and for a given wave vector k. This is achieved via a numerical (finite

difference) solution of the Schrödinger equation following the prescription of ref. [7]. Once this is done, we can calculate the dipole moment in Equation (4) for any chosen intersubband transition, at any chosen magnetic field and for any chosen wave vector.

In the limit of high magnetic fields, when the magnetic length $l(=\sqrt{\hbar/eB}) << W$ one can again obtain an analytical expression for the dipole moment $d_{f,i}$. In this case, the magnetostatic confinement predominates over electrostatic confinement and the envelope functions $\chi_n(y,k,B)$ can be approximated by harmonic-oscillator wave functions:

$$\chi_n(y,k,B) \equiv \chi(y-y_k,B) = N_n H_n(\alpha, y-y_k) e^{-\frac{1}{2}\alpha^2(y-y_k)^2}, \qquad (6)$$

where $N_n = (\alpha/\pi^{1/2}2^2 n!)^{1/2}$ is a normalization constant, $H_n(\alpha,y)$ is the nth Hermite polynomial, $y_k = \hbar k/eB$, and

$$\alpha = \sqrt{\frac{eB}{\hbar}} = \frac{1}{l}. \qquad (7)$$

In order to evaluate the integral in Eq. (4) analytically, we extend the limits of integration to infinity assuming that the wave function tail is negligible at the boundaries of the wire (i.e. at $y = \pm W/2$). This is a very reasonable assumption in a high confining magnetic field. The resulting analytical expression for the dipole moment is

$$\begin{aligned} d_{f,i}(B) = e < \chi_f|y|\chi_i > &= el(\frac{n+1}{2})^{1/2}, \quad if\ m = n+1 \qquad (8) \\ &= el(\frac{n}{2})^{1/2}, \quad if\ m = n-1 \\ &= 0, \quad otherwise. \end{aligned}$$

The physical significance of the two analytical limits - $B \to 0$ and $B \to \infty$ - is obvious. At zero field, the dipole is determined by the width of the wire $d_{f,i} \sim eW$, and at the high field limit it is determined by the magnetic

length $d_{f,i} \sim el$. This is what one would expect intuitively. At zero field, the dipole is confined electrostatically with the wire width being a measure of this confinement while at high magnetic field, the dipole is confined magnetostatically and the magnetic length is the corresponding measure of this confinement.

III. Results

A. Intraband dipoles

We now present results of our calculations. The physical parameters used for the numerical calculations correspond to a $GaAs$ quantum wire with relative dielectric constant $\epsilon_r = 12.9$, and effective masses $m_e = 0.067m_o$ and $m_h = 0.5m_o$ where m_o is the free electron mass.

In Fig. 2, we show the dependence of the dipole moment $d_{f,i}(k, B)$ for three transitions (e1-e2, e2-e3, and e1-e3) on the wave vector k when a magnetic field of 1 tesla is applied (following usual practice, the transitions are numbered by the subband indices). The dipoles corresponding to transitions between states of opposite parity (e1-e2 and e2-e3) have maxima at $k = 0$ and then decrease with increasing wave vector. This can be easily understood as follows. At zero wave vector (no translational velocity) these states do not experience any Lorentz force and hence the wave functions are not skewed. As the wave vector k increases, the translational velocity and the Lorentz force experienced increase. Consequently, the envelope wave functions are skewed more and more and the dipole moment decreases. Real transitions between states of the same parity are forbidden at zero magnetic field, but at a finite magnetic field, they are forbidden only at k=0 when there is no translational velocity and no Lorentz force to skew the wave functions. With increasing k, the wave functions are increasingly skewed and the dipole mo-

ment of forbidden transitions increases. In our chosen prototype wire, d_{e1-e3} reaches a maximum of 28 $e-\mathring{A}$ at $k = 0.0051$ $\mathring{A}$ and then decreases gradually ultimately reaching zero. This intriguing *non-monotonic* dependence on k is explained later on. However, at this point, it is interesting to note that a fairly large forbidden dipole moment of ~ 30 e-Å can be achieved in realistic structures at a moderate magnetic field of 1 tesla.

Fig. 3 presents the dipole moments for the same transitions as a function of magnetic flux density. The propagation wave vector k is chosen to be 0.01/Å. At zero magnetic field, a non-vanishing dipole matrix element occurs only for transitions between states of opposite parity (e1-e2, e2-e3) as expected from Equation (5). This equation also allows us to estimate the strengths of these zero-field dipoles to be 180 $e-\mathring{A}$ for e1-e2 and 195 $e-\mathring{A}$ for e2-e3 transitions. As we can see from Fig. 3, these values are in excellent agreement with our numerical results. From the analytical expression in equation (8), we can estimate the strength of the e1-e2 dipole to be 66 $e-\mathring{A}$ at a magnetic flux density of 15 tesla. This number also agrees with our numerical result. The e1-e3 dipole vanishes at both zero field (because of the spatial symmetry of the particle-in-a-box states) and at high fields because of the symmetry of the Landau states or Hermite polynomials. This behavior is consistent with Equations (5) and (8). Only at intermediate fields, when the wave functions of the subbands are a hybrid between particle-in-a-box states and Hermite polynomials (and thus "non-symmetric" in space), is this transition allowed. This immediately tells us that d_{e3-e1} must have a *non-monotonic* dependence on the magnetic flux density B and indeed it does.

A.1 Non-monotonic behavior of dipole moment d_{e3-e1}.

Let us now examine the non-monotonic behavior of d_{e3-e1} more closely. This transition is forbidden at zero field since the wave functions of the first and third subband have the same parity. At low magnetic fields, the parities are altered by the skewing of the wavefunctions and consequently d_{e3-e1} is no longer zero but increases with the magnetic field. It reaches a maximum of about 30 e-Å and then decreases. This later decreases is related to the following effect. For a fixed wave vector k, a sufficient increase in the flux density B forces the traversing states ("skipping orbits" or "edge states") to condense into closed cyclotron orbits (Landau levels) which are no longer skewed by the magnetic field to the wire edge since they have no translational velocity and hence no Lorentz force. While edge states have a skewed wave function which is not symmetric in space, cyclotron orbits have a wave function that is symmetric about the orbit center y_k. Note that y_k depends only on k and B. Therefore, at a fixed k, the wave functions of the first and third Landau levels are symmetric about a *common* center. Whenever this kind of symmetry holds, d_{e3-e1} vanishes. Therefore, the dipole moment d_{e3-e1} decreases gradually to zero at high magnetic field with the onset of Landau condensation.

The same physics can be elucidated in a different way by considering the energy versus wave vector relation is Fig. 4(a) and 4(b) which show the dispersion of the first and third magneto-electric subbands respectively.

At $B = 0$, velocity (slope of the curves) at $k = 0.01\ /\mathring{A}$ are non-zero for both the e1 and e3 subbands. However, the Lorentz force is zero because $B = 0$ and hence $d_{e1-e3} = 0$. At $B = 5$ tesla, the group velocities for the two subbands are still non-zero and the Lorentz force is finite resulting in skewing of wave functions and a non-vanishing value of d_{e1-e3}. At $B = 10$

tesla, the group velocities at k=0.01 /$\AA$ are zero in both subbands indicating that the corresponding states have undergone Landau condensation. In this case, the Lorentz force (for skewing) is again zero and the dipole moment d_{e1-e3} vanishes once more. The crucial point to note is that the Lorentz force $e\vec{v} \times B$ can vanish in two different ways: (i) $B = 0$, and (ii) $\vec{v} = 0$. These two conditions are met at zero and very high magnetic fields. As a result, the dipole moment d_{e1-e3} exhibits a non-monotonic behavior in magnetic field. One can ask as to why the same physics does not cause non-monotonicity in the e1-e2 and e2-e3 curves. It is not clear apriori that non-monotonicity cannot occur (indeed there are regions of inflexion in the two curves). However, the point to note is that Landau condensation causes recovery of the wave function symmetry (or anti-symmetry), *but does not restore the original zero-field wavefunctions.* This is shown in Fig. 5 where we show the wave functions in e1 subband at 0 and 10 tesla. Both wave functions are "symmetric" in space, but they are otherwise vastly different since the magnetostatic confinement squeezes the wave functions binding them in cyclotron orbits.

The non-monotonicity in the wave vector dependence of d_{e1-e3} in Fig. 2 has a similar origin. As k is increased, the *relative* skewing between the wave functions in e1 and e3 subbands change non-monotonically causing the non-monotonicity in this figure.

The process described above is illustrated in Fig. 6 (a) - (c), where we present wave functions of two electronic states (e1 and e3) for three values of magnetic flux density. At zero magnetic field the wave functions are symmetric about the center of the wire and dipole transition d_{e3-e1} is forbidden (case "a"). At low magnetic field the wave functions are skewed to the edge of the

wire ("edge states" - case "b") and the spatial symmetry is broken for both states. Dipole transition d_{e3-e1} is now allowed. It is important to note here that the symmetry breaking skewing of the wave functions is caused by the simultaneous presence of a magnetic field and the electrostatic potential barriers at the edges of the quantum wire. At higher magnetic fields, when the magnetic length is smaller than the wire width, the electrons do not "feel" the potential barriers at the edges of the wire as they undergo complete Landau condensation and execute cylotron motion with radius much smaller than the width of the wire. In this case, the wave function symmetry is essentially restored (case "c") although the wave functions are now symmetric about a point that is not at the center of the wire. Nonetheless, what is important is that both wave functions are symmetric about the same point. Consequently, the d_{e3-e1} transition vanishes. Simultaneous presence of both electrostatic confinement and magnetostatic confinement is therefore necessary for wave function skewing, formation of edge states and the observation of forbidden transitions.

B. Second Harmonic Generation

It is well known that in systems with inversion symmetry there can be no second order nonlinearity.[8] However, in systems without inversion symmetry, the lowest order optical nonlinearity is of the second order and is expressed by

$$\vec{P^{(2)}}(\vec{k},\omega) = \chi^{(2)}(\omega;\omega_1,\omega_2)\vec{E_1}(\vec{k_1},\omega_1)\vec{E_2}(\vec{k_2},\omega_2), \tag{9}$$

where $\vec{P}$ is the polarization caused by two electric fields $\vec{E_1}$ and $\vec{E_2}$ that are associated with the electromagnetic fields of either two frequency components of the same light beam or two different coherent beams with frequencies ω_i

and wave vectors $\vec{k_i}$. The frequencies and wave vectors obey the energy and momentum conservation laws

$$\hbar\omega = \sum_i \pm\hbar\omega_i, \qquad (10)$$
$$\hbar\vec{k} = \sum_i \pm\hbar\vec{k_i}.$$

It is obvious that the third-ranked tensor $\chi^{(2)}$ will vanish in any structure with inversion symmtery. A quantum confined structure may lack inversion symmetry for two main reasons. (i) the semiconductor material by its intrinsic chemical and crystalline structure may lack inversion symmetry,[9] and this is the case in most III-V, II-VI, and I-VII compounds along certain crystallographic directions. (ii) the quantum confining potential well may be asymmetric (e. g. triangular potential well, asymmetric double square well potential, etc.). In the first case, the asymmetry is related to the intracell charge asymmetry and is not affected by the the confinement since the latter extends over several unit cells. In the second case, the asymmetry is artificially imposed and therefore can be engineered. It clearly depends on the confining potential and hence an applied electric field can alter the potential and change the degree of symmetry-breaking.

In the present work we restrict ourselves to the second case and do not consider intrinsic second order nonlinearities of GaAs which are actually quite large (the nonlinear susceptibility of bulk GaAs is $\chi^{(2)}_{14}$=3.8 10^{-10} m/V.[10]) As mentioned before, we avoid an electric field since it promotes carrier escape and consider a magnetic field instead. Although a magnetic field does not affect the potential to first order, the simultaneous action of *symmetric* electrostatic potential and an external magnetic field may lead to the *uneven charge distribution* along the width ($y-axis$) of the wire caused by different

degrees of skewing of the wave functions. Because of this reason, it is possible to break the inversion symmetry in a symmetric quantum well or wire with a magnetic field alone. This approach is superior to applying a transverse electric fields since the latter will tilt the confining potential wells thereby promoting carrier escape from the well by either tunneling or thermionic emission.

The large magnitude of the dipole moments associated with otherwise forbidden transitions between subbands of the same parity and their sensitivity to the biasing magnetic field open up a possibility of second harmonic generation (SHG) that can be controlled by the magnetic field. In order to evaluate the magnitude and dependences of SHG on the biasing field and wire geometry, we calculate the second order susceptibility using the formula[11]

$$\chi^{(2)}_{\mu\alpha\beta}(-\omega_\sigma;\omega_1;\omega_2) = \frac{Ne^3}{\epsilon_o 2\hbar^2}\hat{S}_T \sum_{abc} \rho_o(a)[\frac{d^\mu_{ab} d^\alpha_{bc} d^\beta_{ca}}{(\Omega_{ba}-\omega_1-\omega_2)(\Omega_{ca}-\omega_2)}], \quad (11)$$

where N is concentration (number density) of conduction electrons, $\hbar\Omega_{\alpha\beta} \equiv \hbar\Omega_{\alpha\beta}(B,W)$ is the energy spacing between α,β subbands which depend on the applied magnetic field and wire width, $d_{mn} \equiv d_{mn}(B,W)$ is a dipole element calculated using Eq. (4), and ω_σ is defined to be $\omega_\sigma = \omega_1+\omega_2$. The total symmetrisation operation $\hat{S}_T$ indicates that the expression which follows it is to be summed over all six permutations of the pairs $(\mu,-\omega_\sigma),(\alpha,\omega_1),(\beta,\omega_2)$. Since $\hat{S}_T$ involves a summation over all possible permutations, it is clear that $\chi^{(2)}_{\mu\alpha\beta}(-\omega_\sigma;\omega_1;\omega_2)$ is invariant under any of them. For simplicity, the Fermi distribution $\rho_o(a)$ was assumed to be unity.

Eq. (11) is an approximation which applies only under the condition that all of the optical frequencies involved (operational frequencies $\omega_\sigma,\omega_1,\omega_2$) are removed far enough from the subband transition frequencies. It means that the medium is assumed to be transparent and loss-free at all the relevant

optical frequencies. This assumption can be relaxed by the introduction of transition damping factors into the expression in Eq. (11). In our consideration we are mainly interested in the effects of an applied magnetic field on the second order susceptibility. Since these effects manifest themselves in Eq. (11) primarily via the magnetic field dependence of the dipole elements $d_{mn} \equiv d_{mn}(B)$, we did not include any damping constants and associated finite linewidths of the electronic states. One should also note here that the Eq. (11) is strictly correct only for dilute media. In this case, one can write $\chi^{(2)} = N\alpha^{(2)}$ with $\alpha^{(2)}$ being the $2nd$-order nonlinear polarization. The above expression is valid only under moderate excitation.

In Fig. 7, we present normalized values of $\chi^{(2)}$ as a function of magnetic field for three different wire widths and a fixed value of the wave vector k (fixed excitation frequency). The operational frequencies $\omega_1 = \omega_2$ are chosen for a CO_2 laser. For wide ranges of magnetic flux densities ($B < 20$ tesla) and wire widths ($100\mathring{A} < W < 1000\mathring{A}$), these frequencies are removed far enough from the subband transition frequencies $\Omega_{\alpha\beta}(B, W)$. As long as the latter is true, the $\chi^{(2)}$ dependence on magnetic field is governed mainly by dipole elements d_{mn}. Consequently, the $\chi^{(2)}$ curve for $W = 1000\mathring{A}$ peaks at the same value of a magnetic flux density (B=0.3 tesla) as the e1-e3 dipole curve of Fig. 3. The magnetic flux density at which $\chi^{(2)}$ reaches its maximum increases with decreasing wire width. This happens because it takes a higher magnetic field to condense electronic states into cyclotron orbits (Landau condensation) when the electrostatic confinement is stronger (narrower wires).

Fig. 8 shows the dependence of the normalized values of $\chi^{(2)}$ on wire width for three different values of a magnetic field and a fixed value of the

wave vector. For weak magnetic field of 0.3 tesla, the $\chi^{(2)}$ curve increases monotonically with increasing wire width (case "b" of Fig. 6). This happens because $d_{m,n}$ is proportional to the wire width W (see Equation 5 which is valid at zero field). The magnetic field is obviously not strong enough for the onset of Landau condensation. At a moderate magnetic flux density of 1 tesla, we can observe some saturation features and for a strong magnetic field of 5 tesla, the curve is non-monotonic, rolling down to almost zero for the wire width of 1000 $\mathring{A}$ (case "c" of Fig. 6). The physics underlying the difference in the behaviors of the three curves is essentially the same as that responsible for the features in Fig. 7. At small values of wire width ($W \approx 170\mathring{A}$), there is an additional peak in the $\chi^{(2)}$ curve. This peak is a manifestation of the fact that Ω_{ab} has become comparable to the operational frequencies. At this point the resonant behavior is strongly suppressed by the near vanishing of the dipole elements.

In our numerical calculations we have used $N = 10^{17}\ cm^{-3}$. For this dilute concentration, high density effects such as screening and bandgap renormalization are not important and Equation (11) is quite valid. In fact, ref. [1] demonstrated an excellent agreement between theory and experiment without accounting for any high density effect even though the carrier concentration in that study was $N = 5 \times 10^{17}/cm^3$. Therefore, we believe that high density effects are not significant in this regime.

The peak value of the second order susceptibility for a wire width of 500 $\mathring{A}$ is $\chi^{(2)} = 1.5\ 10^{-7}$ m/V (the absolute magnitudes of the peak values for various wire widths are given in the caption of Fig. 7). For comparison, the nonlinear susceptibility of electric field biased GaAs quantum wells (W=92 $\mathring{A}$) - calculated theoretically and measured experimentally in ref. [1] - was

$\chi^{(2)} = 2.4\ 10^{-8}$ m/V for an electric field of 36 kV/cm. This shows that relatively weak magnetic fields in quantum wires can produce similar magnitudes of $\chi^{(2)}$ as rather strong electric fields in quantum wells. Unfortunately, there is no theoretical or experimental result available for either electric field biased quantum wires or magnetic field biased quantum wells so that a direct comparison is not possible. Nonetheless, it is obvious that magnetic field biased quantum wires provide a very attractive alternative to other means of producing large $\chi^{(2)}$ values. In fact, the largest value of $\chi^{(2)}$ (obtained at a magnetic flux density of 2 tesla) in a magnetic-field-biased quantum wire is three orders of magnitude higher than what can be achieved in bulk GaAs.

IV. Conclusion

We have theoretically studied the giant dipole effect in magnetic-field-biased semiconductor quantum wires. The dipoles are associated with transitions between magneto-electric subbands within the conduction band, some of which are forbidden in the absence of the magnetic field. The resonant frequencies of these transitions can be tuned by the magnetic field which allows the realization of externally tunable inter-subband lasers. We have also studied the possibility of second harmonic generation in a quantum wire biased with a magnetic field and find a strong second harmonic component of the susceptibility which has applications in non-linear optics.

Acknowledgement

This work is supported by the US Army Research Office under contracts DAAH04-95-1-0586 and DAAH04-95-1-0527.

REFERENCES

[1]. M.M. Fejer, S.J.B. Yoo, R.L.Byer, A. Harwit, J.S. Harris, *Phys. Rev. Lett.*, **62**, 1041 (1989) and references therein; L. C. West and S. J. Eglash, *Appl. Phys. Lett.*, **46**, 1156 (1985); for an overview of current work on intersubband transitions see H.C. Liu, B.F. Levine and S.Y. Anderson eds., *Quantum Well Intersubband Transition Physics and Devices* (NATO ASI Series E270), (Dordrecht: Academic, 1994).

[2]. A. Sa'ar, I. Grave, N. Kuze, and Yariv in *Nonlinear Optics: Materials, Phenomena and Devices,* 113 (1990); B.F. Levine, R.J. Malik, J. Walker, K.K. Choi, C.G. Bethea, D.A. Kleinman, and J.M. Vandenberg, *Appl. Phys. Lett.*, **50**, 273 (1987).

[3]. See, for example, Manfred Helm, *Semicond. Sci. Technol.*, **10**, 557 (1995); J. Faust, et. al., *Appl. Phys. Lett.*, **64**, 1144 (1994).

[4]. E.J. Austin and M. Jaros, *Phys. Rev. B* **31**, 5569 (1985).

[5]. A. Balandin and S. Bandyopadhyay, *J. Appl. Phys.*, **77**, 5924 (1995); A. Balandin, Ph.D. dissertation, University of Notre Dame, 1996.

[6]. Claude Weisbuch and Borge Vinter, *Quantum Semiconductor Structures: Fundamentals and Applications*, (Academic Press, Boston, 1991).

[7] S. Chaudhuri and S. Bandyopadhyay, *J. Appl. Phys.*, **71**, 3027 (1992).

[8] see for example J.M. Hvam in *Nonlinear Spectroscopy of Solids: Advances and Applications,* Edited by B. Di Bartolo and B. Bowlby (Plenum Press, New York, 1994), pp. 91-149.

[9] This lack of symmetry is due to the transfer of a valency charge from one atom to the other bond-forming atom and resultant uneven charge distribution along the bond axis.

[10] *Handbook of Lasers,* Edited by R.J. Pressley (Chemical Rubber Co., Cleveland, 1971), p. 504.

[11] see for example P.N. Butcher, D. Cotter, *The Elements of Nonlinear Optics,* (Cambridge University Press, 1990); A. Yariv, *Quantum Electronics,* (Wiley, N.Y., 1989); or Y.R. Shen, *The Principles of Nonlinear Optics,* (Wiley, N.Y., 1984).

FIGURE CAPTIONS

[1] An electron waveguide (quantum wire) subjected to a magnetic field along the z axis. The width of the wire is much larger than the thicknes.

[2] Dipole moments for various inter-subband transitions as functions of the propagating wave vector k for a magnetic flux density of 1 tesla. At zero translational velocity ($k = 0$) the dipole of the transition e1-e3 vanishes. The $GaAs$ quantum wire is 1000 $\AA$ wide.

[3] The dipoles of three inter-subband transitions as functions of the applied magnetic field. The dipole d_{e1-e3} peaks at a magnetic flux density of 0.3 tesla. The wire width is the same as that in Fig. 2.

[4] Energy vs. wave vector relation of electrons in (a) first subband, and (b) third subband of a 1000 $\AA$ wide quantum wire. The wave vector is along the free propagation direction. The results are shown for three values of a magnetic field. The energy is calculated from the bulk conduction band edge.

[5] The y component of the electron envelope function for the first subband at a magnetic flux density of 0 and 10 tesla.

[6] The y component of the electron envelope functions for the first and third electronic subbands. The results are shown for the cases when (a) no magnetic field is present, (b) when a weak magnetic field is present and, finally, (c) when a strong magnetic field is present.

[7] Second order susceptibility as a function of the biasing magnetic field. The peak values of the susceptibility are 13.2 10^{-7} m/V, 1.5 10^{-7} m/V and 3 10^{-8} m/V for wire widths of 1000 $\AA$, 500 $\AA$ and 300 $\AA$ respectively. The results are shown for the wave vector k=0.01 / $\AA$ (fixed excitation frequency).

[8] Second order susceptibility as a function of the wire width for three values of the biasing magnetic field. The maximum values of the $\chi^{(2)}$ curves are the same as in Fig. 7. The narrow peaks at a wire width of ~ 200 Å are due to resonances occuring when either $\Omega_{ba} = \omega_1 + \omega_2$ or $\Omega_{ca} = \omega_2$ (see Equation 11 in the text).

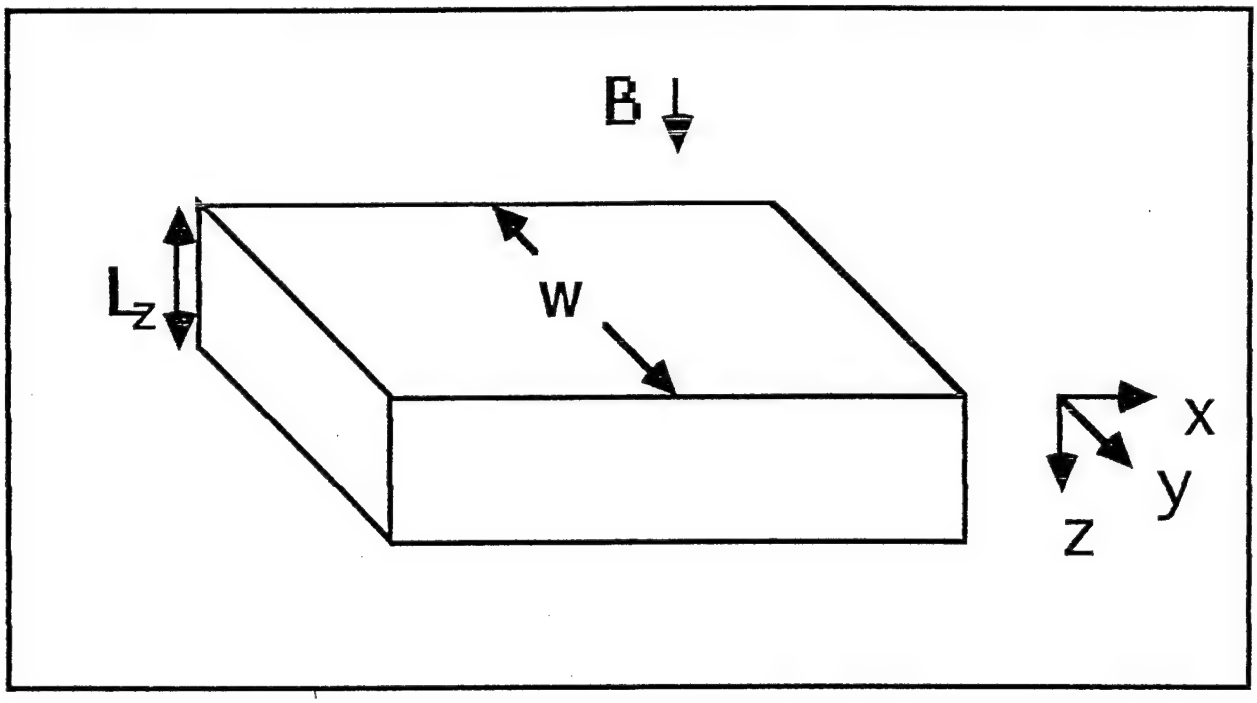

Fig. 1

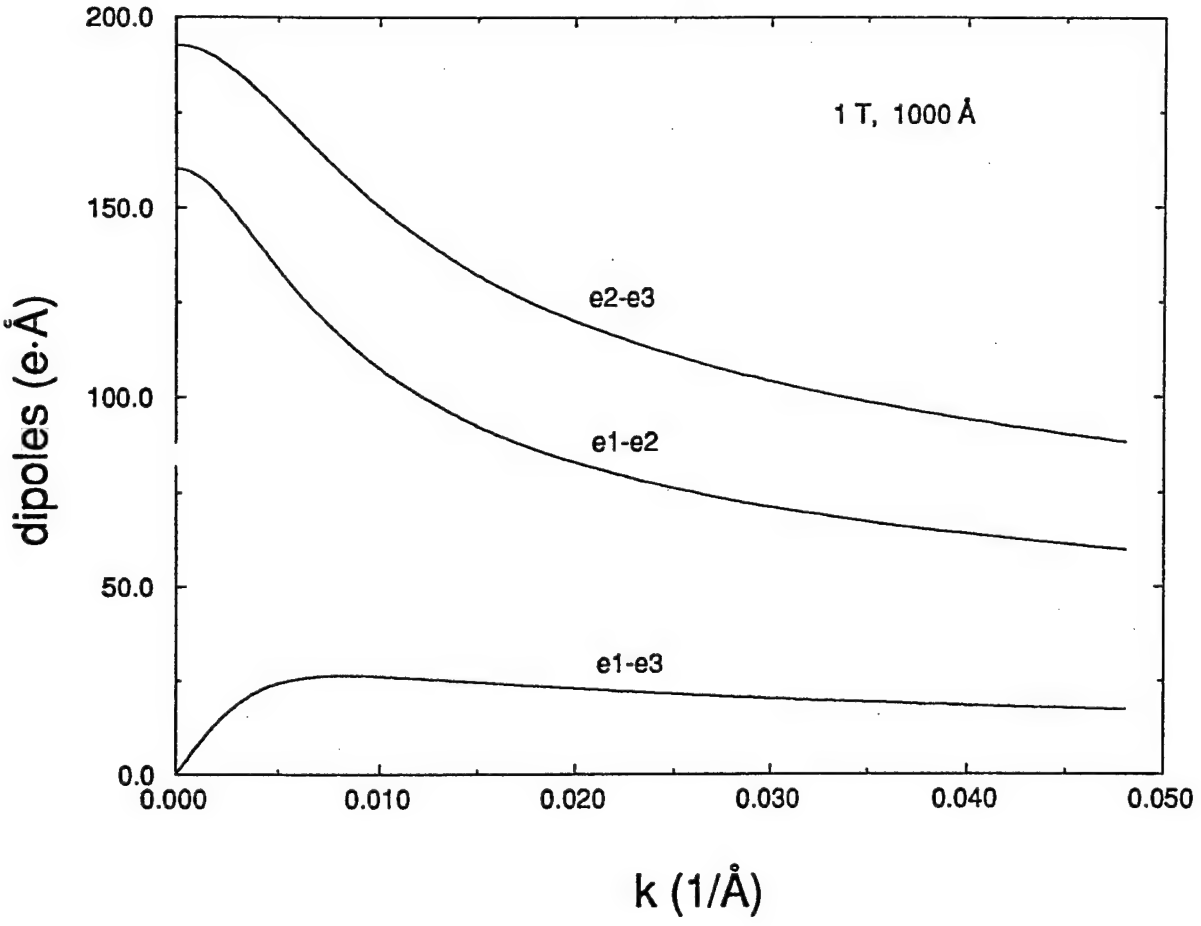
200.0
150.0
100.0
50.0
0.0
dipoles (e·Å)
1 T, 1000 Å
e2-e3
e1-e2
e1-e3
0.000
0.010
0.020
0.030
0.040
0.050
k (1/Å)

Fig. 2

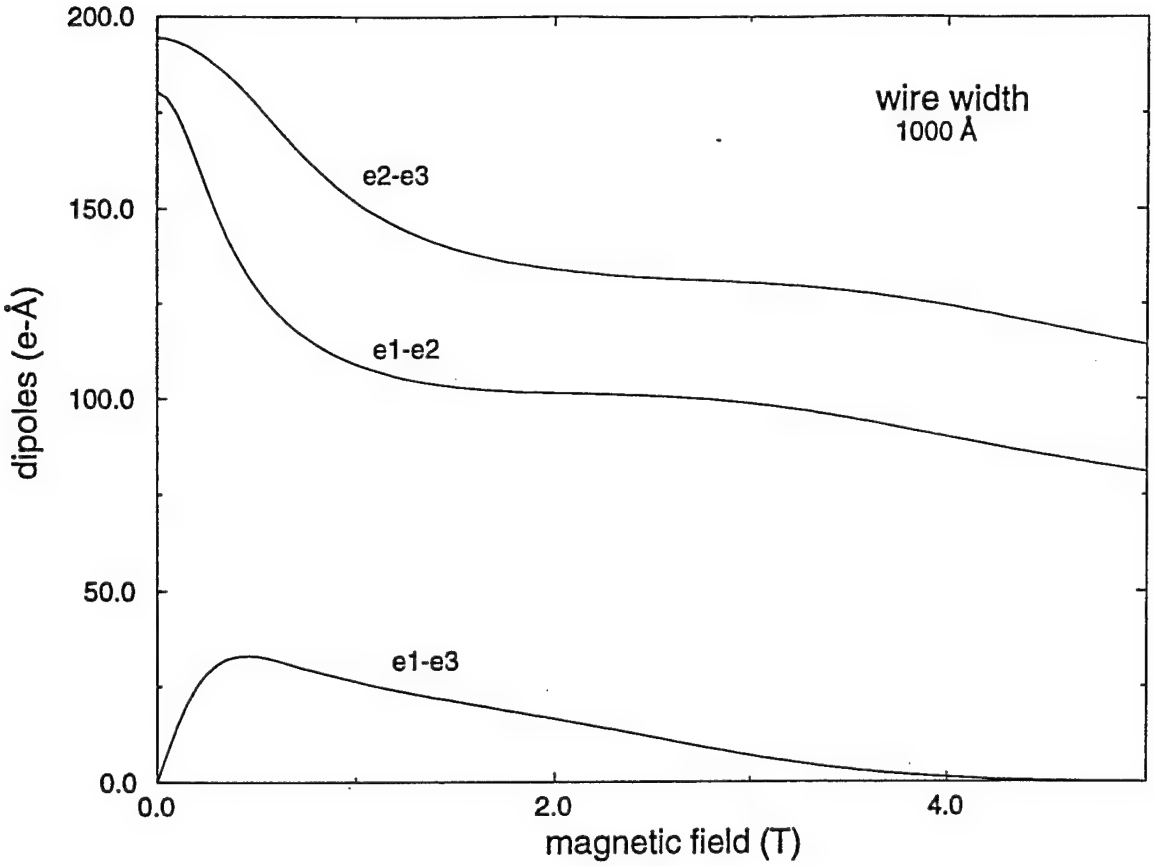
200.0
150.0
100.0
50.0
0.0
dipoles (e-Å)
wire width
1000 Å
e2-e3
e1-e2
e1-e3
0.0
2.0
4.0
magnetic field (T)

Fig. 3

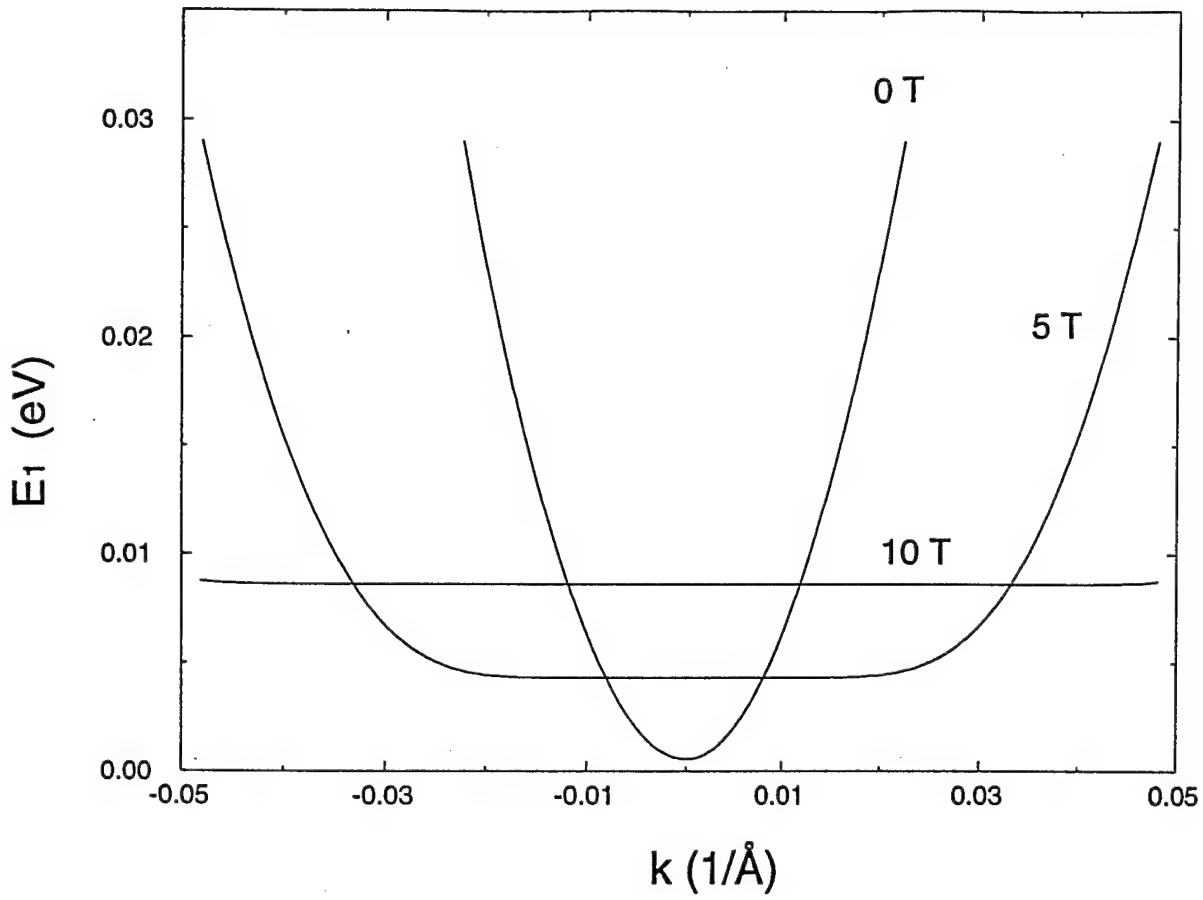

(a)

Fig. 4(a)

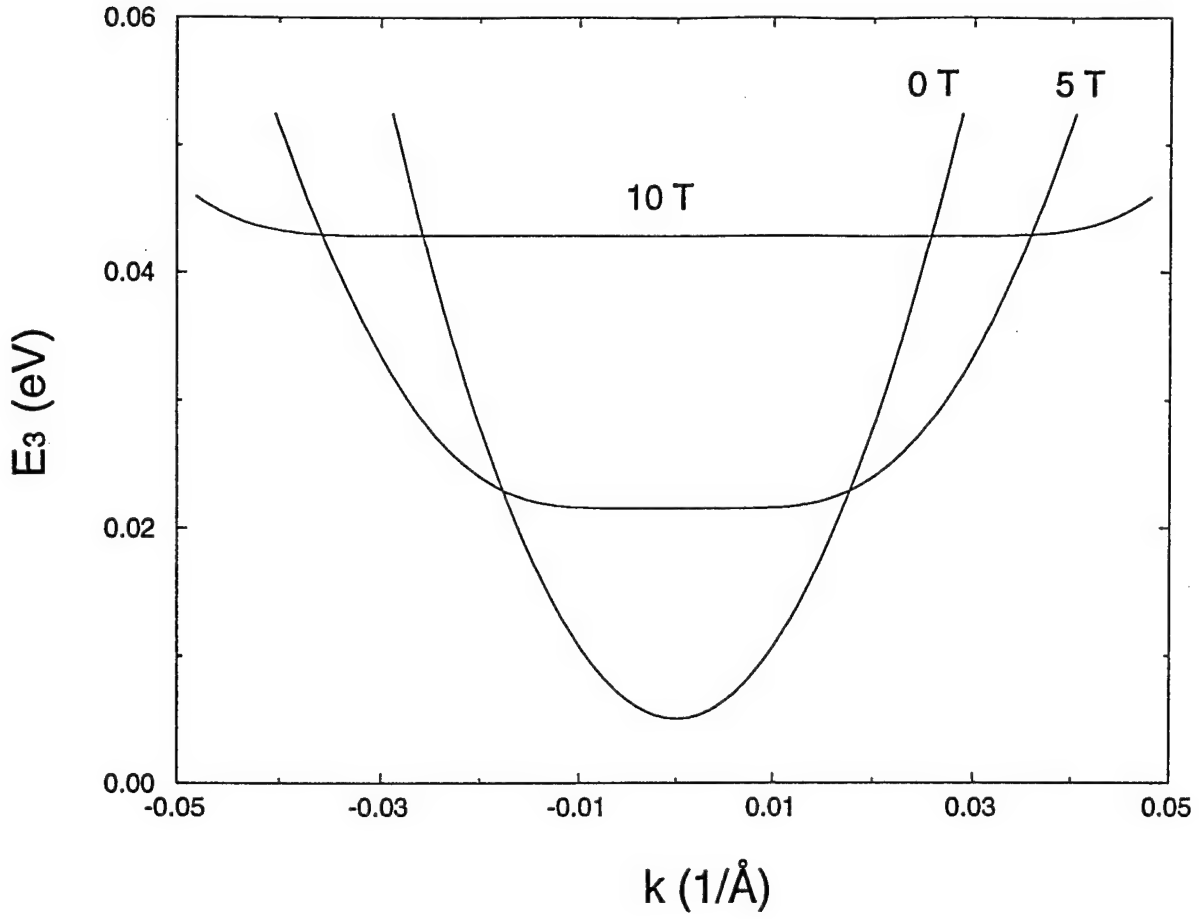

(b)

Fig. 4(b)

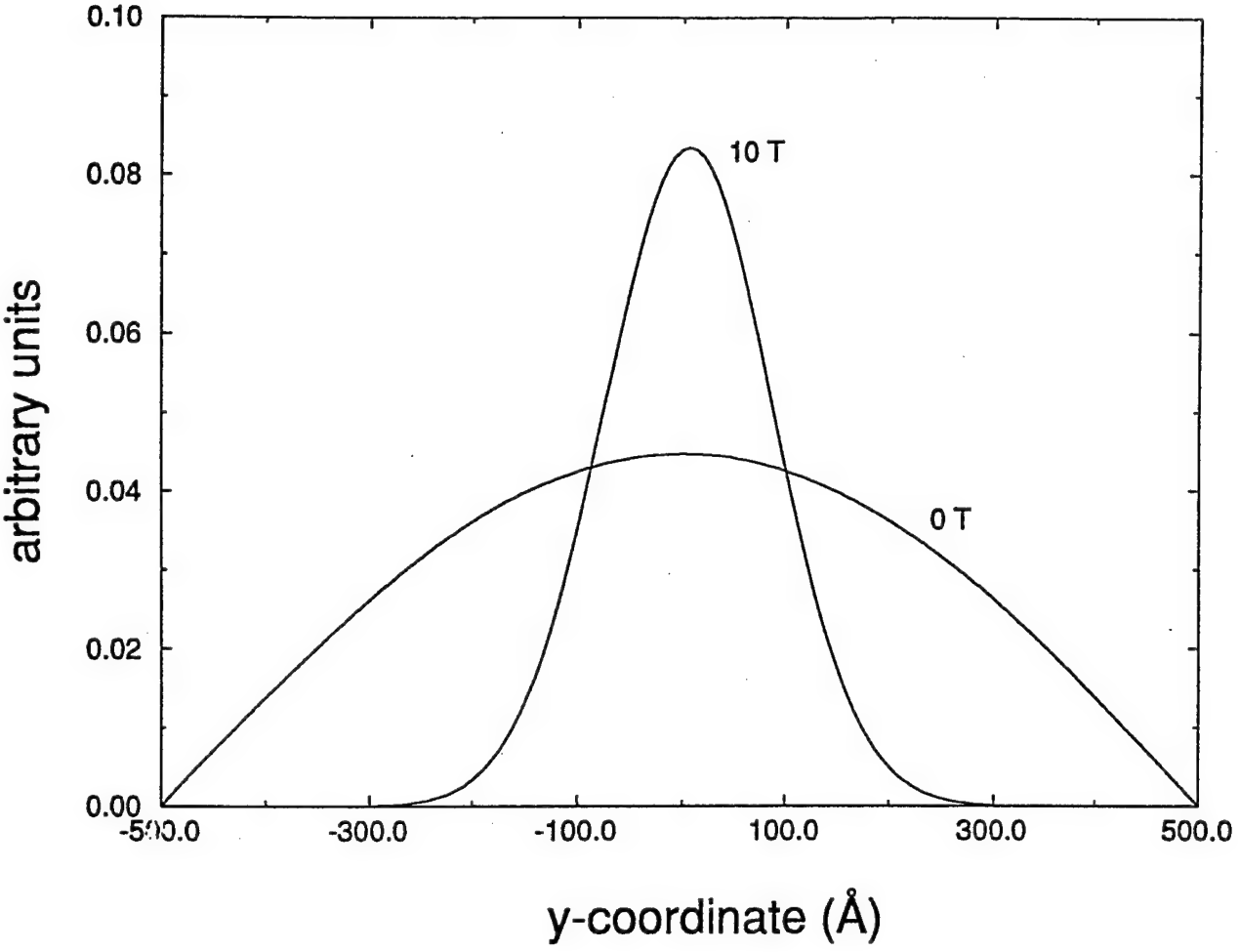
0.10
0.08
0.06
0.04
0.02
0.00
arbitrary units
10 T
0 T
-500.0
-300.0
-100.0
100.0
300.0
500.0
y-coordinate (Å)

Fig. 5

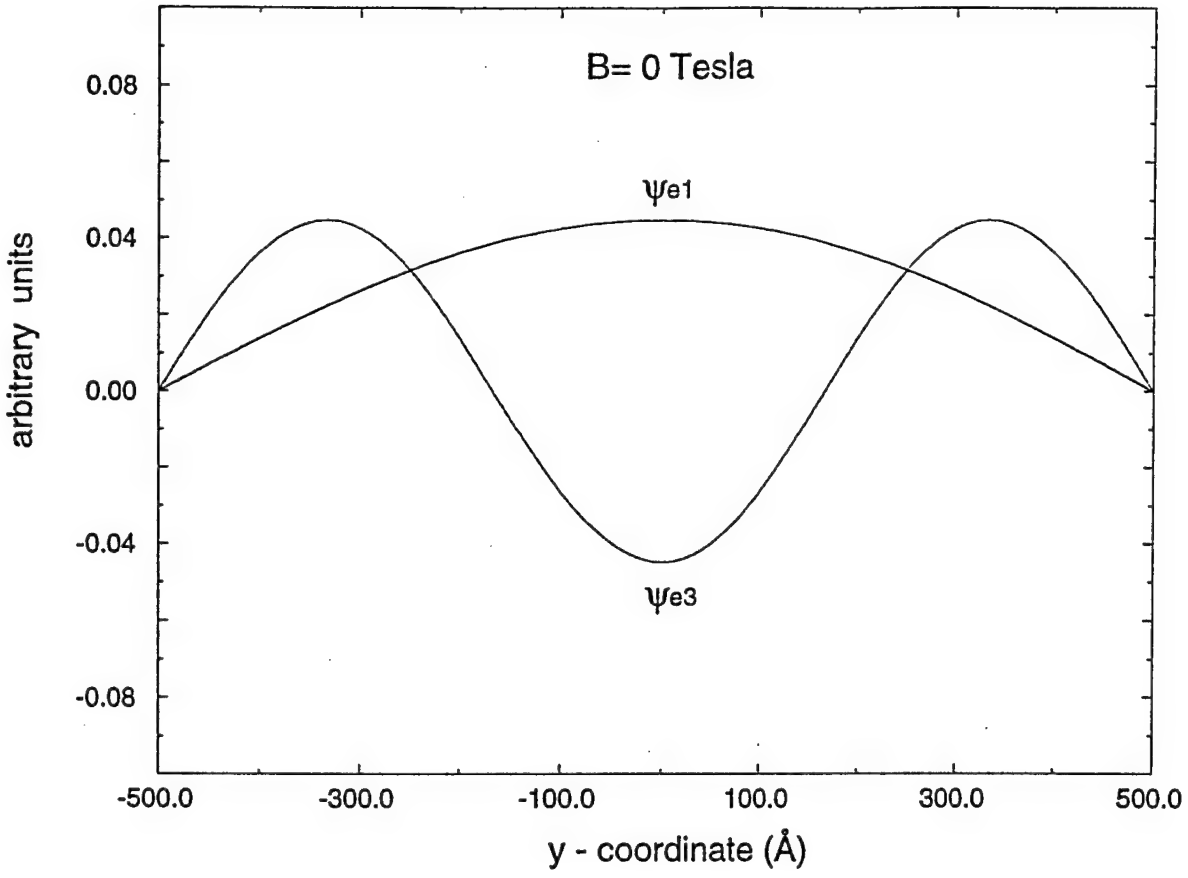
B= 0 Tesla
ψe1
ψe3
0.08
0.04
0.00
-0.04
-0.08
arbitrary units
-500.0
-300.0
-100.0
100.0
300.0
500.0
y - coordinate (Å)

(a)

Fig. 6(a)

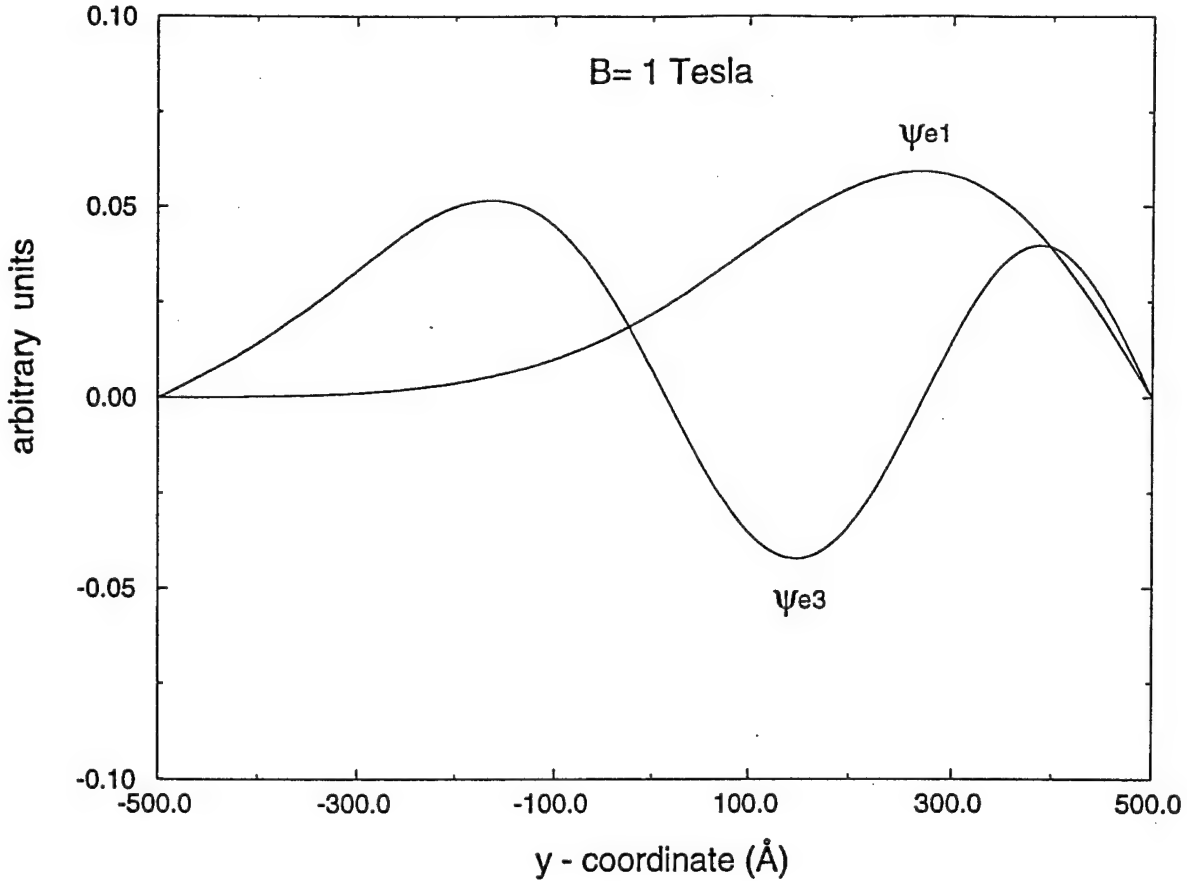
B= 1 Tesla
ψe1
ψe3
0.10
0.05
0.00
-0.05
-0.10
arbitrary units
-500.0
-300.0
-100.0
100.0
300.0
500.0
y - coordinate (Å)

(b)

Fig. 6(b)

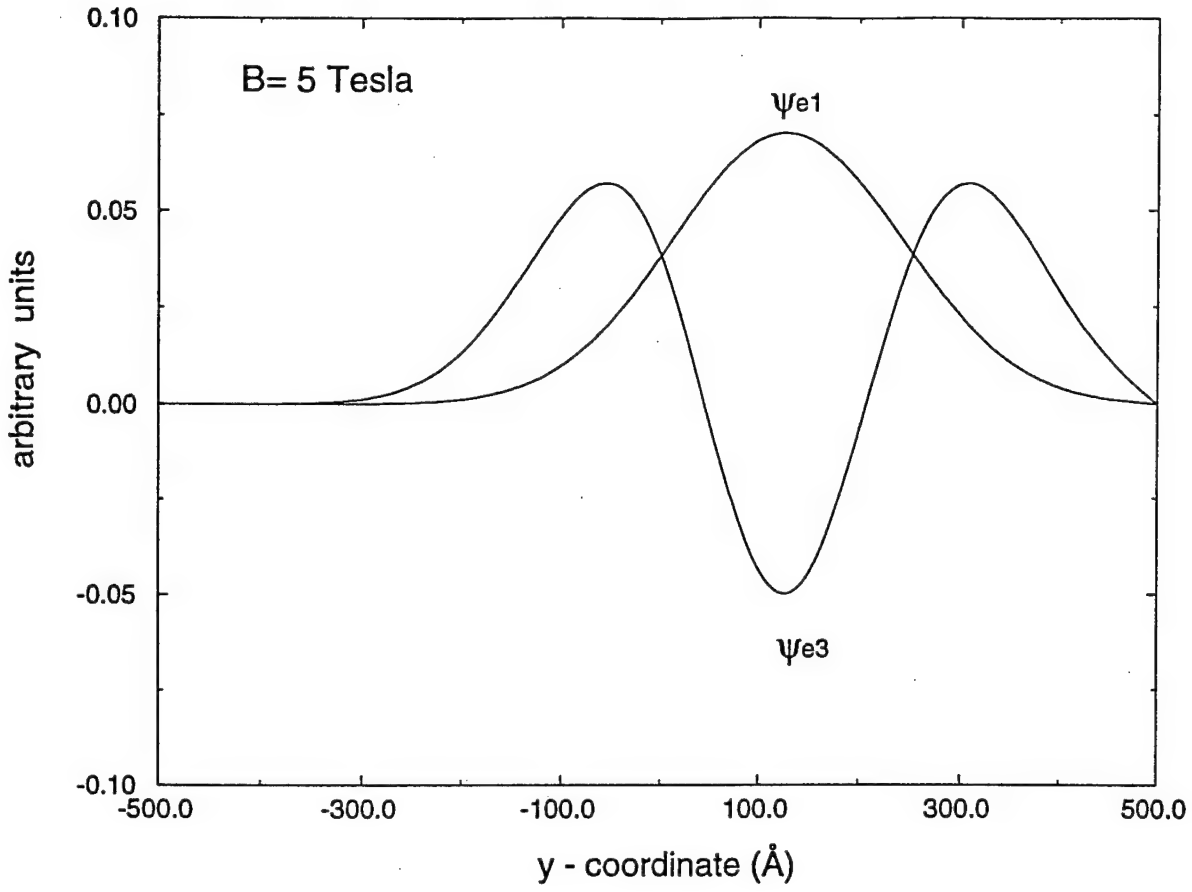
B= 5 Tesla
ψe1
ψe3
0.10
0.05
0.00
-0.05
-0.10
arbitrary units
-500.0
-300.0
-100.0
100.0
300.0
500.0
y - coordinate (Å)

(c)

Fig. 6(c)

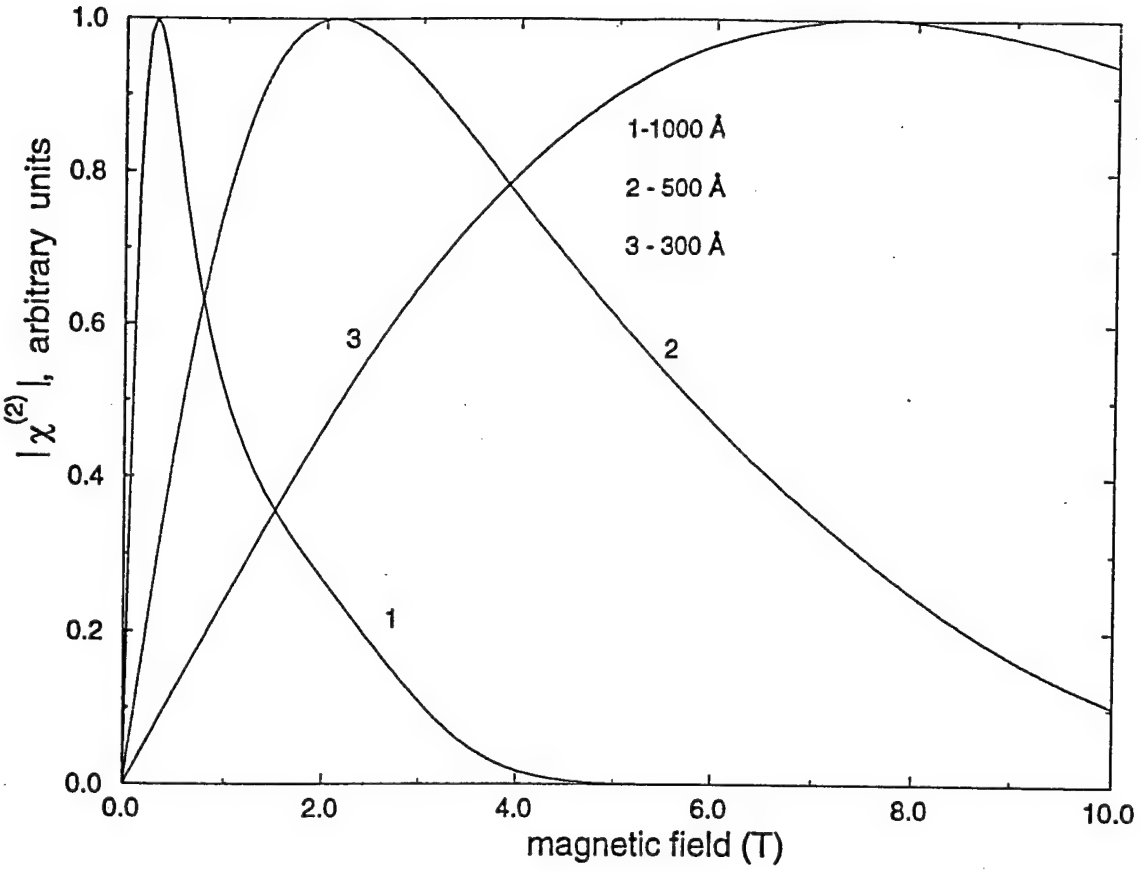
1.0
0.8
0.6
0.4
0.2
0.0
$|\chi^{(2)}|$, arbitrary units
0.0
2.0
4.0
6.0
8.0
10.0
magnetic field (T)
1-1000 Å
2 - 500 Å
3 - 300 Å
1
2
3

Fig. 7

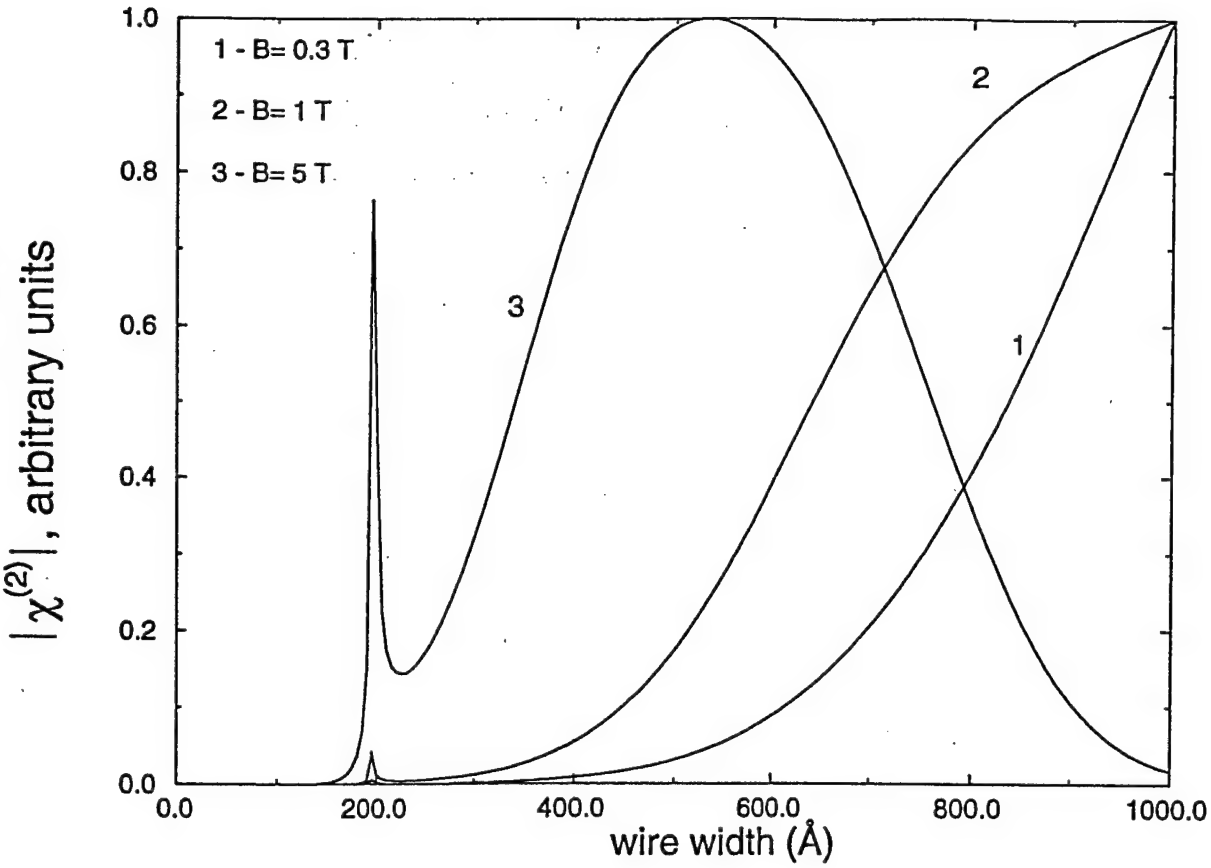
1 - B= 0.3 T
2 - B= 1 T
3 - B= 5 T
1
2
3
1.0
0.8
0.6
0.4
0.2
0.0
0.0
200.0
400.0
600.0
800.0
1000.0
wire width (Å)
$|\chi^{(2)}|$, arbitrary units

Fig. 8

Presented at the Fourth International Symposium on Quantum Confinement: Nanoscale Materials and Devices, 191st Meeting of the Electrochemical Society, Montreal, Canada, July 4-9, 1997

Confined Magneto-Polariton Propagation in Quantum Wires

A. Balandin and S. Bandyopadhyay
Department of Electrical Engineering
University of Nebraska
Lincoln, Nebraska 68588-0511 USA

Abstract

In this paper, we have calculated the refractive index of a quantum wire waveguide in the vicinity of an exciton-polariton resonance. The critical values of the exciton decay parameter, defining the onset of polariton transport regime, and the associated temperature were also found using the combination of a variational approach and a numerical solution. Our theoretical model allows us to include the effects of an external magnetic field. The results show that confinement of excitons to one dimension and the simultaneous application of a magnetic field may lead to the extension of the temperature and spatial limits of polariton transport. The magnetic field can be used to shift refractive index peaks in frequency thus providing a much-desired tuning capability.

I. Introduction

Exciton dynamics in semiconductor quantum confined structures has always been attractive because of its potential applications in optoelectronics. One of the most interesting phenomenon related to excitons in such structures is the formation of exciton-polaritons. In the spectral region around an exciton resonance, a photon, absorbed by a semiconductor, linearly couples with an exciton to create a polariton. Exciton polaritons have been studied extensively in quantum wells by measuring photoluminescence and reflection,

as well as by picosecond time-of-flight measurements.[1,2] It was shown that polaritons are much more stable in quantum wells than in bulk,[3] and they are expected to be even more stable in quantum wires since the exciton binding energy and oscillator strength tend to increase with reducing dimensionality.[4]

The formation of polaritons modifies the transport of light through the medium. In particular, the medium of propagation becomes substantially more transparent[5,6] and the group velocity of light propagating along the waveguide approaches the speed of light in vacuum.[7] At the same time, there is a possibility of controlling polariton transport with an external field. In this paper, we argue that a relatively weak magnetic field is particularly attractive for tuning polariton transport because it increases exciton oscillator strength thus *extending the polariton regime* of energy transfer, while an electric field would decrease exciton oscillator strength and quench polariton transport.

Although existing theoretical models recognize modification of polariton transport due to spatial confinement, they account for it by using heuristically peaked values for exciton oscillator strength and binding energy. The authors are not aware of any attempts to include an external field, particularly magnetic, into consideration.

In this work, we present a model for calculating the exciton-polariton critical decay parameter and the refractive index of a quantum wire around a polariton resonance in the presence of a magnetic field. The decay parameter determines the regime of polariton transport. To our knowledge, this is the first study where the exciton longitudinal-transverse (LT) splitting and exciton resonance frequency - which define the polariton dispersion - are found in a non-ad-hoc manner using the combination of a variational approach and an exact numerical solution of the Schrödinger equation. The calculations are performed for a quantum wire with finite lateral dimensions subjected to a magnetic field.

The rest of the paper is organized as follows. In section II, we establish the polariton dispersion relation used throughout the model; section III presents

the results of calculation of the LT splitting and oscillator strength of the exciton transition in a quantum wire subjected to a magnetic field; in section IV, we examine the exciton critical damping for the onset of the polariton transport regime and calculate refractive index of the wire in the vicinity of exciton resonance. Conclusions are given in section V of the paper.

II. Polariton dispersion

We consider an array of parallel $GaAs$ quantum wires of rectangular cross section separated by infinite potential barriers so that wavefunctions of the excitons from different wires do not overlap. In such a structure, excitons are free to move along the wire axes but are confined in perpendicular directions. The lateral dimension of each wire is comparable to the exciton Bohr radius. The cladding material is assumed to have a similar refractive index so that we can ignore image charges of the exciton and associated dielectric confinement effects. Under these conditions, the dispersion relation of the exciton polaritons can be determined for each separate wire. The multiple wire structure in this case merely forms a waveguide structure analogous to that considered in Ref. [8].

Most theoretical models for exciton polaritons (both in bulk material and nanostructures) embody a semi-classical approach and utilize the dispersion relation of a polariton derived for a single electric-dipole-active exciton resonance.[5,8] Here, we adopt the same philosophy and consider electromagnetic waves propagating through an array of quantum wires with a wavevector k parallel to the wire axis. This choice of the direction of propagation allows for a spatial dispersion of the light waves. In the opposite case of light propagating normal to the wire axis, the translational motion of excitons is suppressed and the spatial dispersion effects do not occur.

In the long-wave approximation ($kL_{y,z} < 1$, where $L_{y,z}$ are the wire lateral dimensions) the array interacts with light waves like an effective medium, and the dielectric function in the vicinity of an isolated exciton resonance can be

written as[9]

$$\epsilon(\omega,k) = \epsilon_o + \frac{2\epsilon_o\omega_{LT}\omega_o}{\omega_o^2 - \omega^2 + \hbar k^2\omega_o/M - i\omega\gamma}. \quad (1)$$

where ϵ_o is the background dielectric constant (contribution made by other resonances), ω is the frequency of light, ω_{LT} is the longitudinal-transverse splitting of the exciton related to its oscillator strength, ω_o is the exciton resonant frequency at $k = 0$, $M = m_e + m_h$ is the translational mass of an exciton, and $\Gamma \equiv \hbar\gamma$ is the exciton damping parameter. Here we have assumed parabolic wavevector dependence of the exciton frequency $\hbar\omega_t(k) = \hbar\omega_o + \hbar^2k^2/2M$, with the caveat that this is valid only in weak magnetic fields when the magnetic length l_m $(= \sqrt{\hbar/eB})$ is much larger than the transverse dimensions of the wire. In the formula above, the quantities $\omega_{LT} \equiv \omega_{LT}(L_{y,z}, B)$ and $\omega_o \equiv \omega_o(L_{y,z}, B)$ are the functions of the wire lateral dimensions and a magnetic field. The exciton damping constant is considered to be independent of the magnetic field since it is known that *energy-averaged* phonon-interaction rates in quantum wires are not terribly sensitive to a magnetic field. In any case, Eq. (1) is a good approximation when the magnetic field applied to the system is relatively weak: $l_m > L_{y,z}$. This equation relates ω and k and is the sought-after dispersion relation of a polariton.

Before we can go further into polariton transport properties, we have to calculate ω_{LT} and ω_o as the functions of wire dimensions $L_{y,z}$ and a magnetic flux density B. This is discussed in the next section.

III. Longitudinal-transverse splitting

Let us assume that the infinite potential barriers of the quantum wire are located at $y = \pm L_y/2$ and $z = \pm L_z/2$. A magnetic field is applied along the z-direction (see inset to Fig. 1). To simplify the calculations, we assume strong quantum confinement of the carriers which enables us to factorize an exciton wavefunction into the product of electron and hole wave functions. Moreover, we limit our consideration to systems with relatively large dielec-

tric constants so that all Coulomb interactions are strongly screened. This assumption, together with the hard-wall boundary condition, allows a coordinate separation. Consequently, the wave function of an exciton in the vicinity of subband bottom (with center-of-mass momentum $\hat{P_X} \approx 0$) is given by[4]

$$\begin{aligned} \Psi \equiv \Psi(x, y_e, y_h, z_e, z_h) &= g_t(x,\eta)\psi_e(y_e, z_e)\psi_h(y_h, z_h) \\ &= g_t(x,\eta)\phi_e(y_e)\phi_h(y_h)\chi_e(z_e)\chi_h(z_h), \end{aligned} \tag{2}$$

where $g_t(x,\eta)$ is chosen to be the Gaussian-type "orbital" function:

$$g_t(x,\eta) = \frac{1}{\eta^{1/2}}(\frac{2}{\pi})^{1/4} e^{-(x/\eta)^2} \tag{3}$$

in which η is a variational parameter which defines the exciton size ("longitudinal length"), and x is the relative electron-hole coordinate. The subscripts in $x_{e,h}, y_{e,h}, z_{e,h}$ identify them as electron or hole coordinates. The variables $\chi_{e,h}(z_{e,h})$ are the z-components of the wave functions which are not affected by the magnetic field. They are given by particle-in-a-box states. The electron and hole wave functions along the y direction, $\phi_{e,h}(y_{e,h})$, are to be calculated numerically when a magnetic field is present. This is done by solving the one-particle Schrödinger equation using a finite difference method.[10]

In order to find an exciton "length" η, we use the variational approach of minimizing the energy given by $< \Psi|\hat{H^X}|\Psi >$, where the exciton Hamiltonian is

$$\begin{aligned} \hat{H^X} &= \frac{\hat{P_X}^2}{2M} + \frac{\hat{p_x}^2}{2\mu} + \frac{\hat{p_{y_e}}^2 + \hat{p_{z_e}}^2}{2m_e} + \frac{\hat{p_{y_h}}^2 + \hat{p_{z_h}}^2}{2m_h} \\ &+ \frac{eB(y_e - y_h)}{M}\hat{P_X} + eB(y_e/m_e + y_h/m_h)\hat{p_x} + \frac{e^2B^2}{2}(y_e^2/m_e + y_h^2/m_h) \\ &+ U_C(x_e, x_h, y_e, y_h, z_e, z_h) + U_S(y_e, y_h, z_e, z_h). \end{aligned} \tag{4}$$

Here we have chosen the Landau gauge $\vec{A} = (-By, 0, 0)$. The quantities m_e, m_h, are the effective masses of electrons and holes respectively, $1/\mu (= 1/m_e + 1/m_h)$ is the exciton's reduced mass, $U_C(x_e, x_h, y_e, y_h, z_e, z_h)$ is the electron-hole Coulomb interaction term, $U_S(y_e, y_h, z_e, z_h)$ is the spatial confinement potentials for electrons and holes along y and z directions.

Details of the variational procedure, calculations of η, etc., can be found in some of our earlier work.[4]

We can find the oscillator strength of the exciton transition α_o and the LT splitting by evaluating the momentum matrix element which is given as

$$|M_{cv}^X|^2 = |\frac{1}{2\pi}\int dk g_t(x,\eta) M_{cv}(k)|^2, \tag{5}$$

where M_{cv} is the valence-band to conduction-band dipole matrix element. and k is again the wave vector along the unconfined direction of the wire. When the k dependence of M_{cv} is neglected, Eq. (5) reduces to the simple expression

$$|M_{cv}^X|^2 = |M_{cv}|^2 |g_t(x=0,\eta)|^2. \tag{6}$$

The exciton oscillator strength per unit length can be written as follows

$$\alpha_o = \frac{2}{m_o \hbar\omega_o}|M_{cv}^X|^2. \tag{7}$$

Here $\hbar\omega_o = E_G + E_{e1} + E_{hh1} - min < \Psi|\hat{H}|\Psi >$ is the exciton ground state energy, E_G is the fundamental bandgap of the bulk material, E_{e1}, E_{hh1} are the lowest electron and the highest heavy hole magneto-electric subband bottom energies in a quantum wire measured from the bottom of the bulk conduction band and the top of the bulk valence band, and m_o is the free electron mass. The exciton LT splitting $\Omega_{LT} \equiv \hbar\omega_{LT}$ can now be written as

$$\hbar\omega_{LT} = \frac{2\pi\alpha_o\hbar\omega_o}{\epsilon_o} = \frac{4\pi}{m_o\epsilon_o}|M_{cv}^X|^2. \tag{8}$$

In Fig. 1 we present the LT splitting calculated for different wire dimensions and magnetic flux densities. The physical parameters used for the calculations correspond to a $GaAs$ quantum wire with $\epsilon = 12.9\epsilon_o$, $E_G = 1.515$eV, $m_e = 0.067m_o$, $m_h = 0.5m_o$, where m_o is free electron mass and ϵ_o is electrical permitivitty of free space, E_{e1}, E_{hh1} are calculated numerically following the prescriptions of Refs. [10, 11]. One can see from the figure, that the exciton splitting is sensitive to the spatial confinement and increases by about 60 % when the wire width decreases from 500 Å to 50 Å. A magnetic field

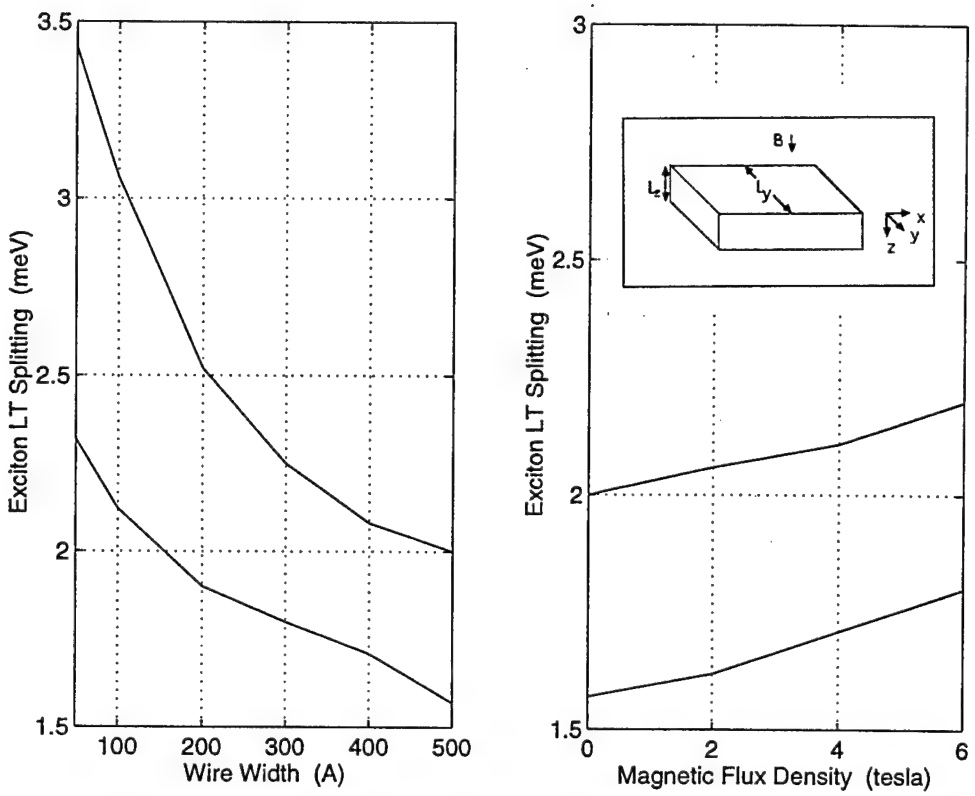

Figure 1: Longitudinal-transverse splitting of an exciton as a function of wire width (left pannel); and as a function of magnetic flux density for a 500 Å wide wire (right panel). For both panels, the upper and lower curves correspond to 200 Å and 500Å thick wires, respectively.

also increases the splitting (and oscillator strength) thus making the exciton polaritons more stable.

IV. Refractive index and decay parameter

The experimentally observed higher transparency of the medium of propagation in polariton transport regime has been attributed to certain features of the dispersion law for excitonic polaritons and to the fact that polariton transport by itself cannot cause true absorption. In order for absorption to occur, polaritons have to be scattered inelastically, e.g., by phonons. The onset of polariton transport through some structure is governed by the exciton

polariton coherence length related to the exciton decay parameter $\Gamma \equiv \hbar\gamma$. It has been shown, both experimentally and theoretically, that there exists a critical value of the exciton decay parameter, Γ_c, which corresponds to a change in the nature of absorption.[5,6] Here we intend to examine the influence of spatial confinement and a magnetic field on this parameter and calculate the refractive index of a quantum wire in the polariton regime.

Confining ourselves to the TE waves relevant to light propagation in the medium, we can write polariton dispersion in the following form

$$\epsilon(\omega, k) = \frac{c^2k^2}{\omega^2} \equiv n^2. \tag{9}$$

Combining this equation with Eq. (1), and after some algebra, we obtain

$$\frac{\hbar\omega_o\omega^2}{Mc^2}n^4 + (\omega_o^2 - \omega^2 - i\gamma\omega - \epsilon_o\frac{\hbar\omega_o\omega^2}{Mc^2})n^2 - \epsilon_o(\omega_o^2 - \omega^2 - i\gamma\omega + 2\omega_{LT}\omega_o) = 0. \tag{10}$$

This equation can be solved for two sets of the refractive indices, n_1 and n_2, corresponding to different transverse polariton branches. It also follows from Eq. (10) that if the damping parameter Γ becomes larger than the critical value

$$\Gamma_c \equiv \Gamma_c(L_{y,z}, B) = 2\hbar\omega_o\sqrt{\frac{2\epsilon_o\hbar\omega_{LT}}{Mc^2}}, \tag{11}$$

then only one light wave mode can propagate in the medium, since there is only one real solution for n. This is the boundary of the polariton propagation regime. The critical value comes about because of the term $\hbar k^2\omega_o/M$ associated with spatial dispersion effects. The physical importance of the critical damping can be illustrated by the following example. It was shown[6] that when the damping exceeds the critical value, the integral absorption is independent of Γ and proportional to the oscillator strength of transitions (non-polariton regime). When $\Gamma < \Gamma_c$, the integral absorption depends on Γ linearly, and decreases with decreasing damping.

Using the results from the previous section, we can calculate Γ_c for different values of wire widths and magnetic field. In Fig. 2 we present the critical exciton damping (decay) parameter as a function of wire width. It is

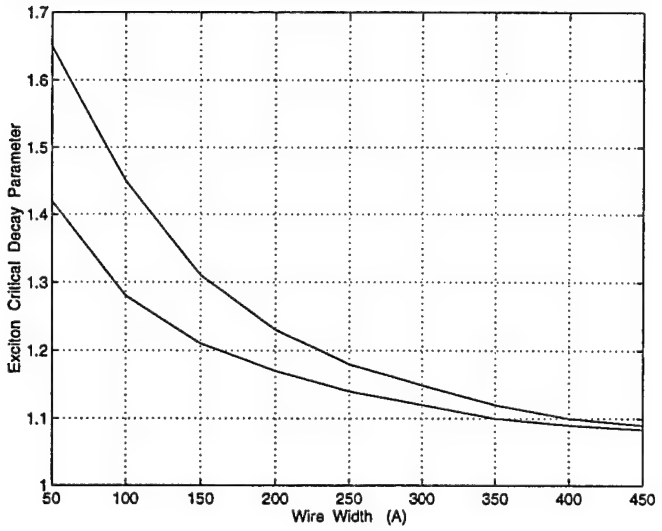

Figure 2: The critical exciton decay parameter (damping) as a function of wire width. The upper and lower curves correspond to the thickness along the z-direction of 200 Å and 300 Å, respectively.

normalized by the value of the decay parameter of a very wide wire (L_y=700 Å) which is wide enough to be approaching the 2D limit. For this wide wire, $\Gamma_c \approx 1.01$ meV. Combining Eqs. (7, 8, 11) we can also estimate the magnetic field dependence of the critical decay parameter using the formula $\Gamma_c(B)/\Gamma_c(0) = (\omega_o(B)/\omega_o(0))\sqrt{\omega_{LT}(B)/\omega_{LT}(0)}$. Although not shown here, the magnetic field dependence of the critical parameter is weak; it increases only 5% at a magnetic flux density of 5 tesla. The strong dependence of the critical damping on the wire width may lead to a pronounced modification of the integral (total) absorption of systems consisting of a number of narrow quantum wires.

We can now find a temperature which corresponds to the critical damping from the relation $\Gamma_c = \Gamma_o + \Gamma_{ph}(T_c)$, where Γ_o is the damping associated with the impurity and other temperature-independent elastic scattering, while $\Gamma_{ph}(T_c)$ represents interactions with acoustic and optical phonons. By increasing Γ_c one can increase T_c which defines the onset of polariton transport and, as a consequence, higher transparency.

Since there is no data available on quantum wires, we assume that the half-width at half maximum (HWHM) of the exciton resonance in a quantum wire is the same as in a 200 Å thick $GaAs/AlGaAs$ quantum well. Using the approximation of Ref [11] we may write for our case (energy units are meV)

$$\Gamma_c = \Gamma_o^+ + 0.00147T_c + 4.0(e^{\hbar\omega_{ph}/k_BT_c} - 1)^{-1} + \Gamma_{imp}e^{-E_b/k_BT_c}, \qquad (12)$$

where $\hbar\omega_{ph} = 36$ meV is a longitudinal optical phonon energy, k_B is the Boltzman constant, $E_b \approx 10$ meV is the everage binding energy for donor impurities in GaAs, $\Gamma_{imp} = 0.75$ meV is a linewidth due to fully ionized impurity scattering, $\Gamma_o^+ \approx 0.45$ meV is the linewidth due to inhomogeneous fluctuations of the wire thickness. The values chosen for the various parameters are typical of experimental systems reported in the literature.

Table I. Critical temperature vs. wire width

$L_y, (\AA)$	500	300	100
$\Gamma_c, (meV)$	1.09	1.16	1.45
$T_c, (K)$	118	138	169

Solving Eq. (12) for the temperature T_c for each value of $\Gamma_c(L_{y,z}, B)$, we are able to obtain the dependence of the critical temperature on the wire width. The thickness of the wire, L_z, was fixed at 200Å for this calculation. As one can see from Table I, that the critical temperature T_c, that defines the onset of polariton transport, can be controlled over a wide range by changing the wire width L_y.

Now let us assume that $\Gamma < \Gamma_c$ (exciton polariton regime) and find the refractive index of the quantum wire in the vicinity of polariton resonance. In order to do this, we make use of Pekar's additional boundary condition (total polarization is zero at the boundary) and write the effective refractive index as

$$n_{eff} = \frac{n_1 n_2 + \epsilon_o}{n_1 + n_2}. \qquad (13)$$

In Fig. 3, we present the real (upper panel) and imaginary (lower panel) parts of the refractive index of a quantum wire with thickness 200 Å and

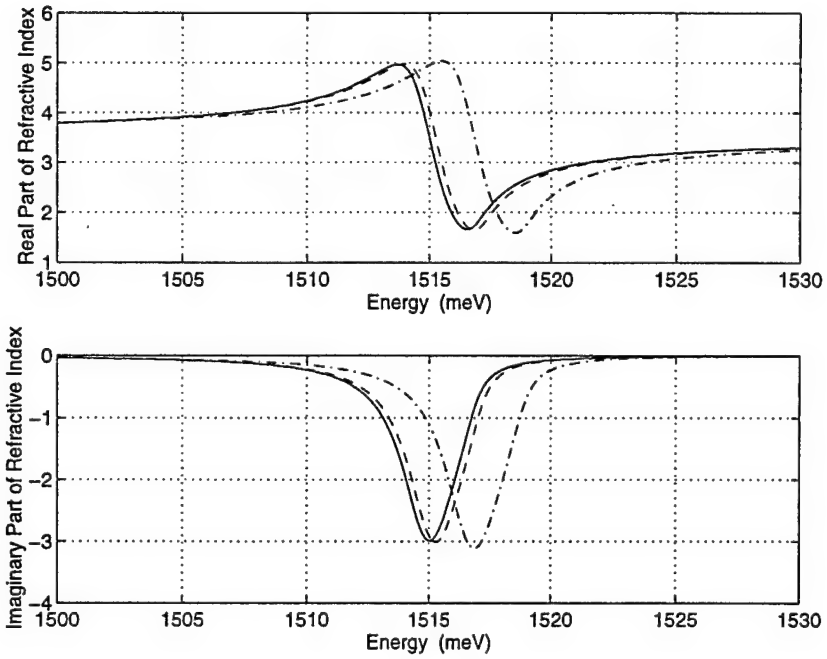

Figure 3: The refractive index of the wire in the vicinity of exciton resonance. The solid, dashed and dash-dotted curves correspond to a 0, 1, and 5 tesla magnetic flux density, respectively.

width 300 Å. An external transverse magnetic field is applied along the thickness. The decay parameter is chosen to be $\Gamma = 1\text{meV}$ which is less than Γ_c for the given wire dimensions. As one can see from the figure, the maximum of the real part of the refractive index is as large as 4.97 at zero field and 5.04 at 5 tesla magnetic field. It is about 1.4 times larger than that of the bulk material. The refractive index attains its maximum value at a photon energy slightly lower than the resonance energy $\hbar\omega_o(L_{y,z}, B)$ at any given magnetic field B. The minimum value of the refractive index, which is 1.66 for zero field and 1.59 for 5 tesla, is located at a frequency of $\omega_o(L_{y,z}, B) + \omega_{LT}(L_{y,z}, B)$. It is interesting to note that efficient waveguiding can be achieved in the spectral range where the real part of the refractive index increases. However, in this region, the imaginary part of the refractive index (extinction coefficient) also peaks and this increases the transmission

loss. The mitigating factor in all this is that the two peaks do not occur at exactly the same frequency so that an optimal region for optical waveguiding exists.

A magnetic field of 5 tesla blue-shifts the refractive index peak by 2 meV. According to Ref. [13], approximately the same magnitude of an opposite red-shift can be achieved by applying an electric field of about 4×10^4 V/cm. However, the electric field leads to a 15-20 % increase in exciton radius and a concomitant decrease in the binding energy. This, in turn, causes a decrease in exciton LT splitting and makes exciton polaritons less stable. Note that while an electric field will tend to ionize an exciton by pulling the electron and hole apart, a magnetic field has the opposite effect. It squeezes the electron and hole even tighter together and increases the binding energy. Therefore, the magnetic field can be used to advantage in this context since it shifts the peaks in frequency while actually increasing polariton stability. This frequency tuning capability, acquired without a penalty in polariton stability, is obviously very attractive and has device applications.

VI. Conclusions

In this paper, we have calculated the refractive index of a quantum wire waveguide in the vicinity of polariton resonance. The critical values of the exciton decay parameter and associated temperature were also found taking into account the effects of spatial confinement and an external magnetic field. Our results show that confinement of excitons to one dimension and the application of a magnetic field may lead to the extension of temperature and spatial limits of polariton transport. The magnetic field can be used to shift refractive index peaks in frequency - without compromising polariton stability - thus providing a much-desired tuning capability.

Acknowledgement: This work was supported by the US Army Research Office under grant number DAAH04-95-1-0527. The authors are indebted to the Electrochemical Society, Inc. for providing travel support.

REFERENCES

[1]. E.L. Ivchenko, V.P. Kochereshko, P.S. Kopev, V.A. Kosobukin, I.N. Uraltsev, D.R. Yakovlev, *Solid State Commun.*, **70**, 529 (1989).

[2]. K. Ogawa, T. Katsuyama, H. Nakamura, *Phys. Rev. Lett.*, **64**, 796 (1990).

[3]. T. Katsuyama, K. Ogawa, *Semicond. Sci. Technol.*, **5**, 446 (1990).

[4]. A. Balandin and S. Bandyopadhyay, *Phys. Rev. B*, **52**, 8312 (1995); A. Balandin and S. Bandyopadhyay, *Phys. Rev. B*, **54**, 5712 (1996).

[5]. V.A. Kosobukin, R.P. Seisyan, S.A. Vaganov, *Semicond. Sci. Technol.*, **8**, 1235 (1993).

[6]. N. Akhmediev, *Zh. Eksp. Teor. Fiz.*, **79**, 1554 (1980).

[7]. K. Oimatsu, T. Iida, S. Nishimura, K. Ogawa, T. Katsuyama *Journal of Luminescence*, **48**, 713 (1991).

[8]. T. Katsuyama, S. Nishimura, K. Ogawa, T. Sato, *Semicond. Sci. Technol.*, **8**, 1226 (1993).

[9]. see for example E.L. Ivchenko in *Excitons* (North-Holland, Amsterdam, 1992), edited by E.I. Rashba and M.D. Sturge, p.141.

[10]. S. Chaudhuri, S. Bandyopadhyay, *J. Appl. Phys.*, **71**, 3027 (1992).

[11]. A. Balandin and S. Bandyopadhyay, *J. Appl. Phys.*, **77**, 5924 (1995).

[12]. J. Lee, E.S. Koteles, M.O. Vassell, *Phys. Rev. B*, **33**, 5512 (1986).

[13]. D.A.B. Miller, D.S. Chemla, T.C. Damen, A.C. Gossard, W. Wiegmann, T.H. Wood, C.A. Burrus, *Phys. Rev. Lett.*, **53**, 2173 (1984); *Phys. Rev. B*, **32**, 1043 (1985).

Presented at the Fourth International Symposium on Quantum Confinement: Nanoscale Materials and Devices, 191st Meeting of the Electrochemical Society, Montreal, Canada, July 4-9, 1997

Infrared Second Harmonic Generation in Magnetic-Field-Biased Quantum Wires

A. Svizhenko, A. Balandin, and S. Bandyopadhyay
Department of Electrical Engineering
University of Nebraska
Lincoln, Nebraska 68588

Abstract

We have theoretically studied non-linear frequency conversion in a semiconductor quantum wire biased with a magnetic field. In these systems, efficient second harmonic generation occurs as a result of the large value of the second-order dielectric susceptibility $\chi^{(2)}$ arising from dipole transitions between magneto-electric subbands. The magnitude and peak frequency of $\chi^{(2)}$, as well as the absorption and refractive index associated with $\chi^{(2)}$, can be tuned with the magnetic field. This allows one to achieve low insertion loss and efficient phase matching by manipulating the absorption and refractive index with a magnetic field.

I. Introduction

Most ordinary solids are not efficient frequency converters because they exhibit extremely small even-order dielectric susceptibilties. Ideally, even-order susceptibilities vanish in solids with inversion symmetry.[1] Consequently, a semiconductor structure can exhibit a large value of the second order susceptibility $\chi^{(2)}$ only if the inversion symmetry of the conduction-band potential is broken artificially either by an external electric field, or by the intentional growth of an asymmetric structure. Obviously, the former is the preferred method since an electric field can be varied continuously and

this allows one to tune the degree of symmetry-breaking and the magnitude of $\chi^{(2)}$. However, an electric field has a practical shortcoming. In a quantum confined structure, it tilts the potential barriers confining the photogenerated carriers. As a result, carriers can escape by tunneling or thermionic emission and this is especially serious in *GaAs/AlGaAs* systems where the barrier height is relatively small. Indeed, it has been pointed out that the electronic states in a quantum confined system biased by a transverse electric field are never true bound states since the particles can always lower their energy by escaping from the well[2]. Consequently, optical transitions (and their higher order harmonics) associated with these states have inconveniently large linewidths and small oscillator strengths.

Recently, we proposed magnetostatic biasing as an attractive alternative to mitigate this problem.[3] We showed that a magnetic field can break inversion symmetry in a quantum wire without tilting potential barriers. A transverse magnetic field, applied to a wire, exerts a Lorentz force on an electron moving along the length. As a result, its wave function (in any magneto-electric subband) will be skewed towards one edge of the wire. This skewing does not tilt potential barriers to first order (the barriers may tilt slightly because of a second-order effect associated with space-charges and the self-consistent (Hall) electric field). However, it effectively breaks inversion symmetry since it causes net charges to accumulate at either edge of the wire. This leads to a non-vanishing even-order susceptibility in an otherwise symmetric structure. The skewing has another subtle effect. The degree to which the wave function is skewed is *different in different subbands* since an electron has different kinetic energies (and hence experiences different Lorentz forces) in different subbands. As a result, transitions between subbands whose wave functions have the same parity - which are forbidden without a magnetic field - are now allowed since the parities are altered by different amounts in different subbands. This effect has some similarity with the quantum confined Lorentz effect (QCLE) previously examined by us[4] in

the context of interband transitions between conduction and valence band states.

In this paper, we first calculate the second-order susceptibility $\chi^{(2)}$ in a symmetric quantum wire whose inversion symmetry (along the width) has been broken with a magnetic field. We restrict ourselves to narrow GaAs wires with a width of about 150$\mathring{A}$. The energy spacing between the first and second subband is $\Delta E_{12} \approx 72$ meV. This choice of the wire dimension puts the resonant frequency (for transitions between the lowest subbands) in the mid-infrared spectral region. The wavelength of the second harmonic component of this transition is about 8.6 μm. Here we will be mainly interested in $\chi^{(2)}$ arising from resonant and near-resonant inter-subband transitions which are governed by the interplay of dipoles and resonant excitations. In contrast, Ref. [3] focussed on the off-resonance regime which was governed solely by the dipoles. We will also calculate absorption and refractive index in the frequency region of interest for both pump and second harmonic frequencies and show how they can be manipulated with an external magnetic field to realize low insertion loss and efficient phase matching.

The rest of the paper is organized as follows. In the next section, we describe the theoretical formulation, followed by results. Finally, in section IV, we present the conclusions.

II. Theory

We consider a generic *GaAs* quantum wire (as shown in the inset of Fig. 1) with a magnetic field applied along the z direction. The thickness along the z direction is so small (and consequently the subband separation in energy in this direction is so large) that for the range of photon energies considered, an electron cannot be excited (by real transition) into a subband which has more than two nodes along the z-direction. In other words, such a transition will not be accessible in energy. This restriction, coupled with the fact that a magnetic field does not affect the z-component of the electron wave function, allows us to drop the z-component from further consideration. The width

of the wire along the y-direction is however large enough ($W = 150\mathring{A}$) that subbands with more than two nodes along the y-direction are accessible in energy.

In systems without inversion symmetry, the lowest order optical nonlinearity is of the second order and is expressed by

$$\vec{P^{(2)}}(\vec{k},\omega) = \chi^{(2)}(\omega;\omega_1,\omega_2)\vec{E_1}(\vec{k_1},\omega_1)\vec{E_2}(\vec{k_2},\omega_2), \qquad (1)$$

where $\vec{P}$ is the polarization caused by two electric fields $\vec{E}_1$ and $\vec{E}_2$ that are associated with the electromagnetic fields of either two frequency components of the same light beam or two different coherent beams with frequencies ω_i and wave vectors $\vec{k_i}$. It is well known that the third-ranked tensor $\chi^{(2)}$ will vanish in any structure with inversion symmetry. A quantum confined structure may lack inversion symmetry for two main reasons. (i) the semiconductor material by its intrinsic chemical and crystalline structure may lack inversion symmetry,[5] and this is the case in most III-V, II-VI, and I-VII compounds along certain crystallographic directions, or (ii) the quantum confining potential well may be asymmetric (e. g. triangular potential well, asymmetric double square well potential, etc.). In the first case, the asymmetry is related to the intracell charge asymmetry and is not affected by the confinement since the latter extends over several unit cells. In the second case, the asymmetry is artificially imposed and therefore can be engineered. It clearly depends on the confining potential. Insofar as an applied electric field can alter the potential, it can change the degree of symmetry-breaking and hence modulate $\chi^{(2)}$.

In the present work we restrict ourselves to the second case and do not consider intrinsic second order nonlinearities which can be quite large in some materials (the nonlinear susceptibility of bulk GaAs is $\chi^{(2)}_{14}$=3.8 10^{-10} m/V).[6] As mentioned before, we avoid the use of a symmetry-breaking electric field since it promotes carrier escape. Instead, we consider a magnetic field. Although a magnetic field does not directly affect the potential, it leads to an *uneven charge distribution* along the width ($y - axis$) of the wire because of

the different degrees of skewing of the wave functions in different magnetoelectric subbands. This has the effect of breaking inversion symmetry.

As mentioned before, a magnetic field induces forbidden transitions between subbands of the same parity. The large magnitude of the dipoles associated with these transitions and their extreme sensitivity to the field open up the possibility of *controllable* second harmonic generation (SHG) that can be manipulated by the magnetic field. In order to evaluate the magnitude and dependence of SHG on the biasing field and wire geometry, we calculate the second order susceptibility using the formula[1]

$$\chi^{(2)}(2\omega;\omega;\omega) = \frac{Ne^3}{\epsilon\epsilon_o 2\hbar^2}\hat{S}_T \sum_{abc} \frac{d^{\mu}_{ab} d^{\alpha}_{bc} d^{\beta}_{ca}}{(\Omega_{ba} - \omega - i\gamma)(\Omega_{ca} - 2\omega - i\gamma)}, \qquad (2)$$

where N is concentration (number density) of conduction electrons, γ is a damping factor associated with elastic and inelastic scattering, $\hbar\Omega_{ba} \equiv \hbar\Omega_{ba}(B, W, k)$ is the energy spacing between the b-th and a-th magnetoelectric subbands which depends on the applied magnetic field, wire width and electron wave vector and $d_{mn} \equiv d_{mn}(B, W, k)$ is a dipole element of transitions between different subbands. The total symmetrisation operation $\hat{S}_T$ indicates that the expression which follows is to be summed over all permutations of the pairs $(\mu, 2\omega), (\alpha, \omega), (\beta, \omega)$. Since $\hat{S}_T$ involves a summation over all possible permutations, it is clear that $\chi^{(2)}_{\mu\alpha\beta}(2\omega;\omega;\omega)$ is invariant under any of them.

In order to calculate dipole elements $d_{mn}(B, W)$, we proceed as in Ref. [3]. Under the electric dipole approximation, the matrix element of photoinduced inter-subband transitions within the conduction band is given by[7]

$$d_{f,i}(k, B) = e \int \chi_f(y, k, B)\hat{\eta} \cdot \vec{r}\chi_i(y, k, B)d\vec{r} \int u^*_f(x, y, k)u_i(x, y, k)d\Omega \qquad (3)$$

where $d\Omega$ is a volume element, $\hat{\eta}$ is the unit vector along the direction of the incident photon polarization, $\vec{r} = x\vec{a}_x + y\vec{a}_y$ is the two-dimensional radius vector, and subscripts i, f stand for initial and final states respectively. Now, if we assume that the incident light is polarized along the y-direction so that

$\hat{\eta} = \hat{a_y}$, the above equation simplifies to

$$d_{f,i}(k,B) = e < \chi_f|y|\chi_i >= e\int_{-W/2}^{W/2} y\chi_f(y,k,B)\chi_i(y,k,B)dy, \qquad (4)$$

where W is the width of the quantum wire along the y-direction. One should note here, that if there is no magnetic (or electric) field applied, the envelope functions χ_i are just particle-in-box states and the dipole moment in Eq. (4) is non zero only for the transitions between subband states of opposite parity. However, this is obviously not the case when a magnetic field is present. It is clear from Eq. (4) that to calculate the dipole moments in the presence of a magnetic field, all we need to compute are the wave functions $\chi_{f,i}(y,k,B)$ at a given magnetic field B, for given magnetoelectric subbands f and i, and for a given wave vector k. This is achieved via a numerical (finite difference) solution of the Schrödinger equation for the y-component of the wavefunction

$$\frac{\partial^2\chi(y)}{\partial y^2} + \frac{2m^*}{\hbar^2}E\chi(y) - \left(\frac{y}{l^2}\right)^2\chi(y) + 2\frac{y}{l^2}k\chi(y) - k^2\chi(y) = 0 \qquad (5)$$

with l being the magnetic length given by $l = \sqrt{\hbar/eB}$, assuming hardwall boundary conditions

$$\chi(y = W/2) = \chi(y = -W/2) = 0 \qquad (6)$$

and following the prescription of Ref. [8]. Once this is done, we can calculate the dipole moment in Eq. (4) for any chosen intersubband transition, at any chosen magnetic field and for any chosen wave vector.

The absorption of both the fundamental frequency (pump) and its second-order harmonic is very important when considering frequency conversion with *low insertion loss*. In general, it is desirable to have large absorption coefficient $\alpha(\omega)$ for the pump frequency and small $\alpha(2\omega)$ for the converted frequency so that the latter is not re-absorbed to cause large insertion loss. In order to obtain the absorption coefficients in the whole range of frequencies and for different values of a magnetic flux density, we need to calculate the first-order susceptibility as follows

$$\chi^{(1)}(\omega) = \frac{Ne^2}{\epsilon\epsilon_o\hbar}\sum_{ab}\frac{(d_{ab})^2}{\Omega_{ba} - \omega - i\gamma}, \qquad (7)$$

where we have used the same notation as in Eq. (2). The imaginary part of $\chi^{(1)}(\omega)$ is related to the absorption coefficient while the real part is related to the refractive index.

II. Results

We now present results of our calculations. The physical parameters used for the numerical calculations are relevant for a $GaAs$ quantum wire with relative dielectric constant $\epsilon_r = 12.9$, and effective masses $m_e = 0.067m_o$ and $m_h = 0.5m_o$ where m_o is the free electron mass.

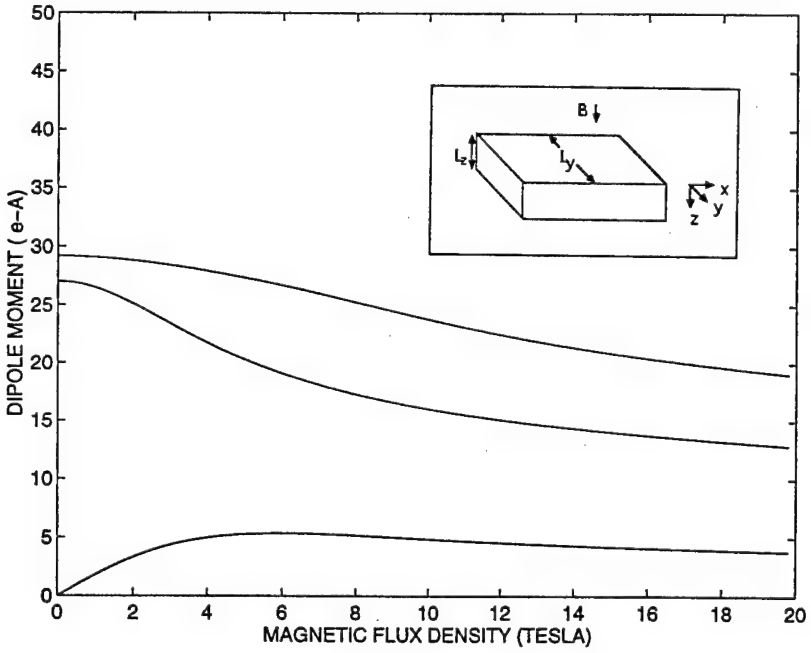

Figure 1: The dipoles of three inter-subband transitions as functions of the applied magnetic field. The induced dipole d_{e1-e3} peaks at a magnetic flux density of 5.3 tesla.

Fig. 1 presents the dipole moments for the lowest intraband transitions as a function of magnetic flux density. At zero magnetic field, a non-vanishing dipole matrix element occurs only for transitions between states of opposite parity (e1-e2, e2-e3) as expected from Eq. (4). Transition dipole d_{e3-e1}

has a non-monotonic dependence on the magnetic field. This transition is forbidden at zero field since the wave functions of the first and third subband have the same parity. At low and moderate magnetic fields, the parities are altered by the skewing of the wavefunctions. The skewing effect of the wave functions of the first and the third subbands is shown in Fig. 2 (top). Its degree depends on a subband number, which causes a breaking of inverion symmetry and, consequently, non-zero value of dipole matrix element d_{e3-e1} for otherwise forbidden transition.

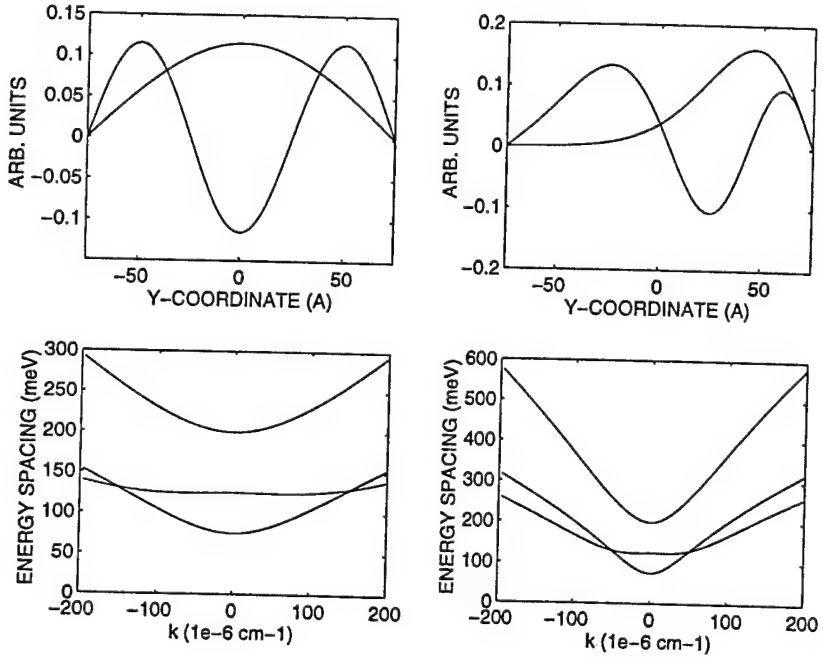

Figure 2: (Top left and right). Skewing of the wave functions of the first and third subbands in a magnetic field. The left panel corresponds to zero magnetic flux density and the wave functions are particle-in-a-box states. The right panel corresponds to a flux density of 3 tesla and the wave functions are those of "edge states". (Bottom left and right). The energy spacing $\hbar\Omega_{mn}$ between the mth and nth subbands vs. wave vector k at a magnetic flux density B=1 tesla (left) and B=3 tesla (right). The lowest curve (at k=0) corresponds to e1-e2, the intermediate curve to e2-e3, and the highest to e1-e3.

The dipole moment reaches a maximum of about 6 e-Å and then de-

creases. This later decrease is related to the following effect. For some fixed wave vector k (electron velocity), a sufficient increase in the flux density B forces the traversing states ("skipping orbits" or "edge states") to condense into closed cyclotron orbits (Landau levels) which are no longer skewed by the magnetic field to the wire edge since they have no translational velocity and hence experience no Lorentz force. While edge states have a skewed wave function which is not symmetric in space, cyclotron orbits have a wave function that is symmetric about the orbit center. Note that the orbit center's coordinates depend only on k and B. Therefore, at a fixed k, the wave functions of the first and third Landau levels are symmetric about a *common* center. Whenever this kind of symmetry holds, d_{e3-e1} vanishes. Therefore, the dipole moment d_{e3-e1} decreases gradually to zero at high magnetic field with the onset of Landau condensation (5 tesla for this wire dimensions).

In Fig. 3, we plot the absolute values of $\chi^{(2)}$ as a function of photon energy for two different values of the magnetic field. In our numerical calculations we have used a dilute carrier concentration of N=10^{17} cm^{-3} which allows us to neglect high density effects such as screening and bandgap renormalization. Both susceptibility curves have pronounced three-peak resonant structure which corresponds to two one-photon transitions e1-e2 (at 72 meV) and e2-e3 (at 124 meV) and one two-photon transition e1-e3 (at 100 meV) between magneto-electric subbands. These three peaks have different broadenings because the sum in Eq. (2) represents an integral effect of all direct transitions with different values of electron wave vector k and because of the complex dependence of the subband spacing $\hbar\Omega_{mn}$ on k and B (see Fig. 2 (bottom)). The latter also gives rise to an uneveness in the second order susceptibility peaks. The peak value of the second order susceptibility is $\chi^{(2)} = 14.5\mathring{A}/V$ for 1 tesla field (left panel); and $\chi^{(2)} = 43.1\mathring{A}/V$ for 3 tesla (right panel). For comparison, the nonlinear susceptibility of electric field biased GaAs quantum wells (W=92 $\mathring{A}$) - calculated theoretically and measured experimentally in Ref. [9] - was $\chi^{(2)}$=240Å/V for an electric field of 36

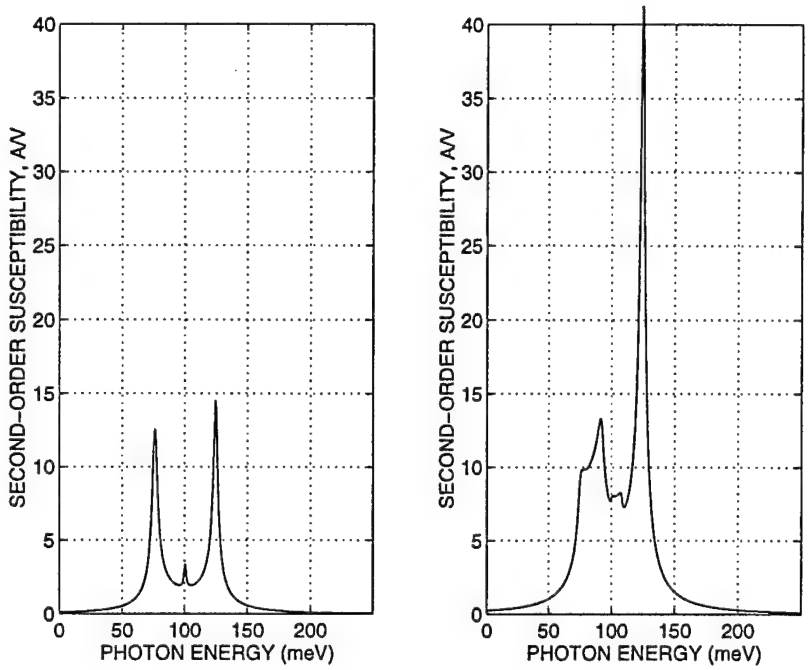

Figure 3: Second order susceptibility as a function of the photon energy for two values of the biasing magnetic field. The left panel corresponds to a magnetic flux density B=1 tesla, the right panel to B=3 tesla. The maximum values of the $\chi^{(2)}$ curves are $14.5\mathring{A}/V$ for 1 tesla field and $43\mathring{A}/V$ for 3 tesla field.

kV/cm. The carrier concentration used in their calculations was $N = 5\times10^{17}$ cm^{-3}. Adjusted to that carrier concentration, the second order susceptibility for a 3-tesla magnetic field is about $215\mathring{A}/V$ compared to $240\mathring{A}/V$ of Ref. [9]. This shows that relatively weak magnetic fields in quantum wires can produce similar magnitudes of $\chi^{(2)}$ as rather strong electric fields in quantum wells.

Fig. 4 shows the dependence of the imaginary part of the first-order susceptibility $Im(\chi^{(1)})$ as a function of photon energy for two different values of the magnetic field. We have used the same wire dimensions and carrier concentrations for this plot as in the previous one. The same physics pertinent to the previous plot explains different broadening; however, the peaks are now attenuated because of averaging over different transition probabilities.

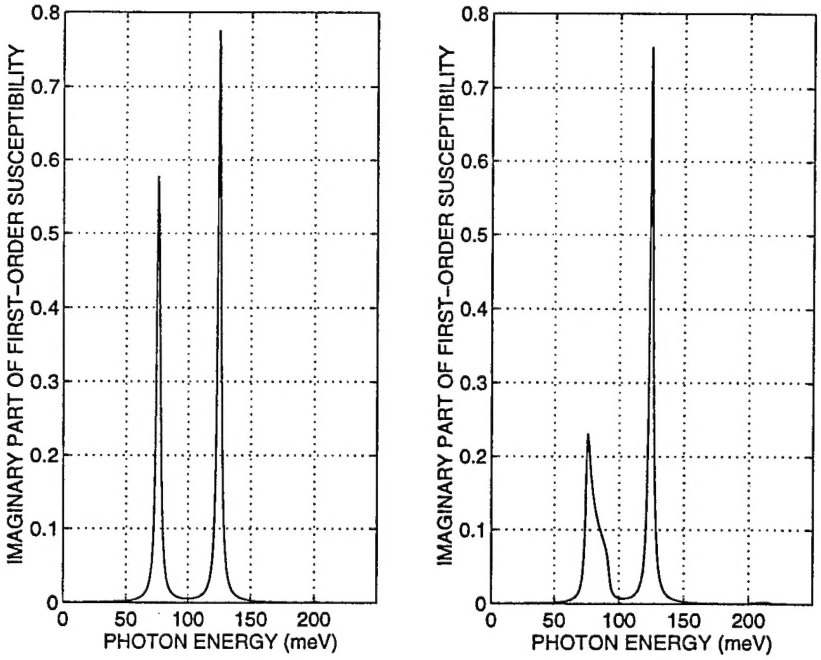

Figure 4: Imaginary part of the first-order susceptibility as a function of the photon energy for B=1 tesla (left panel) and B=3 tesla (right panel).

Since $Im(\chi^{(1)})$ is related to the absorption coefficient $\alpha(\omega)$ as

$$\alpha(\omega) = \frac{4\pi\omega}{c} Im(\chi^{(1)}), \tag{8}$$

one can estimate the absorption over the whole frequency range. At resonant photon energies of 72 meV and 124 meV, the absorption coefficient $\alpha = 1.5\ 10^4\ cm^{-1}$ and $\alpha = 4.5\ 10^4\ cm^{-1}$, respectively. It is clear from the figure, that the absorption coefficient at twice these frequencies, $\alpha(2\omega)$ is much less. This implies that a large portion of the pump energy at these resonant frequencies will be absorbed by the structure and converted into second harmonic signal which will not be significantly re-absorbed.

Another important factor for efficient second harmonic generation is *phase matching*. Since the refractive index $n(\omega)$ of most materials is frequency dependent, the following inequality holds $n(\omega) \neq n(2\omega)$. As a result, the coherence length $l_{coh} = \lambda_\omega/4(n_{2\omega} - n_\omega)$ for $GaAs$ (typical non-birefringent crystal)

varies between 10μm and 100μm. The efficiency of nonphase-matched interactions are about 10^{-5} times less than that of the phase-matched interactions over a length scale of 1 cm.

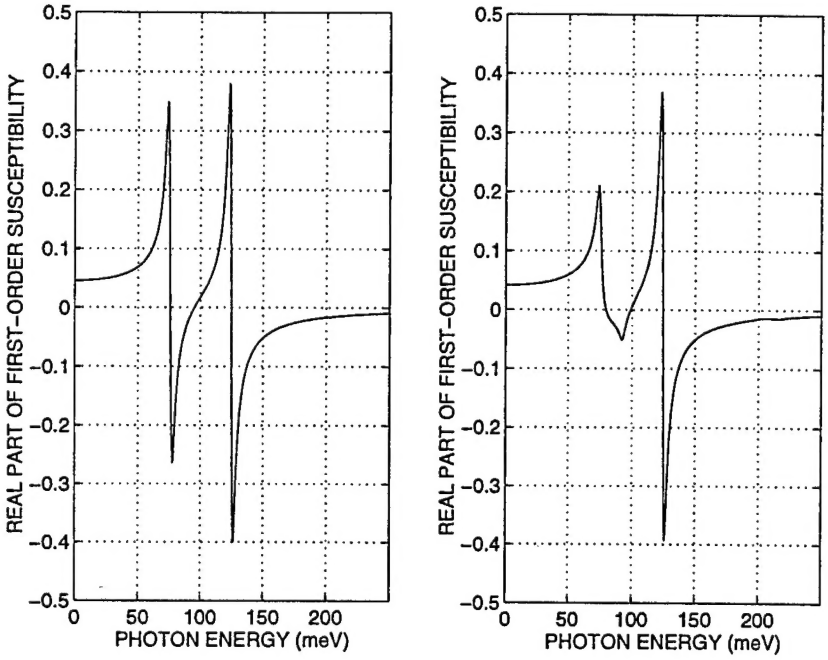

Figure 5: Real part of the first-order susceptibility as a function of the photon energy for B=1 tesla (left panel) and B=3 tesla (right panel).

Using a magnetic field as an additional degree of freedom, we may try to adjust $n(\omega)$. In Fig. 5 we present the dependence of the real part of the first-order susceptibility $Re(\chi^{(1)})$ as a function of photon energy for two different values of the magnetic field. Using the relation

$$\Delta n(\omega) = 2\pi Re(\chi^{(1)}), \tag{9}$$

and Eq. (8), one can determine the frequencies where two conditions simultaneously hold: $n(\omega) \approx n(2\omega)$ and $\alpha(\omega) >> \alpha(2\omega)$. For the 3-tesla field, this frequency $\hbar\omega$ corresponds to 75 meV.

IV. Conclusion

We have theoretically studied second harmonic generation in a semiconductor quantum wire biased with a magnetic field. A strong second-harmonic component of the dielectric susceptibility, due to the dipoles associated with transitions between magneto-electric subbands, is found. We have also calculated absorption coefficient and refractive index in the appropriate frequency range to assess the efficiency of frequency conversion and insertion loss. We have shown that a magnetic field can be used as an additional degree of freedom in optimizing second harmonic generation efficiency. This may have important applications in nonlinear optics.

Acknowledgement

This work is supported by the US Army Research Office under contracts DAAH04-95-1-0586 and DAAH04-95-1-0527. The authors are indebted to the Electrochemical Society, Inc. for partial travel support.

REFERENCES

[1] see for example P.N. Butcher, D. Cotter, *The Elements of Nonlinear Optics,* (Cambridge University Press, 1990); A. Yariv, *Quantum Electronics,* (Wiley, N.Y., 1989); or Y.R. Shen, *The Principles of Nonlinear Optics,* (Wiley, N.Y., 1984).

[2]. E.J. Austin and M. Jaros, *Phys. Rev. B* **31**, 5569 (1985).

[3]. A. Svizhenko, A. Balandin and S. Bandyopadhyay, *J. Appl. Phys.*, (in press, 1997).

[4]. A. Balandin and S. Bandyopadhyay, *J. Appl. Phys.*, **77**, 5924 (1995); A. Balandin, Ph.D. dissertation, University of Notre Dame, 1996.

[5] This lack of symmetry is due to the transfer of a valency charge from one atom to the other bond-forming atom and resultant uneven charge distribution along the bond axis.

[6] *Handbook of Lasers,* Edited by R.J. Pressley (Chemical Rubber Co., Cleveland, 1971), p. 504.

[7]. Claude Weisbuch and Borge Vinter, *Quantum Semiconductor Structures: Fundamentals and Applications*, (Academic Press, Boston, 1991).

[8] S. Chaudhuri and S. Bandyopadhyay, *J. Appl. Phys.*, **71**, 3027 (1992).

[9]. M.M. Fejer, S.J.B. Yoo, R.L.Byer, A. Harwit, J.S. Harris, *Phys. Rev. Lett.*, **62**, 1041 (1989).